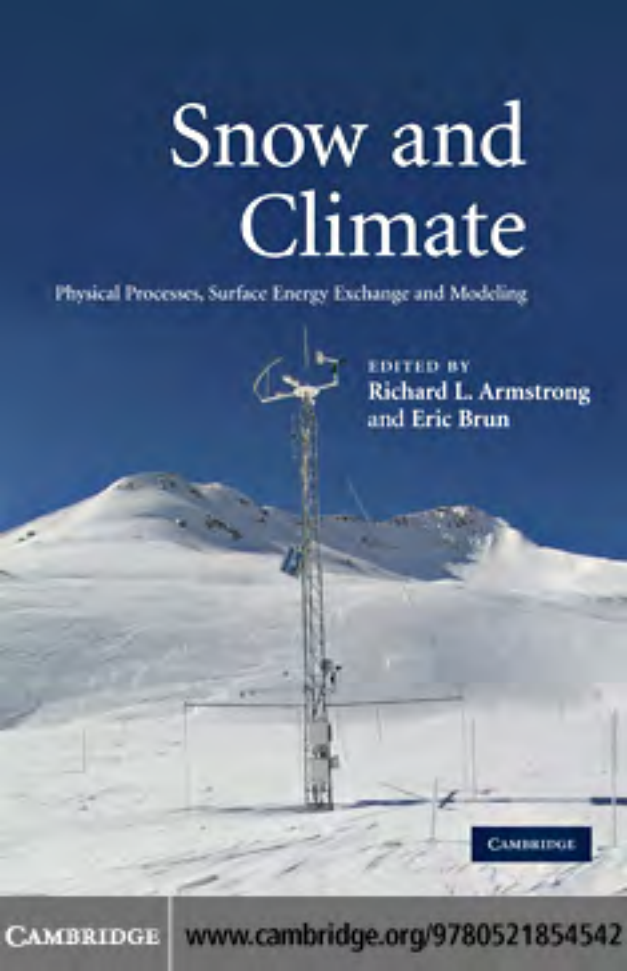


# Snow and Climate

Physical Processes, Surface Energy Exchange and Modeling

EDITED BY  
Richard L. Armstrong  
and Eric Brun



CAMBRIDGE

CAMBRIDGE

[www.cambridge.org/9780521854542](http://www.cambridge.org/9780521854542)

This page intentionally left blank

## SNOW AND CLIMATE

The extent and variability of seasonal snow cover are important parameters in the climate system, due to their effects on energy and moisture budgets, and because surface temperature is highly dependent on the presence or absence of snow cover. In turn, snow-cover trends serve as key indicators of climate change.

In the last two decades many new methods and techniques have become available for studying snow–climate relationships. Satellites provided the first capability for monitoring snow-cover extent at continental and hemispheric scales, enabling the investigation of synoptic-scale snow cover–climate linkages. This global view of snow cover has been accompanied by rapid advances in snow modeling physics to represent snow cover and snow processes in Global Climate Models (GCMs). These advances have changed the way we look at snow cover, and the main goal of this book is to provide an up-to-date synthesis of the current state of snow–climate science that reflects this new perspective. This volume will provide an excellent synthesis for researchers and advanced students.

**RICHARD ARMSTRONG** is a Senior Research Scientist at the National Snow and Ice Data Center, the World Data Center for Glaciology and the Cooperative Institute for Research in Environmental Sciences at the University of Colorado. His current research includes remote sensing and evaluation of fluctuations in snow cover and glaciers as indicators of climate change.

**ERIC BRUN** is Head of Research at Météo-France and Director of the Centre National de Recherche Météorologiques. He is a specialist in snow and avalanches and developed original methods to assess the impact of climate change on snow cover and alpine rivers.



# SNOW AND CLIMATE

Physical Processes, Surface Energy Exchange and Modeling

*Editors:*

RICHARD L. ARMSTRONG

*Cooperative Institute for Research in Environmental Sciences,  
University of Colorado*

ERIC BRUN

*CNRM/GAME  
(Météo-France, CNRS)*



**CAMBRIDGE**  
**UNIVERSITY PRESS**

CAMBRIDGE UNIVERSITY PRESS  
Cambridge, New York, Melbourne, Madrid, Cape Town, Singapore, São Paulo

Cambridge University Press  
The Edinburgh Building, Cambridge CB2 8RU, UK  
Published in the United States of America by Cambridge University Press, New York

[www.cambridge.org](http://www.cambridge.org)

Information on this title: [www.cambridge.org/9780521854542](http://www.cambridge.org/9780521854542)

© Cambridge University Press 2008

This publication is in copyright. Subject to statutory exception and to the provision of relevant collective licensing agreements, no reproduction of any part may take place without the written permission of Cambridge University Press.

First published in print format 2008

ISBN-13 978-0-511-45533-9 eBook (EBL)

ISBN-13 978-0-521-85454-2 hardback

Cambridge University Press has no responsibility for the persistence or accuracy of urls for external or third-party internet websites referred to in this publication, and does not guarantee that any content on such websites is, or will remain, accurate or appropriate.

This book is dedicated to the memory of Professor Donald M. Gray, (1929–2005), Chairman of the Division of Hydrology, University of Saskatchewan, and editor (with David Male) of the *Handbook of Snow: Principles, Processes, Management and Use* (1981), which is one of the earliest books to include a complete review of snow physics, accumulation and ablation processes and associated meteorology and climatology. Don pioneered the study of snow in Canada with an insistence that its study include a strong physical and observational basis, the full coupling of the mass and energy equations and consideration of atmospheric as well as surface processes. His contributions to this book are greatly appreciated.



# Contents

<i>List of contributors</i>	page ix
<i>Preface</i>	xi
<i>Acknowledgments</i>	xiii
<i>Nomenclature</i>	xiv
1 Introduction	1
<i>Richard L. Armstrong and Ross Brown</i>	
1.1 Basic properties of snow	1
1.2 Importance of snow in the climate system	4
1.3 Importance of snow in natural and human systems	6
1.4 Climate change implications	7
1.5 Layout of book	9
2 Physical processes within the snow cover and their parameterization	12
<i>Rachel E. Jordan, Mary R. Albert, and Eric Brun</i>	
2.1 Introduction	12
2.2 General characteristics	19
2.3 Thermal behavior of snow	35
2.4 Fluid flow behavior in snow	40
2.5 Radiative properties of snow	53
3 Snow–atmosphere energy and mass balance	70
<i>John C. King, John W. Pomeroy, Donald M. Gray, Charles Fierz, Paul M. B. Föhn, Richard J. Harding, Rachel E. Jordan, Eric Martin, and Christian Plüss</i>	
3.1 Introduction	70
3.2 Equations of energy and mass balance	70
3.3 The fluxes involved in the energy balance	73
3.4 Snow accumulation	83
3.5 Examples of energy and mass balances	92

4	Snow-cover parameterization and modeling	125
	<i>Eric Brun, Zong-Liang Yang, Richard Essery, and Judah Cohen</i>	
4.1	History of numerical modeling of snow cover	125
4.2	Description of recent snow models	129
4.3	Sensitivity of energy and mass fluxes at the snow–atmosphere interface to internal and interface parameters	136
4.4	Snow parameterization in GCMs	145
4.5	The global snow coverage in climate change scenarios	156
5	Snow-cover data: measurement, products, and sources	181
	<i>Ross Brown and Richard L. Armstrong</i>	
5.1	Introduction	181
5.2	<i>In situ</i> snow data	182
5.3	Remote sensing data	192
5.4	Operational snow-cover products	203
5.5	Global–continental snow-cover climatology: measured and modeled	205
	<i>Appendix: Snow model questionnaire</i>	217
	<i>Index</i>	220

*The color plates are between pages 104 and 105*

## List of contributors

**Mary Remley Albert** U.S. Army Cold Regions Research and Engineering Laboratory, Hanover, New Hampshire, U.S.A.

**Richard L. Armstrong** Cooperative Institute for Research in Environmental Sciences, University of Colorado, Boulder, Colorado, U.S.A.

**Ross Brown** Environment Canada, Climate Research Division, Montréal, Québec, Canada

**Eric Brun** CNRM/GAME (Météo-France, CNRS), Toulouse, France

**Judah Cohen** Atmospheric and Environment Research, Lexington, Massachusetts, U.S.A.

**Richard Essery** School of Geosciences Grant Institute, University of Edinburgh, Edinburgh, UK

**Charles Fierz** WSL Institute for Snow and Avalanche Research SLF, Davos, Switzerland

**Paul Föhn** WSL Institute for Snow and Avalanche Research SLF, Davos, Switzerland

**Don M. Gray** Division of Hydrology, University of Saskatchewan, Saskatoon, Canada, † deceased

**Richard J. Harding** Centre for Ecology and Hydrology, Institute of Hydrology, Wallingford, UK

**Rachel E. Jordan** U.S. Army Cold Regions Research and Engineering Laboratory, Hanover, New Hampshire, U.S.A.

**John C. King** British Antarctic Survey, Natural Environmental Research Council,  
Cambridge, UK

**Eric Martin** Météo-France/CNRM, Toulouse, France

**Christian Plüss** WSL Institute for Snow and Avalanche Research SLF, Davos,  
Switzerland, Now at Erdgas Ostschweiz AG

**John W. Pomeroy** Centre for Hydrology, University of Saskatchewan, Saskatoon,  
Canada

**Zong-Liang Yang** Department of Geological Sciences, University of Texas,  
Austin, Texas, U.S.A.

# Preface

While the idea of a book with a focus on snow and climate had been discussed for several years previous, it first took formal shape at a meeting of the International Commission on Snow and Ice (ICSI) of the International Association of Hydrological Sciences (IAHS) in Victoria, British Columbia, Canada in 1996. At that time, a group was formed within the ICSI Division of Snow Cover and Avalanches (chaired by Eric Brun) to begin work on an outline of a state-of-the-art book that would focus on the relationships between snow and climate. A basic outline of the book was developed and section leads were assigned to coordinate the development of detailed outlines of each individual chapter. We recognized that the study of snow and climate was a rapidly evolving science and that there were new demands for detailed representations of snow processes to provide an up-to-date understanding of the physical processes in snow and to support modeling for climate change scenarios. The earlier *Handbook of Snow* (Gray and Male, 1981) provided excellent information on the principles, processes, management, and uses of snow, but no similar book had been published in the intervening two decades. Because we envisioned that this book would perhaps be the only example of an overview of snow and climate available, we agreed that the audience should be broad. Our intent is that this new scientific and comprehensive treatment of the subject of snow and climate becomes a fundamental reference text for university undergraduate and graduate students as well as a reference guide for instructors in secondary schools to assist them in teaching about snow and climate. Because of the world wide interest in snow and snow processes among winter recreationists and much of the general public living in cold regions, this book should also offer a source of basic information for those with only a limited scientific background. Regardless of audience, the fundamental purpose of this book is to introduce the basic scientific principles that enable us to understand the relationships between snow and climate.

Researchers have long been aware of the important role of snow in the climate system. For example, studies on snowfields in Scandinavia were undertaken by

Sverdrup (1935) and Wallen (1949). Later, Houghten (1954), Budyko (1956), and Geiger (1959) included the effect of snow in their studies of the surface heat balance and the associated snow–albedo feedback while Lamb (1955) was one of the first to look at the synoptic-scale influence of snow cover. Williams (1975) was one of the first to explore the influence of snow cover on atmospheric circulation and climate change. In the decades since these studies, many new methods and techniques have become available to study snow–climate relationships. Satellites provided the first capability for monitoring snow-cover extent at continental and hemispheric scales, thus enabling the investigation of synoptic-scale snow cover–climate linkages. This global view of snow cover was accompanied by rapid advances in snow modeling physics to represent snow cover and snow processes in Global Climate Models (GCMs). These processes have changed the way we look at snow cover, and the main goal of this book is to provide an up-to-date synthesis of the current state of snow–climate science that reflects this new perspective.

### References

- Budyko, M. I. (1956). *Teplovoi Balans Zemnoi Poverkhnosti*. Leningrad: Gidrometeorologicheskoe Izdatel'stvo. (English transl.: Stepanova, N. A. (1958). *The Heat Balance of the Earth's Surface*. Office of Technical Services, U.S. Dept. of Commerce, Washington, DC.)
- Geiger, R. (1959). *The Climate near the Ground*. Cambridge, MA: Harvard University Press.
- Gray, D. M. and Male, D. H. (1981). *Handbook of Snow*. Toronto: Pergamon Press.
- Houghten, H. G. (1954). On the annual heat balance of the Northern Hemisphere. *J. Meteorol.*, **11**, 1–9.
- Lamb, H. H. (1955). Two-way relationships between the snow or ice limit and 100–500 mb thickness in the overlying atmosphere. *Q. J. Roy. Meteorol. Soc.* **181**, 172–189.
- Sverdrup, H. U. (1935). Scientific results of the Norwegian–Swedish Spitzbergen expedition in 1934. Part IV. The ablation on Isachsen's Plateau and on the 14th of July Glacier. *Geogr. Ann.*, **17**, 53–166.
- Wallen, C. C. (1949). Glacial–meteorological investigations on the Karsa Glacier in Swedish Lapland 1942–1948. *Geogr. Ann.*, **30**, 451–672
- Williams, J. (1975). The influence of snow cover on the atmospheric circulation and its role in climate change. *J. Appl. Meteorol.*, **14**, 137–152.

# Acknowledgments

The editors wish to express their gratitude to the reviewers of the book sections. Their comments and suggestions were extremely helpful and very much appreciated. We would also like to thank the support and encouragement provided by the International Commission on Snow and Ice (ICSI) of the International Association of Hydrological Sciences (IAHS), as well as by the newly formed (2007) International Association of Cryospheric Sciences (IACS).

The work of Ms. Rachel Jordan was funded primarily by the Director of Research and Development, U.S. Army Corps of Engineers, through projects at ERDC-CRREL, and partly by the National Science Foundation via awards OPP-98-14024 and OPP-00-84190. Dr. Mary Albert's contribution to chapter 2 was supported by the National Science Foundation under grant OPP-01-39988. The work of M. Eric Brun was funded primarily by the Centre National de Recherches Météorologiques at Météo-France.

Rachel Jordan is grateful to Dr. Robert E. Davis and Dr. Edgar L. Andreas for their continued support and helpful discussions, as well as to ERDC-CRREL's technical staff for maintaining the CRREL snow research site.

Zong-Liang Yang is indebted to Dr. R. C. Bales who suggested that he read the WMO-led snow model survey while designing his questionnaire. He also wishes to thank Dr. R. E. Dickinson for his encouragement and Dr. W. J. Shuttleworth for reading the early draft. All those who took time to complete the snow model questionnaire are gratefully acknowledged.

# Nomenclature

Symbol	Description	Section	Value	Units (SI)
$a$	Parameter, saturation vapor pressure	2		hPa
$a_1$	Parameter, effective thermal conductivity	4		$\text{W m}^{-2} \text{K}^{-1}$
$a_2$	Parameter, albedo weight function	4		$\text{m}^{-1}$
$a_3$	Parameter, albedo weight function	4		$\text{m}^{-1}$
$a_4$	Parameter, dimensionless sensible heat flux	3		
$a_5$	“Saltation efficiency” coefficient	3	0.68	$\text{m s}^{-1}$
$A$	Specific surface of snow	2		$\text{m}^2 \text{m}^{-3}$
$b$	Parameter, saturation vapor pressure	2		
$b_1$	Parameter, effective thermal conductivity	4		$\text{m}^6 \text{kg}^{-1} \text{s}^{-3} \text{K}^{-1}$
$B$	Bowen ratio $H_S/H_L$	3		
$B_*$	Lower limit for Bowen ratio	3		
$c$	Parameter, saturation vapor pressure	2		$^{\circ}\text{C}$
$c_1$	Parameter, apparent change in roughness length	3	0.1203	
$c_2$	New snow drift coefficient	3	$0.8 \times 10^{-4}$	$\text{s}^3 \text{m}^{-2}$
$c_{\text{susp}}$	Mass concentration of suspended snow	3		
$c_{\text{can}}$	Canopy closure	3		
$c_{\text{p,a}}$	Specific heat of air at constant pressure and at 273.15 K	2, 3	1005	$\text{J kg}^{-1} \text{K}^{-1}$

Symbol	Description	Section	Value	Units (SI)
$c_{p,i}$	Specific heat of ice at constant pressure and at 273.15 K	2, 3	2114	$\text{J kg}^{-1} \text{K}^{-1}$
$c_{p,\ell}$	Specific heat of water at constant pressure and at 273.15 K	2	4217	$\text{J kg}^{-1} \text{K}^{-1}$
$c_{p,s}$	Specific heat of snow at constant pressure	2		$\text{J kg}^{-1} \text{K}^{-1}$
$C$	Shape factor	2		m
$C_{hq}$	Bulk transfer coefficient	3		
$C_D$	Bulk transfer coefficient for momentum	3		
$C_H$	Bulk transfer coefficient for heat	3		
$C_Q$	Bulk transfer coefficient for water vapor	3		
$C_{DN}, C_{HN}, C_{QN}$	Parameters, bulk transfer coefficients in terms of the bulk Richardson number	3		
$d$	Geometrical grain size or diameter	2		m
$d_{\text{opt}}$	Optical grain size	2		m
$D_g, D_a$	Diffusion coefficient of water vapor in air	2, 3		$\text{m}^2 \text{s}^{-1}$
$D_s$	Diffusion coefficient of water vapor in snow	2		$\text{m}^2 \text{s}^{-1}$
$D_{\text{bs}}$	Horizontal blowing snow transport	3		$\text{kg m}^{-1}$
$D_{\text{salt}}$	Saltating transport of blowing snow	3		$\text{kg m}^{-1} \text{s}^{-1}$
$D_{\text{susp}}$	Suspension transport of blowing snow	3		$\text{kg m}^{-1} \text{s}^{-1}$
$E$	Sum of sublimation and evaporation rate at surface	3		$\text{kg m}^{-2} \text{s}^{-1}$
$E_{\text{subl}}$	Surface sublimation rate	3		$\text{kg m}^{-2} \text{s}^{-1}$
$E_{\text{evap}}$	Surface evaporation rate	3		$\text{kg m}^{-2} \text{s}^{-1}$
$E_{\text{bs}}$	Sublimation rate of blowing snow	3		$\text{kg m}^{-2} \text{s}^{-1}$
$f$	Parameter, compaction	2		
$F$	Heat flux	2		$\text{W m}^{-2}$
$f_s$	Weight function for albedo	4		
$g$	Acceleration due to gravity	2, 3	9.81	$\text{m s}^{-2}$

Symbol	Description	Section	Value	Units (SI)
$G$	Ground heat flux	3		$\text{W m}^{-2}$
$G_g$	Enhancement factor for grain growth	2		m
$h$	Capillary rise	2		m
$h_{S,b}$	Portion of bare ground sensible heat advected to a snow patch	3		$\text{W m}^{-2}$
$h_*$	Lower boundary for suspended snow (upper boundary for saltating snow)	3		m
$\tilde{h}$	Mass transfer coefficient	2		$\text{m s}^{-1}$
$\mathcal{H}$	Internal energy of the snowpack	3		$\text{J m}^{-2}$
$H_L$	Latent heat flux	3		$\text{W m}^{-2}$
$H_P$	Energy flux carried by precipitation and blowing snow	3		$\text{W m}^{-2}$
$H_S$	Sensible heat flux	3		$\text{W m}^{-2}$
$H_{S,b}$	Sensible heat flux over bare ground	3		$\text{W m}^{-2}$
$H_{S,s}$	Sensible heat flux over a completely snow-covered fetch	3		$\text{W m}^{-2}$
$H'_S$	Dimensionless sensible heat flux	3		
$HN_w$	New snow depth due to blowing and drifting snow	3		m
$HS, H$	Depth of snowpack, snow depth	2, 3, 4, 5		m
$I$	Snow interception	3		$\text{kg m}^{-2}$
$I_1$	Interception before unloading	3		$\text{kg m}^{-2}$
$k$	Thermal conductivity	2		$\text{W m}^{-1} \text{K}^{-1}$
$k_a$	Thermal conductivity of air	3		$\text{W m}^{-1} \text{K}^{-1}$
$K_\ell$	Permeability of the interconnected water pathways in wet snow	2		$\text{m}^2$
$K_F$	Cryoscopic constant for water	2	1.855	$\text{K kg mol}^{-1}$
$k_{cl}$	Snow clump shape coefficient	3		
$k_{\text{eff}}$	Effective thermal conductivity	2		$\text{W m}^{-1} \text{K}^{-1}$
$k_i$	Thermal conductivity of ice	4		$\text{W m}^{-1} \text{K}^{-1}$
$K$	Intrinsic or saturated permeability	2		$\text{m}^2$
$K_k$	Permeability of phase $k$ in unsaturated wet snow	2		$\text{m}^2$
$K_{rk}$	Relative permeability of phase $k$ in unsaturated wet snow ( $=K_k/K$ )	2		
$L_{i\ell}, L_{\ell i}$	Latent heat of fusion for ice at 273.15 K	2, 3	$3.335 \times 10^5$	$\text{J kg}^{-1}$

Symbol	Description	Section	Value	Units (SI)
$L_{iv}, L_{vi}$	Latent heat of sublimation for ice at 273.15 K	2, 3	$2.838 \times 10^6$	$\text{J kg}^{-1}$
$L_{\ell v}, L_{v\ell}$	Latent heat of evaporation for water at 273.15 K	2, 3	$2.505 \times 10^6$	$\text{J kg}^{-1}$
$L_{ji}$	Latent heat of phase change from phase $j$ to phase $i$	2		$\text{J kg}^{-1}$
$\mathcal{L}_L$	Snow load	3		$\text{kg m}^{-2}$
$\mathcal{L}_{L,o}$	Initial snow load	3		$\text{kg m}^{-2}$
$\mathcal{L}_L^*$	Maximum canopy snow load	3		$\text{kg m}^{-2}$
$\mathcal{L}_{L,b}$	Maximum snow load per unit area of branch	3		$\text{kg m}^{-2}$
$L_O$	Obukhov length	3		m
$L_N$	Net flux of longwave radiation, $L_{\downarrow} + L_{\uparrow}$	3		$\text{W m}^{-2}$
$LAI$	Winter leaf and stem area index	3		$\text{m}^2 \text{m}^{-2}$
$L_L^*$	Maximum canopy snow load	3		$\text{kg m}^{-2}$
$L_{\downarrow}$	Downward component of longwave radiation	3		$\text{W m}^{-2}$
$L_{\uparrow}$	Upward component of longwave radiation	3		$\text{W m}^{-2}$
$m$	Parameter, water saturation (van Genuchten)	2		
$M$	Molality of species	2		$\text{mol kg}^{-1}$
$m_p$	Mass of single blowing snow particle	3		kg
$\dot{m}$	Mass growth rate of snow particle	2		$\text{kg s}^{-1}$
$\mathcal{M}$	Snow mass per unit surface area	3		$\text{kg m}^{-2}$
$n$	Parameter, water saturation (van Genuchten)	2		
$Nu$	Nusselt number	3		
$N_{Re}$	Particle Reynolds number	3		
$p$	Pressure	2		Pa
$p_a$	Atmospheric or air pressure	2		hPa or Pa
$p_e$	Air-entry pressure	2		Pa
$p_k$	Pressure of constituent $k$	2		Pa
$p_{a\ell}$	Capillary pressure or pressure drop ( $p_a - p_{\ell}$ ) across air/water interface	2		Pa

Symbol	Description	Section	Value	Units (SI)
$p_{ij}$	Pressure drop ( $p_i - p_j$ ) across $i/j$ interface	2		Pa
$p_{v,\text{sat},k}$	Saturation vapor pressure over a flat surface with respect to constituent $k$	2		hPa
$p'_{v,\text{sat},k}$	Saturation vapor pressure over a curved surface with respect to constituent $k$	2		hPa
$P$	Precipitation rate	3		$\text{kg m}^{-2} \text{s}^{-1}$
$\mathcal{P}$	Accumulated precipitation	3		$\text{kg m}^{-2}$
$Pe$	Peclet number	2		
$P_{\text{bs}}$	Probability of blowing snow occurrence	3		
$q$	Phase change thermal source term	2		$\text{W m}^{-3}$
$Q$	Specific humidity	3		$\text{kg/kg}$
$Q_o$	Specific humidity at the snow surface	3		$\text{kg/kg}$
$Ra$	Rayleigh number	2		
$r_{\text{pt}}$	Particle radius	3		m
$r_{\text{pt},n}$	Nominal snow particle radius	3	0.0005	m
$r_p$	Tube radius or equivalent pore radius	2		m
$r_g$	Snow grain radius	2, 3		m
$Ra_{\text{crit}}$	Critical Rayleigh number for onset of convection	2		
$Re$	Reynolds number	3		
$Ri_B$	Bulk Richardson number	3, 4		
$R_v$	Gas constant for water vapor	2	461.50	$\text{J kg}^{-1} \text{K}^{-1}$
$R_F$	Freezing rate	3		$\text{kg m}^{-2} \text{s}^{-1}$
$R_M$	Melt rate	3		$\text{kg m}^{-2} \text{s}^{-1}$
$R_N$	Net radiative flux at the snow surface, $S_N + L_N$	3		$\text{W m}^{-2}$
$R_{\text{runoff}}$	Runoff rate at snow–soil interface	3		$\text{kg m}^{-2} \text{s}^{-1}$
$s$	Liquid water saturation ( $\theta_l/\phi$ )	2		
$s_i$	Irreducible or immobile liquid water saturation	2		
$s^*$	Effective liquid water saturation [[ $(s - s_i)/(1 - s_i)$ ]]	2		
$S$	Phase change mass source term	2		$\text{kg m}^{-3} \text{s}^{-1}$
$Sh$	Sherwood number	3		

Symbol	Description	Section	Value	Units (SI)
$S_{\text{toa}}$	Solar radiation flux at the top of the atmosphere	3		$\text{W m}^{-2}$
$SCA$	Proportion of snow-covered area	3		
$S_{\text{N}}$	Net flux of shortwave radiation, $S_{\downarrow} + S_{\uparrow}$	3		$\text{W m}^{-2}$
$SWE$	Snow water equivalent	2, 3, 4, 5		$\text{kg m}^{-2}$ (or $\text{mm w.e.}$ )
$S_{\downarrow}$	Downward component of solar radiation	3		$\text{W m}^{-2}$
$S_{\uparrow}$	Reflected component of solar radiation	3		$\text{W m}^{-2}$
$t$	Time	2, 3, 4		s
$t_{\text{h}}$	Snow surface age	3		hours
$T$	Temperature	2, 3		K or $^{\circ}\text{C}$
$T_{\text{d}}$	Melting point depression, $273.15 - T$	2		K
$T_0$	Melting temperature 273.15 or $0^{\circ}\text{C}$	2		K or $^{\circ}\text{C}$
$T_{\text{o}}, T_{\text{0}}$	Snow surface temperature	3, 4		K or $^{\circ}\text{C}$
$T_{\text{o,sp}}$	Ice sphere surface temperature	3		K
$T_{\text{a}}$	Air temperature	3, 4		K or $^{\circ}\text{C}$
$T_{\text{s}}$	Snow temperature	3		K or $^{\circ}\text{C}$
$T'$	Snow temperature gradient	2		$\text{K m}^{-1}$ or $^{\circ}\text{C m}^{-1}$
$T_{\text{mean}}$	Mean air temperature in layer of depth $\zeta_{\text{ref}}$	3		K
$u$	Wind speed	3		$\text{m s}^{-1}$
$u_{10}$	Average hourly 10-m wind speed	3		$\text{m s}^{-1}$
$\bar{u}$	Mean wind speed	3		$\text{m s}^{-1}$
$\bar{u}_{\text{crest}}$	Mean wind speed measured on a crest	3		$\text{m s}^{-1}$
$u_{*}$	Friction velocity	3		$\text{m s}^{-1}$
$u_{*\text{n}}$	Friction velocity applied to small-scale non-erodible elements	3		$\text{m s}^{-1}$
$u_{*\text{t}}$	Threshold friction velocity	3		$\text{m s}^{-1}$
$U_{\text{I}}$	Snow unloading coefficient	3		$\text{s}^{-1}$
$v_i$	Velocity of ice matrix	2		$\text{m s}^{-1}$
$v_k$	Flow (filter) velocity of fluid $k$ (a = air, $\ell$ = water)	2		$\text{m s}^{-1}$

Symbol	Description	Section	Value	Units (SI)
$V$	Volume per unit mass or reciprocal density	2		$\text{m}^3 \text{kg}^{-1}$
$w$	Vertical (wind) velocity	3		$\text{m s}^{-1}$
$w_*$	Dimensionless vertical velocity	3		
$x, y, z$	Coordinate system with $z$ positive upward relative to the ground	2, 3		m
$x$	Spatial coordinate along the direction of flow	2		m
$x_M, x_H$	Parameters, similarity function	3		
$X$	Dimensionless distance downwind of snow patch	3		
$z_{\text{ref}}$	Reference height above ground	3		m
$z_b$	Upper boundary for suspended snow	3		m
$z_o, z_0$	Momentum (or aerodynamic) roughness length; surface roughness length	3, 4		m
$z_H$	Roughness length for heat	3		m
$z_Q$	Roughness length for water vapor	3		m
$z_*$	Scale of roughness elements	3		m
$\alpha$	Snow (surface) albedo	2, 3		
$\alpha_b$	Albedo of snow-free (bare) surface	4		
$\alpha_{\text{max}}$	Upper limit on snow albedo	4		
$\alpha_{\text{min}}$	Lower limit on snow albedo	4		
$\alpha_s$	Albedo of deep, homogeneous snow	4		
$\beta$	Coefficient of solar absorption	2		$\text{cm}^{-1}$
$\tilde{\beta}$	Coefficient of thermal expansion	2		$\text{K}^{-1}$
$\beta_{1H}, \beta_{1M}$	Parameters, similarity function	3		
$\beta_1$	Parameter, similarity function, $\beta_1 = \beta_{1M} = \beta_{1H}$	3		
$\Delta t$	Time interval	4		s
$\Delta x$	Characteristic distance	2		m
$\gamma_1, \gamma_2$	Parameters, similarity function	3		
$\delta$	Standard deviation of wind speed	3		$\text{m s}^{-1}$
$\varepsilon$	Snow infrared emissivity	3		
$\varepsilon_{\text{eff}}$	Effective emissivity for the atmosphere	3		
$\varepsilon$	Exponent, phase permeability	2		

Symbol	Description	Section	Value	Units (SI)
$\zeta$	Height above snow surface	3		m
$\zeta_{\text{ref}}$	Reference height above snow surface	3		m
$\zeta_{ij}$	Radius of curvature of $i/j$ interface	2		m
$\eta$	Newtonian viscosity of snow	2		Pa s
$\eta_0$	Newtonian viscosity of snow at $T = 0\text{ }^\circ\text{C}$ and $\rho_s = 0.0\text{ kg m}^{-3}$	2		Pa s
$\eta_k$	Dynamic viscosity of fluid $k$	2		Pa s
$\theta$	Contact angle between solid and liquid	2		rad.
$\theta_k$	Volume fraction of constituent $k$	2, 3		
$\kappa$	Von Kármán constant	3		
$\kappa_s$	Turbulent diffusion coefficient for snow particles	3		$\text{m}^2\text{ s}^{-1}$
$\lambda$	Wavelength	2		$\mu\text{m}$
$\lambda_p$	Pore-size distribution index	2		
$\Lambda$	Leaf area index	4		
$\Lambda$	Thermal diffusivity ( $k/\rho_a \cdot c_{p,a}$ )	2		$\text{m}^2\text{ s}^{-1}$
$\mu_a$	Kinematic viscosity of air ( $\eta_a / \rho_a$ )	3		$\text{m}^2\text{ s}^{-1}$
$\rho_a$	Density of air	2, 3		$\text{kg m}^{-3}$
$\rho_{0,a}$	Reference density of air	2		$\text{kg m}^{-3}$
$\rho_i$	Density of ice	2, 3	917	$\text{kg m}^{-3}$
$\rho_k$	Density of fluid or solid $k$	2		$\text{kg m}^{-3}$
$\rho_\ell$	Density of water	2, 3, 4	1000	$\text{kg m}^{-3}$
$\rho_{\text{max}}$	Maximum permitted snow density	4		
$\rho_s$	Density of snow	2, 3, 4, 5		$\text{kg m}^{-3}$
$\rho_v$	Density of water vapor	2		$\text{kg m}^{-3}$
$\rho_{v,a}$	Density of water vapor in air	3		$\text{kg m}^{-3}$
$\rho_{v,\text{pt}}$	Density of water vapor at particle surface	3		$\text{kg m}^{-3}$
$\rho_{v,\text{sat}}$	Saturation density of water vapor	2, 3		$\text{kg m}^{-3}$
$\sigma_{\text{SB}}$	Stefan–Boltzmann constant	3	$5.6697 \times 10^{-8}$	$\text{W m}^{-2}\text{ K}^{-4}$
$\sigma_{a\ell}, \sigma_{\ell v}$	Surface tension of air/water interface	2	0.076	$\text{N m}^{-1}$
$\sigma_{i\ell}$	Surface tension of ice/water interface	2	0.028	$\text{N m}^{-1}$
$\sigma_{iv}$	Surface tension of ice/vapor interface	2	0.104	$\text{N m}^{-1}$
$\sigma_{ij}$	Surface tension of $i/j$ interface	2		$\text{N m}^{-1}$

Symbol	Description	Section	Value	Units (SI)
$\tau_o$	Surface stress	3		$\text{N m}^{-2}$
$\tau_{\text{atm}}$	Atmospheric shear stress	3		$\text{N m}^{-2}$
$\tau_n$	Atmospheric shear stress on non-erodible surface	3		$\text{N m}^{-2}$
$\tau_p$	Atmospheric shear stress on saltating bed of snow particles	3		$\text{N m}^{-2}$
$\tau_s$	Atmospheric shear stress on stationary erodible surface	3		$\text{N m}^{-2}$
$\tau_\alpha$	Time constant for albedo	4		s
$\tau_\rho$	Time constant for density	4		s
$\phi$	Snow porosity	2		
$\Phi$	Surface-layer similarity function	3		
$\chi_I$	Exponent for bulk transfer coefficient	3		
$\psi$	Angle between direction of flow and downward vertical	2		rad.
$\Psi_H$	Integrated form of surface-layer similarity function for heat	3		
$\Psi_M$	Integrated form of surface-layer similarity function for momentum	3		
$\Psi_Q$	Integrated form of surface-layer similarity function for water vapor	3		

### Subscripts

Subscript	Description
a	Air or atmosphere
b	Bare ground
i	Ice
<i>i</i>	Phase
<i>j</i>	Phase
<i>k</i>	Constituent
<i>l</i>	Liquid water
s	Snow
sat	Saturated or equilibrium state
v	Vapor

# 3

## Snow–atmosphere energy and mass balance

John C. King, John W. Pomeroy, Donald M. Gray,  
Charles Fierz, Paul M. B. Föhn, Richard J. Harding, Rachel E. Jordan,  
Eric Martin and Christian Plüss

### 3.1 Introduction

*John C. King, John W. Pomeroy, Donald M. Gray, and Charles Fierz*

Climates at the global, the regional, and the local scale determines the relative contributions of radiation, turbulent, and mass fluxes to the corresponding balance at the atmosphere–ground interface. In particular conditions, these fluxes induce the formation of a snowpack on the ground and predominantly effect its accumulation (depth), ablation (melt), sublimation, evaporation, as well as its structure (layering). Presence and transformation of the snow pack change the physical properties of the atmosphere–ground interface, which in turn affects the above fluxes, thereby influencing the properties of the lower atmosphere. For instance, the nearly black body emissivity of snow in the longwave range as well as surface temperature never exceeding 0 °C (273.15 K) promote an often persistent stable atmospheric boundary layer over the snowpack’s surface, even in daytime. In addition, fluxes involved at the snow–atmosphere interface depend much on the ground vegetation, on the snowpack being continuous or patchy, as well as on topography.

These features, along with other particular physical properties of the snowpack such as its high albedo, its capability to store both frozen and liquid water and its low thermal conductivity lead to a strong feedback between the atmosphere and the snowpack, as well as to substantially altered climatic signals over seasonal snowpacks as compared with bare soil.

This chapter first presents general equations for both energy and mass balances (Section 3.2). Detailed discussions of each component of the energy balance follow (Section 3.3), including effects due to either vegetation or topography. Next, the influence of vegetation, blowing snow, as well as topography, on snow

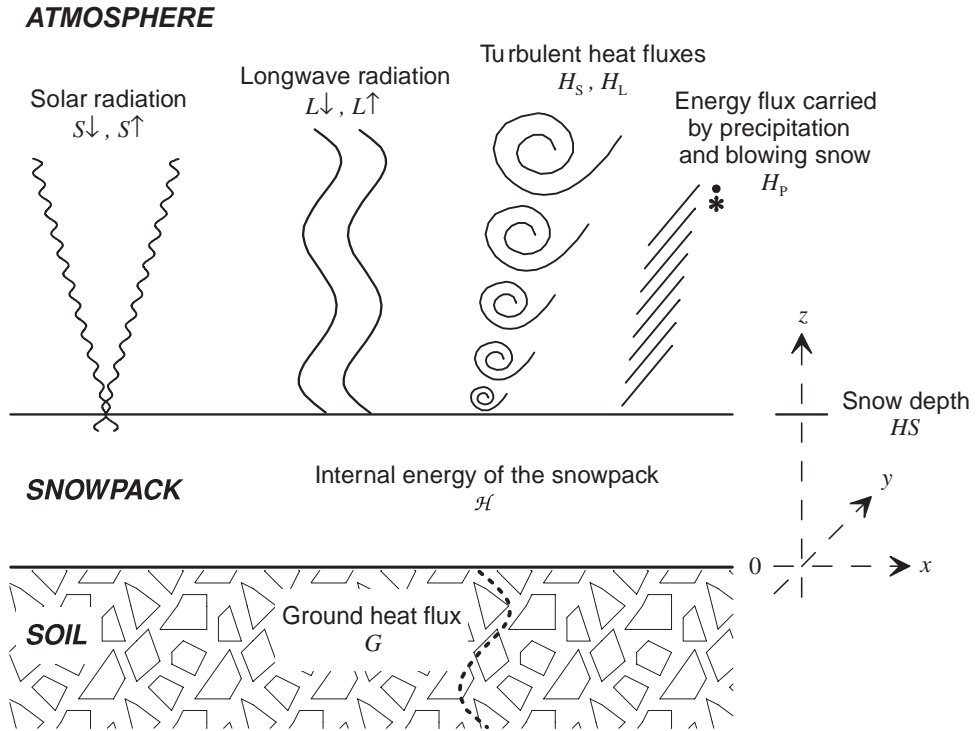


Figure 3.1. Energy balance for an open snowpack.

accumulation is treated (Section 3.4), including some considerations of the coupling of energy and mass balances. Finally, in order to give the reader a sense of the magnitude of the fluxes involved, some examples are presented (Section 3.5), considering either daily averages over typical periods (season) or the processes in detail.

### 3.2 Equations of energy and mass balance

*John C. King, John W. Pomeroy, Donald M. Gray, and Charles Fierz*

Energy balance is often formulated in terms of energy exchanges taking place at an interface (see e.g. Oke, 1987). Such an active surface has to be thought of as being infinitesimally thin and having neither mass nor specific heat. Penetration of shortwave radiation into the snowpack as well as mass movements and phase changes within the snowpack make this concept barely applicable to snow. A better approach is to consider a volume balance of the fluxes as shown in Fig. 3.1. Neglecting horizontal energy transfers as well as effects due to blowing snow or

vegetation, the balance for an open and flat snow cover is given in units of  $\text{W m}^{-2}$  by:<sup>1</sup>

$$-\frac{d\mathcal{H}}{dt} = S\downarrow + S\uparrow + L\downarrow + L\uparrow + H_S + H_L + H_P + G, \quad (3.1)$$

where  $d\mathcal{H}/dt$  is the net change rate of the snowpack's internal energy per unit area.  $S\downarrow$  and  $S\uparrow$  are the downward and reflected components of shortwave radiation respectively,  $L\downarrow$  and  $L\uparrow$  are the downward and upward components of longwave radiation respectively,  $H_S$  and  $H_L$  are the turbulent fluxes of sensible and latent heat through the atmosphere,  $H_P$  is the flux of energy carried as sensible or latent heat by both precipitation and blowing snow. It is generally small, but may become significant in the case of warm rain falling onto and penetrating a cold snowpack. However, it will not be discussed further here. Finally,  $G$  is the ground heat flux.

Since the change of internal energy is related to either warming and melting (positive change, i.e. energy gain) or cooling and freezing (negative change, i.e. energy loss) within the snowpack, it is also given by:

$$-\frac{d\mathcal{H}}{dt} = L_{\ell i}(R_F - R_M) - \int_{z=0}^{HS} \left[ \frac{d}{dt}(\rho_s(z)c_{p,i}T_s(z)) \right] dz, \quad (3.2)$$

where  $R_F$  and  $R_M$  are the freezing and melting rate, respectively,  $L_{\ell i}$  the latent heat of fusion of ice ( $3.34 \times 10^5 \text{ J kg}^{-1}$ ) and  $c_{p,i}$  the specific heat capacity of ice ( $2.1 \times 10^3 \text{ J kg}^{-1} \text{ K}^{-1}$ );  $\rho_s$  is the snow density and  $T_s$  is the snow temperature,<sup>2</sup> both at height  $z$ . The integral is over the snowpack depth  $HS$  and is often referred to as the snowpack's cold content. Freezing and melting rates couple the energy balance through Equation (3.2) to the mass  $\mathcal{M}$  per unit area of the snowpack which, neglecting the mass of air, is given by:

$$\mathcal{M} = \int_z (\theta_i(z)\rho_i(z) + \theta_\ell(z)\rho_\ell(z)) dz, \quad (3.3)$$

where  $\theta_i$  and  $\theta_\ell$  are the volumetric fractions of ice and water taken at height  $z$  with densities  $\rho_i$  and  $\rho_\ell$ , respectively. The mass balance of the snowpack is given in units of  $\text{kg m}^{-2} \text{ s}^{-1}$  by (see Fig. 3.2):

$$\frac{d\mathcal{M}}{dt} = P \pm E - R_{\text{runoff}}, \quad (3.4)$$

where  $d\mathcal{M}/dt$  is the snowpack mass change rate (positive in the case of accumulation);  $P$  is the precipitation rate (accumulation) and  $E = E_{\text{subl}} + E_{\text{evap}}$

<sup>1</sup> Here energy fluxes are the dot product of energy flux densities and the unit normal to the surface. Using the coordinate system shown in Fig. 3.1, energy flux densities directed away from a surface lead to a positive energy flux.

<sup>2</sup> Because  $0^\circ\text{C}$  ( $273.15 \text{ K}$ ) is the melting point of ice, the Celsius scale is the natural choice for describing temperature conditions. However, the absolute Kelvin scale is used in the equations unless stated otherwise.

**ATMOSPHERE**

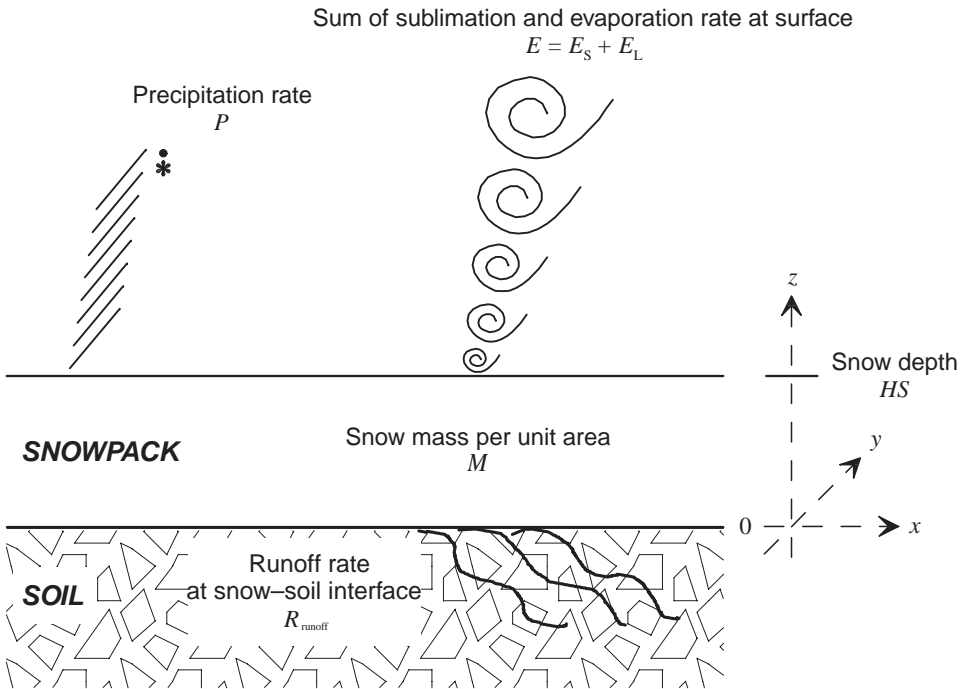


Figure 3.2. Mass balance for an open snowpack.

is the sum of sublimation and evaporation rates at the surface that may contribute either positively or negatively to the mass balance. The runoff rate,  $R_{\text{runoff}}$ , is strongly coupled to the melting rate of so-called isothermal snowpacks ( $T_s = 0^\circ\text{C}$  throughout the snowpack) and contributes to ablation only.

A further coupling of energy and mass balances arises because the latent heat flux is simply related to both sublimation and evaporation rates through:

$$H_L = L_{vi}E_{\text{subl}} + L_{v\ell}E_{\text{evap}} \approx L_{vi}E, \tag{3.5}$$

where  $L_{vi}$  is the latent heat of sublimation for ice ( $2.838 \times 10^6 \text{ J kg}^{-1}$  at  $0^\circ\text{C}$ ) and  $L_{v\ell}$  is the latent heat of evaporation for water ( $2.505 \times 10^6 \text{ J kg}^{-1}$  at  $0^\circ\text{C}$ ).

**3.3 The fluxes involved in the energy balance**

*John C. King, John W. Pomeroy, Donald M. Gray, and Charles Fierz*

In the following sections, these fluxes will be discussed in greater detail and schemes for modeling them will be presented.

### 3.3.1 Shortwave radiation

The starting point for calculating insolation at the surface is the solar radiation flux at the top of the atmosphere,  $S_{\text{toa}}$ , 99.9% of which lies in the spectral band from 0.2 to 100  $\mu\text{m}$ .  $S_{\text{toa}}$  may easily be calculated as a function of geographical location, season, and time (see, e.g., Iqbal, 1983). The part of the solar spectrum up to 4.0  $\mu\text{m}$  is usually called shortwave radiation, representing about 99.2% of  $S_{\text{toa}}$ . However, solar radiation is absorbed by some atmospheric constituents and is reflected and scattered by clouds and aerosol. Accurate calculation of incoming shortwave radiation at the earth's surface,  $S_{\downarrow}$ , from  $S_{\text{toa}}$  thus requires the use of a radiative transfer model, but the data required for driving such models are rarely available in practical snow-cover applications. Incoming shortwave radiation is the most important energy source for snow cover in most situations (see Section 3.5). The net flux of shortwave radiation,  $S_N$ , at the snow surface is given by:

$$S_N = S_{\downarrow} + S_{\uparrow} = S_{\downarrow} (1 - \alpha), \quad (3.6)$$

where  $S_{\uparrow}$  is the reflected shortwave radiation and  $\alpha$  is the albedo, i.e. the spectrally integrated reflectance as discussed in Section 2.5.2. As snow albedo ranges between 0.50 for old, wet snow and 0.95 for new snow, changes in snow albedo lead to substantially different amounts of energy absorbed by the snowpack. Moreover, the interaction between the surface and the atmosphere is substantially altered over seasonal snow covers because albedo is quite different over snow-covered ground as opposed to bare ground.

If measurements of  $S_{\downarrow}$  are not available, it is generally necessary to parameterize this flux in terms of solar zenith angle and easily observed quantities such as total cloud cover. Key *et al.* (1996) discuss and evaluate a number of such parameterizations. Generally,  $S_{\downarrow}$  is calculated first evaluating the insolation under clear sky conditions and then applying a correction for cloud cover. Clouds are reflective; hence, increasing cloud cover tends to *reduce* the magnitude of the downward component of shortwave radiation  $S_{\downarrow}$ . Over high-albedo surfaces, such as snow, it is important to include the effect of multiple reflections between the snow surface and the cloud base in any parameterization used (Shine, 1984; Gardiner, 1987).

A non-negligible part of downward shortwave radiation  $S_{\downarrow}$  reaches the ground as diffuse, nearly isotropic radiation. Its percentage depends primarily on cloudiness and isotropy greatly simplifies its parameterization. As Varley *et al.* (1996) pointed out, many areas in heterogeneous terrain (e.g. alpine topography) receive little or no direct radiation in wintertime, making the separate modeling of direct and diffuse radiation an important issue there. In addition, diffuse radiation reflected from the surrounding topography has to be taken into account (e.g. Dozier, 1980; Plüss, 1997).

### 3.3.2 Longwave radiation

Longwave or terrestrial radiation encompasses wavelengths from approximately 4 to 100  $\mu\text{m}$ . Downward longwave radiation at the surface,  $L\downarrow$ , results from thermal emission from both atmospheric gases (notably water vapor and carbon dioxide) and clouds while upward longwave radiation,  $L\uparrow$ , is thermally emitted from the surface.

While an accurate evaluation of  $L\downarrow$  once again requires the use of a radiative transfer model, the relatively strong absorption of infrared radiation by water vapor means that  $L\downarrow$  is largely determined by conditions in the lowest few hundred meters of the atmosphere (Ohmura, 2001) and, consequently, can be parameterized sufficiently well for many practical applications in terms of near-surface variables. In analogy with the Stefan–Boltzmann equation, parameterizations generally take the form:

$$L\downarrow = -\varepsilon_{\text{eff}} \sigma_{\text{SB}} T_{\text{a}}^4, \quad (3.7)$$

where  $\sigma_{\text{SB}}$  is the Stefan–Boltzmann constant,  $T_{\text{a}}$  is a near-surface air temperature (in K) and  $\varepsilon_{\text{eff}}$  is an “effective” emissivity for the atmosphere.  $\varepsilon_{\text{eff}}$  is usually specified as a function of cloud cover only, cloud cover and near-surface humidity (Konzelmann *et al.*, 1994) or near-surface humidity only under clear sky (Brutsaert, 1975). Clouds are very efficient infrared emitters and have effective emissivities close to unity, while, under clear skies,  $\varepsilon_{\text{eff}}$  is typically around 0.75 but may reach values as low as 0.55 in alpine regions (Marty, 2000). Thus, for fixed  $T_{\text{a}}$ , increasing cloud cover will *increase* the magnitude of the downward component of longwave radiation  $L\downarrow$ . Key *et al.* (1996) as well as König-Langlo and Augstein (1994) give further examples of such parameterizations.

Upward longwave radiation can be calculated from the snow surface temperature,  $T_{\text{o}}$  (in K), and snow infrared emissivity  $\varepsilon$  (see Section 2.5.3) as:

$$L\uparrow = \varepsilon \sigma_{\text{SB}} T_{\text{o}}^4 - (1 - \varepsilon) L\downarrow. \quad (3.8)$$

In the stably stratified conditions that often prevail in the surface boundary layer over snow-covered surfaces,  $T_{\text{o}}$  may be several degrees colder than  $T_{\text{a}}$  and the use of  $T_{\text{a}}$  instead of  $T_{\text{o}}$  in (3.8) may result in a significant overestimate of  $L\uparrow$ . Over a melting snow cover,  $T_{\text{o}}$  may be set to 273.15 K (0 °C). It should be further noted that both downward and upward longwave radiation are usually assumed to be isotropic, resulting in negligible errors only (Plüss, 1997).

To account for longwave radiation in heterogeneous terrain, it is necessary to calculate the incoming fluxes from the sky and the surrounding terrain separately (Plüss and Ohmura, 1997). They showed that in snow-covered environments, where the surface temperature is usually below the air temperature, neglecting the effects

due to air temperature leads to an underestimation of the incoming longwave radiation flux on inclined slopes.

### 3.3.3 Net radiation

In summary, the net radiative flux at the surface is:

$$R_N = S_N + L_N = S\downarrow(1 - \alpha) + (L\downarrow + L\uparrow). \quad (3.9)$$

The value of  $\alpha$  is crucial to the sign of net radiation. Under clear sky, e.g., albedo needs often to be below 0.75 before  $R_N$  becomes negative and hence represents a positive energy gain to the snowpack (see Equation 3.1). However,  $R_N$  is mostly negative under overcast conditions, independent of the value of  $\alpha$ .

Furthermore, as we have seen above, cloud cover has opposite effects on  $S\downarrow$  and  $L\downarrow$ . So it is not immediately clear how an increasing cloud cover will effect net radiation. Over a high-albedo surface such as snow, the increase in magnitude of  $L\downarrow$  with increasing cloud cover can more than outweigh the reduction in net shortwave radiation, leading to an increased energy gain to the snowpack (Ambach, 1974). This situation of positive cloud radiative forcing is most likely to arise in the polar regions, where both surface albedo and cloud transmissivities in the shortwave region are high and the sun is low. However, the effect of cloud radiative forcing depends critically on surface and cloud properties and both positive and negative forcing has been observed over polar snow surfaces (Bintanja and van den Broeke, 1996).

### 3.3.4 Turbulent heat fluxes

Sensible and latent heat may be carried to or from a snow surface by the action of turbulent eddies in the surface boundary layer (Morris, 1989). Formally, these fluxes may be written as the covariance of fluctuations in vertical velocity,  $w$ , with those either in temperature,  $T_a$ , or specific humidity,  $Q$ , i.e.:

$$\begin{aligned} H_S &= \rho_a c_{p,a} \overline{w' T'_a}, \\ H_L &= \rho_a L_{vi} \overline{w' Q'}, \end{aligned} \quad (3.10)$$

where the overbar denotes a mean over time, primes denote deviations from time averaged values,  $\rho_a$  is the air density and  $c_{p,a}$  is the specific heat of air at constant pressure ( $1.01 \times 10^3 \text{ J kg}^{-1} \text{ K}^{-1}$ ). Given suitable fast-response instrumentation, it is possible to measure these covariances and hence obtain direct estimates of the fluxes. However, such measurements are rarely available and in many experimental applications or modeling studies it is necessary to parameterize these fluxes. Most commonly this is done using a bulk transfer formulation, in which fluxes are

expressed in terms of differences between surface variables and the values of those variables at some reference height,  $z_{\text{ref}}$ , in the surface boundary layer, i.e.:

$$\begin{aligned}\tau_o &= \rho_a C_D u^2(z_{\text{ref}}), \\ H_S &= -\rho_a c_{p,a} C_H u(z_{\text{ref}})(T_a(z_{\text{ref}}) - T_o), \\ H_L &= -\rho_a L_{vi} C_Q u(z_{\text{ref}})(Q(z_{\text{ref}}) - Q_o).\end{aligned}\quad (3.11)$$

Here,  $T_a(z_{\text{ref}})$ ,  $Q(z_{\text{ref}})$  and  $u(z_{\text{ref}})$  are the air temperature, specific humidity, and wind speed respectively at the reference height  $z_{\text{ref}}$ , while  $T_o$  and  $Q_o$  are the temperature and specific humidity at the snow surface.  $Q_o$  may be taken as the specific humidity of air saturated with respect to ice at temperature  $T_o$ .  $\tau_o$  is the surface stress and  $C_D$ ,  $C_H$ , and  $C_Q$  are the bulk transfer coefficients for momentum, heat, and water vapor, respectively. In order to calculate fluxes using (3.11), it is necessary to determine these coefficients that, in general, will depend on both surface roughness and atmospheric stability. This is most satisfactorily accomplished through the framework of the Monin–Obukhov surface layer similarity theory (see, e.g. Garratt, 1992, pp. 49–58). This approach also takes into account that the reference height  $\zeta_{\text{ref}} = z_{\text{ref}} - HS$  above a snowpack of depth  $HS$  will change with time as  $HS$  increases or decreases.

The bulk transfer coefficients are related to the integrated forms of the surface layer similarity functions by:

$$\begin{aligned}C_D &= \kappa^2 [\ln(\zeta_{\text{ref}}/z_o) - \Psi_M(\zeta_{\text{ref}}/L_O)]^{-2}, \\ C_H &= \kappa^2 [\ln(\zeta_{\text{ref}}/z_o) - \Psi_M(\zeta_{\text{ref}}/L_O)]^{-1} [\ln(\zeta_{\text{ref}}/z_H) - \Psi_H(\zeta_{\text{ref}}/L_O)]^{-1}, \\ C_Q &= \kappa^2 [\ln(\zeta_{\text{ref}}/z_o) - \Psi_M(\zeta_{\text{ref}}/L_O)]^{-1} [\ln(\zeta_{\text{ref}}/z_Q) - \Psi_Q(\zeta_{\text{ref}}/L_O)]^{-1},\end{aligned}\quad (3.12)$$

where  $\kappa$  is von Kármán's constant (generally taken to be around 0.4),  $z_o$ ,  $z_H$ , and  $z_Q$  are the roughness lengths for momentum, heat, and water vapor respectively and  $\Psi_M$ ,  $\Psi_H$ ,  $\Psi_Q$  are the corresponding integrated forms of the surface layer similarity functions  $\Phi_\xi$ :

$$\Psi_\xi = \int_{\zeta_0}^{\zeta_{\text{ref}}} (1 - \Phi_\xi(\zeta'/L_O)) d(\ln \zeta'); \quad \xi = M, H, Q; \quad \zeta_0 = z_o, z_H, z_Q.\quad (3.13)$$

The surface layer similarity functions express how profiles of wind speed, temperature and humidity deviate from the logarithmic forms that are observed under neutral conditions ( $\zeta_{\text{ref}}/L_O = 0$ ) as a result of stability effects. These functions depend solely on the dimensionless height  $\zeta_{\text{ref}}/L_O$ , where  $L_O$  is the Obukhov length defined as:

$$L_O = -\frac{u_*^3 T_{\text{mean}} \rho_a c_{p,a}}{\kappa g H_S}\quad (3.14)$$

and

$$u_*^2 = \frac{\tau_o}{\rho_a}, \quad (3.15)$$

where  $u_*$  is the friction velocity,  $T_{\text{mean}}$  is the mean air temperature in the layer of depth  $\zeta_{\text{ref}}$ , and  $g$  is the acceleration due to gravity. Note the negative sign on the right-hand side of Equation (3.14), which results from the chosen sign convention (see Stull, 1988). Since  $L_O$  is a function of the fluxes to be calculated, the equation set (3.11, 3.12 and 3.14) must generally be solved iteratively. However, as shown below, if some simplifying assumptions are made concerning the form of the  $\Psi$ -functions, a direct solution is possible under some circumstances.

Experimental studies have determined the forms of the similarity functions in (3.12) even though little has been based on measurements over snow covers (Morris, 1989). Under stable conditions, where the sensible heat flux is directed towards the surface ( $H_S < 0$ ), it is found that, for  $0 \leq \zeta_{\text{ref}}/L_O \leq 1$ :

$$\begin{aligned} \Psi_M &= \beta_{1M} \zeta_{\text{ref}}/L_O, \\ \Psi_H &= \Psi_Q = \beta_{1H} \zeta_{\text{ref}}/L_O, \end{aligned} \quad (3.16)$$

while for unstable conditions ( $H_S > 0$ ), for  $-5 \leq \zeta_{\text{ref}}/L_O \leq 0$ :

$$\begin{aligned} \Psi_M &= 2 \ln[(1 + x_M)/2] + \ln[(1 + x_{M^2})/2] - 2 \tan^{-1} x_M + \pi/2, \\ \Psi_H &= \Psi_Q = 2 \ln[(1 + y_H)/2], \end{aligned} \quad (3.17)$$

where:

$$\begin{aligned} x_M &= (1 + \gamma_1 \zeta_{\text{ref}}/L_O)^{1/4}, \\ y_H &= (1 + \gamma_2 \zeta_{\text{ref}}/L_O)^{1/2}. \end{aligned} \quad (3.18)$$

Measurements indicate  $\beta_{1M} \approx \beta_{1H} \approx 5$  and  $\gamma_1 \approx \gamma_2 \approx 16$ , but there is a considerable range in experimentally determined values (see Garratt 1992, appendix 4).

In what follows, we shall concentrate on stable conditions, since this regime tends to prevail over snow covers. In winter, particularly in high latitudes,  $R_N$  is positive for much of the time, leading to a downward heat flux, while advection of warm air over a melting snow cover also leads to the establishment of stable stratification since  $T_o$  cannot rise above  $0^\circ\text{C}$ . If we simplify (3.16) by assuming  $\beta_{1M} = \beta_{1H} = \beta_1$ , manipulation of (3.12) and (3.14) yields an explicit expression for the transfer coefficients in terms of the bulk Richardson number (Garratt, 1992):

$$Ri_B = gz(T_a(z_{\text{ref}}) - T_o)/(T_{\text{mean}} u(z_{\text{ref}})^2), \quad (3.19)$$

where  $Ri_B \geq 0$  for stable conditions and  $T_{\text{mean}}$  is the mean temperature in the layer of depth  $\zeta_{\text{ref}} = z_{\text{ref}} - (HS + z_o)$ .

For  $0 \leq Ri_B < \beta_1^{-1}$ :

$$\begin{aligned} C_D &= \kappa^2 [\ln(\zeta_{\text{ref}}/z_o)]^{-2} (1 - \beta_1 Ri_B)^2 = C_{DN} f(Ri_B), \\ C_H &= \kappa^2 [\ln(\zeta_{\text{ref}}/z_o) \ln(\zeta_{\text{ref}}/z_H)]^{-1} (1 - \beta_1 Ri_B)^2 = C_{HN} f(Ri_B), \\ C_Q &= \kappa^2 [\ln(\zeta_{\text{ref}}/z_o) \ln(\zeta_{\text{ref}}/z_Q)]^{-1} (1 - \beta_1 Ri_B)^2 = C_{QN} f(Ri_B), \end{aligned} \quad (3.20)$$

and for  $Ri_B \geq \beta_1^{-1}$ :

$$C_D = C_H = C_Q = 0. \quad (3.21)$$

In practice, there may be problems with using (3.20) and (3.21) as presented above. In runs of coupled surface boundary layers – snow-cover models that parameterize turbulent fluxes using (3.20) and (3.21), it has been found that, when strong radiative cooling is imposed, snow surface temperatures can drop to the point where  $Ri_B = \beta_1^{-1}$ , at which point the fluxes are “switched off” and the snow surface becomes effectively decoupled from the atmosphere. This leads to further rapid (and unrealistic) cooling as the surface temperature evolves towards a pure radiative equilibrium (e.g. Morris *et al.*, 1994). Measurements (e.g. King, 1990) show that small but non-zero heat fluxes persist even when  $Ri_B \geq \beta_1^{-1}$  and this effect should be incorporated into any heat flux parameterization used in snow models. Theoretical understanding of turbulent transport in this high-stability regime is still developing but a number of practical alternative schemes to (3.20) and (3.21) have been proposed to avoid the problem of decoupling (Beljaars and Holtslag, 1991; King and Connolley, 1997).

The ratio of  $H_S/H_L$  is known as the Bowen ratio,  $B$ . Over snow surfaces, the air is often close to saturation, so  $Q(z)$  may be related to  $T_a(z)$  through the Clausius–Clapeyron equation. It can be demonstrated (Andreas, 1989) that, if supersaturation is forbidden and if both  $H_S$  and  $H_L$  are directed downwards,  $B$  is limited by:

$$B \geq B_* = \frac{\rho_a c_{p,a}}{L_{vi}(\partial \rho_{v,\text{sat}}/\partial T)} \Big|_{T=T_o}, \quad (3.22)$$

where  $\rho_{v,\text{sat}}$  is the saturation water vapor density. Andreas and Cash (1996) have extended this result to other combinations of  $H_S$  and  $H_L$  and have deduced general formulations for  $B$  over saturated surfaces. Such relationships can be of value if estimates of  $H_L$  are required but no humidity measurements are available.

In order to calculate the turbulent fluxes, it is necessary to know the appropriate roughness lengths for momentum, heat and water vapor. The momentum (or aerodynamic) roughness length,  $z_o$ , is related to the geometric roughness characteristics of the snow surface. Snow cover is one of the smoothest land surface types encountered in nature and, consequently, measurements of  $z_o$  over snow (Table 3.1) indicate small values, of the order  $10^{-4}$  to  $10^{-3}$  m. Usually,  $z_Q$  and  $z_H$  are assumed to be one

Table 3.1 Aerodynamic roughness lengths measured over various snow and ice surfaces.

Surface	Roughness length $z_o(m)$	Location	Reference
Seasonal snow cover	$2.3 \times 10^{-4}$	Finse	Kondo and Yamazawa (1986)
	$2.0 \times 10^{-4}$ to $4.0 \times 10^{-3}$		Harding (1986)
	$2.0 \times 10^{-4}$ to $2.0 \times 10^{-2}$	Spitsbergen	Konstantinov (1966)
	$2.5 \times 10^{-3}$		Sverdrup (1936)
Antarctic ice shelves	$5.6 \times 10^{-5}$		King and Anderson (1994)
	$1.0 \times 10^{-4}$		Heinemann (1989)
	$1.0 \times 10^{-4}$		König (1985)
Antarctic blue ice	$2.8 \times 10^{-6}$		Bintanja and van den Broeke (1995)
Sea ice	3 to $5 \times 10^{-4}$		Joffe (1982)
Subantarctic glacier		Snow-covered	Poggi (1976)
		Fresh snow	van den Broeke (1997)
		Accumulation zone	van den Broeke (1997)
		Ablation zone	Grainger and Lister (1966)
		Sastrugi	Grainger and Lister (1966)
Icelandic glacier		Undulating wet snow	Grainger and Lister (1966)
	$2 \times 10^{-3}$ to $1 \times 10^{-1}$	Ablation zone	Smeets <i>et al.</i> (1998)

order of magnitude smaller, as suggested by Garrat (1992) and Morris (1989). With values this small, it is clear that roughness elements of the scale of individual snow grains must be making the greatest contribution to the surface drag, with larger micro-topographic features, such as sastrugi, making a lesser contribution (Kondo and Yamazawa, 1986; Inoue, 1989). Ablating glaciers can develop large roughness elements on their surfaces, leading to aerodynamic roughness lengths of up to 0.1 m. The roughness of such surfaces can change rapidly as surface features develop during the ablation season (Smeets *et al.*, 1998). Bare ice surfaces have particularly small roughness lengths (Bintanja and van den Broeke, 1995; see Table 3.1). Flow over such surfaces is “aerodynamically smooth,” i.e. the surface Reynolds number:

$$Re = \frac{u_* z_*}{\mu_a}, \quad (3.23)$$

where  $\mu_a$  is the kinematic viscosity of air and  $z_*$ , the scale of the roughness elements, is less than about 5. In this low Reynolds number regime, flow around individual roughness elements is laminar and the roughness length is given by:

$$z_o = 0.135 \frac{\mu_a}{u_*}. \quad (3.24)$$

If the surface stress is great enough to generate blowing snow (see Section 3.4), suspended snow grains may contribute to the momentum transfer from atmosphere to surface and may thus cause an apparent change in  $z_o$ . Owen (1964), Tabler (1980), Chamberlain (1983), and others have suggested that, under these conditions, the apparent roughness length is increased by drag exerted on saltating snow and will therefore be proportional to the surface stress, i.e.

$$z_o = c_1 \frac{u_*^2}{2g}. \quad (3.25)$$

Experimental evidence for such a relationship is variable. Tabler (1980), Tabler and Schmidt (1986) as well as Pomeroy and Gray (1990) present extensive quantitative measurements that support such behavior with values of  $c_1$  of 0.1203 over continuous snowfields (Pomeroy and Gray, 1990) and  $c_1$  of 0.02648 over a mixture of snow and lake ice (Tabler, 1980).

Bintanja and van den Broeke (1995), however, suggest that, in some cases, the alteration of surface characteristics by the transport of fresh snow onto a smoother underlying snow or ice surface may be the dominant process leading to an apparent increase in  $z_o$  with wind speed. More observations are needed to resolve this issue.

Fewer measurements exist for the scalar roughness lengths,  $z_H$  and  $z_Q$ , largely because of the difficulty of defining  $T_o$  and  $Q_o$  other than over a melting snow

surface, when  $T_0$  may be taken as  $0^\circ\text{C}$ . Heat and water vapor transfer at the snow surface must ultimately be accomplished purely by molecular diffusion, since there is no equivalent to the form drag of roughness elements that is responsible for the majority of the momentum transport. Andreas (1989) developed a theory that predicts the ratio of  $z_0$  to the scalar roughness lengths as a function of the surface Reynolds number (see Equation 3.23). In the aerodynamically smooth regime,  $z_H/z_0 = 3.49$  and  $z_Q/z_0 = 5.00$ . As  $Re$  increases, the ratio of scalar roughness length to momentum roughness length decreases rapidly and, for moderate wind speeds over a typical snow cover, the scalar roughness lengths will be one or two orders of magnitude smaller than  $z_0$ . Measurements (Kondo and Yamazawa, 1986; Bintanja and van den Broeke, 1995) generally support this functional dependence. However, in many modeling applications, the scalar roughness lengths are set equal to  $z_0$  for simplicity, on the grounds that the ensuing errors in surface fluxes will be no greater than the uncertainties resulting from other parts of the flux computation procedure.

### 3.3.5 Heat fluxes over a non-uniform snow cover

The results of Section 3.3.4 are strictly applicable only over an extensive and uniform snow cover, where the atmospheric conditions at the reference height used for the flux computation are in equilibrium with the underlying surface. This will not, in general, be the case over a patchy snow cover. Areas of bare ground will have different roughness and albedo characteristics from snow-covered areas. Advection of air warmed over bare ground onto a snow-covered area will lead to an enhanced downward heat flux at the upwind edge of the snow patch, with heat fluxes decreasing with increased fetch over the snow as the air comes into a new equilibrium with the snow surface. For instance, Weisman (1977) showed that the dimensionless sensible heat flux  $H'_S$  at any point downwind of the leading edge of a snow patch varies with snow-covered fetch distance as

$$H'_S = -a_4 X^{-0.125}, \quad (3.26)$$

where  $X$  is a dimensionless distance downwind of the leading edge of the snow patch (influenced by roughness length) and  $a_4$  is controlled by a temperature difference stability parameter (Weisman, 1977).

Marsh and Pomeroy (1996) proposed that the additional sensible heat advected to a snow patch is a function of the snow-free fraction of the upwind domain,

$$H_S - H_{S,s} = (-H_{S,b}(1 - \text{SCA})/\text{SCA}) h_{S,b}, \quad (3.27)$$

where  $H_{S,s}$  is the sensible heat flux to snow over a completely snow-covered fetch,  $H_{S,b}$  is sensible heat over bare ground, SCA is the proportion of snow-covered area

and  $h_{s,b}$  expresses the portion of bare ground sensible heat that is advected to the snow patch. Neumann and Marsh (1998) showed that  $h_{s,b}$  declines from 0.3 to 0.001 as SCA decreases from 1 to 0.01 and that for SCA of 0.5,  $h_{s,b}$  ranges from 0.02 to 0.2 depending on wind speed and snow patch size. Even more extreme effects may occur over a sea-ice cover interspersed with leads of open water (Claussen, 1991). Interactions with the vegetation will also affect the heat fluxes. They will be discussed in more detail in Sections 3.5.4 and 3.5.5.

The computation of surface fluxes over such non-uniform surfaces is very important for climate simulation (see Section 4.3) and it is a developing subject that requires the application of numerical or analytic models of varying degrees of complexity. A detailed description of such techniques is beyond the scope of the present work and the reader is referred to Weisman (1977), Liston (1995), Essery (1997), and Marsh *et al.* (1997) for further information.

To conclude, few authors have investigated the variation of the turbulent fluxes in heterogeneous terrain although it was termed a priority research topic by Garratt (1992). Based on such an investigation, a simplified approach is presented in Plüss (1997).

### 3.4 Snow accumulation

*John C. King, John W. Pomeroy, Donald M. Gray, and Charles Fierz*

The surface mass balance described in Equation (3.4) is affected by distinctive snow accumulation fluxes that are influenced by the air mass characteristics, surface snow conditions, vegetation, and topography. Interception and unloading must be considered in forested environments where evergreen canopies intercept substantial portions of snowfall. Blowing snow fluxes are significant in exposed, poorly vegetated regions such as alpine terrain, steppes, prairies, tundra, and ice sheets.

#### 3.4.1 Interception by vegetation

Vegetation intercepts snow as a function of its winter leaf and stem area and the size of the snowfall event. Because sublimation and melt remove snow from canopies, interception (the snowfall trapped in the canopy, normally event-based) is distinguished from snow load (the snow held in the canopy at a particular time). Hedstrom and Pomeroy (1998) developed and field tested a model of snow interception and snow unloading of the following form (see Fig. 3.3):

$$I = I_1 e^{-U_1 t}, \quad I_1 = (\mathcal{L}_L^* - \mathcal{L}_{L,o}) (1 - e^{c_{\text{can}} \mathcal{P} / \mathcal{L}_L^*}), \quad (3.28)$$

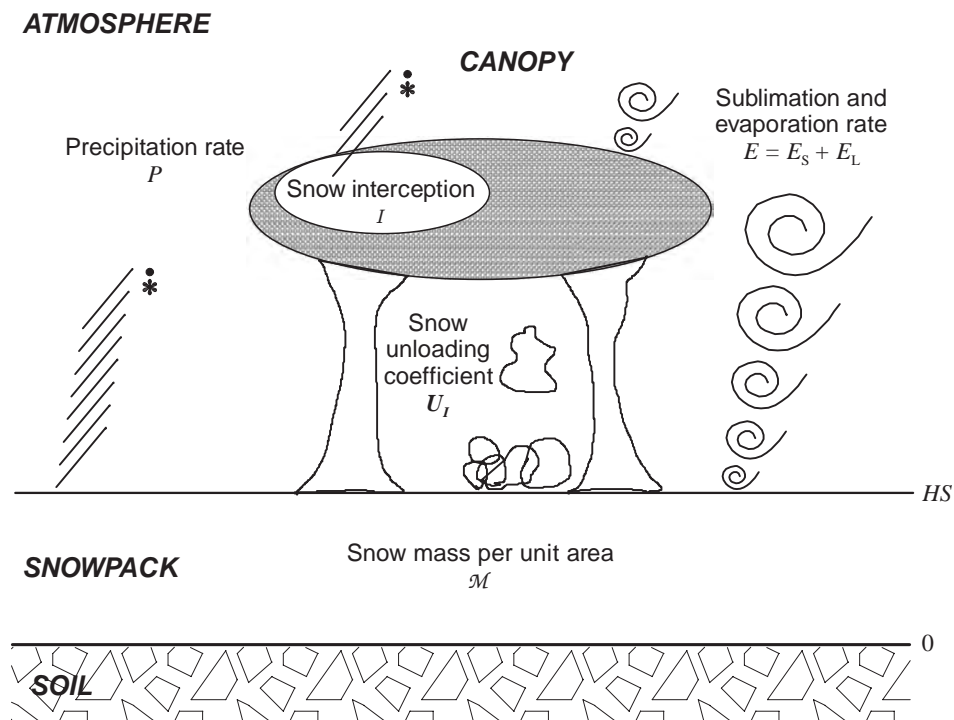


Figure 3.3. Interception and unloading by vegetation.

where  $I$  is snow interception after unloading has occurred ( $\text{kg m}^{-2}$ ),  $I_1$  is interception at the start of unloading,  $U_I$  is a snow unloading coefficient,  $t$  is time (s),  $\mathcal{L}_L^*$  is the maximum canopy snow load,  $\mathcal{L}_{L,0}$  is the initial snow load,  $\mathcal{P}$  is the accumulated snowfall ( $\text{kg m}^{-2}$ ) and  $c_{\text{can}}$  is the canopy closure.

In a southern boreal forest, Hedstrom and Pomeroy (1998) found that  $e^{-U_I t} = 0.678$  using empirical data with a weekly time resolution.  $\mathcal{L}_L^*$  can be determined using an empirical relationship developed by Schmidt and Gluns (1991), where:

$$\mathcal{L}_L^* = \mathcal{L}_{L,b} \left( 0.27 + \frac{46}{\rho_s} \right) LAI \quad (3.29)$$

and  $\mathcal{L}_{L,b}$  is the maximum snow load per unit area of branch ( $\text{kg m}^{-2}$ ),  $\rho_s$  is the density of fresh snow ( $\text{kg m}^{-3}$ ) and  $LAI$  is winter leaf and stem area index ( $\text{m}^2 \text{m}^{-2}$ ).  $\mathcal{L}_{L,b}$  ranges from  $5.9 \text{ kg m}^{-2}$  for spruce to  $6.6 \text{ kg m}^{-2}$  for pine. Equation (3.28) is an extension of the expression proposed by Calder (1990), which is based on formulations used for the interception of rainfall. Important differences from earlier formulations are the consideration of canopy snow load in reducing interception efficiency and the substantially high maximum canopy snow loads that are found,

compared to maximum rainfall interception. Interception efficiency ( $I/P$ ) varies from small values up to 0.6 for dense conifer canopies and declines with increasing storm snowfall amounts and initial canopy snow loads.

Snow in the canopy represents a “snow surface” with very different characteristics from snow on the ground (Harding and Pomeroy, 1996). For instance, it is relatively well-exposed to the atmosphere and subject to high net radiation because snow-filled canopies retain their low snow-free albedo (Pomeroy and Dion, 1996; Yamazaki *et al.*, 1996), are aerodynamically rough (Lundberg *et al.*, 1998), and are usually associated with slightly unstable surface boundary layers (Nakai *et al.*, 1999). The varying snow load and degree of its exposure in the canopy means that snow-filled canopies do not behave as a continuous, saturated surface; this affects the free availability of moisture in the canopy. Nakai *et al.* (1999) accounted for this effect by varying the ratio of bulk transfer coefficients  $C_Q/C_H$  (see Equation 3.12) from 0.1 for the low moisture case (low snow load) to 1.0 for the high moisture case (high snow load). Lundberg *et al.* (1998) used a Penman–Monteith combination model with a resistance parameterization to estimate sublimation from snow-covered canopies, and found that the resistance of a snow-covered canopy had to be set at 10 times that of a rain-covered canopy to provide results that matched measurements. Parviainen and Pomeroy (2000) use a coupled calculation scheme where turbulent transfer from snow clumps is calculated (presuming no evaporation from the snow-free canopy) to provide a within-canopy humidity and temperature field that is then matched with the bulk transfer formulation for the whole canopy as shown in Equation (3.11). Both sensible and latent heat transfer from snow clumps are calculated from variants of Equation (3.11) where the terms  $C_H$  and  $C_Q$  are replaced with  $C_{hq}$  and  $u(z)$  is replaced with the Sherwood and Nusselt numbers for turbulent transfer of heat and water vapor from particles respectively and solved with the assumption that sublimating snow clumps are in thermodynamic equilibrium at the ice-bulb surface temperature (Schmidt, 1991).  $C_{hq}$  is then found as:

$$C_{hq} = \frac{3\mathcal{L}_L k_{cl}}{2r_{pt,n}^2 \rho_i} \left( \frac{\mathcal{L}_L}{\mathcal{L}_L^*} \right)^{-\chi_1}, \quad (3.30)$$

where  $\mathcal{L}_L$  is snow load (equal to initial interception,  $I_1$ , less any sublimation and unloading),  $k_{cl}$  is a dimensionless snow clump shape coefficient,  $r_{pt,n}$  is a nominal snow particle radius (0.0005 m),  $\rho_i$  is the density of ice ( $\text{kg m}^{-3}$ ), and  $\chi_1$  is 1.0 less the fractal dimension of intercepted snow (Pomeroy and Schmidt, 1993). Pomeroy *et al.* (1998a) found  $\chi_1$  is normally 0.4 for mature evergreens and Parviainen and Pomeroy (2000) report empirically derived values of  $k_{cl}$  (given the nominal  $r_{pt,n}$ ) of 0.0114 for a mature conifer forest and 0.0105 for a young conifer plantation in western Canada.

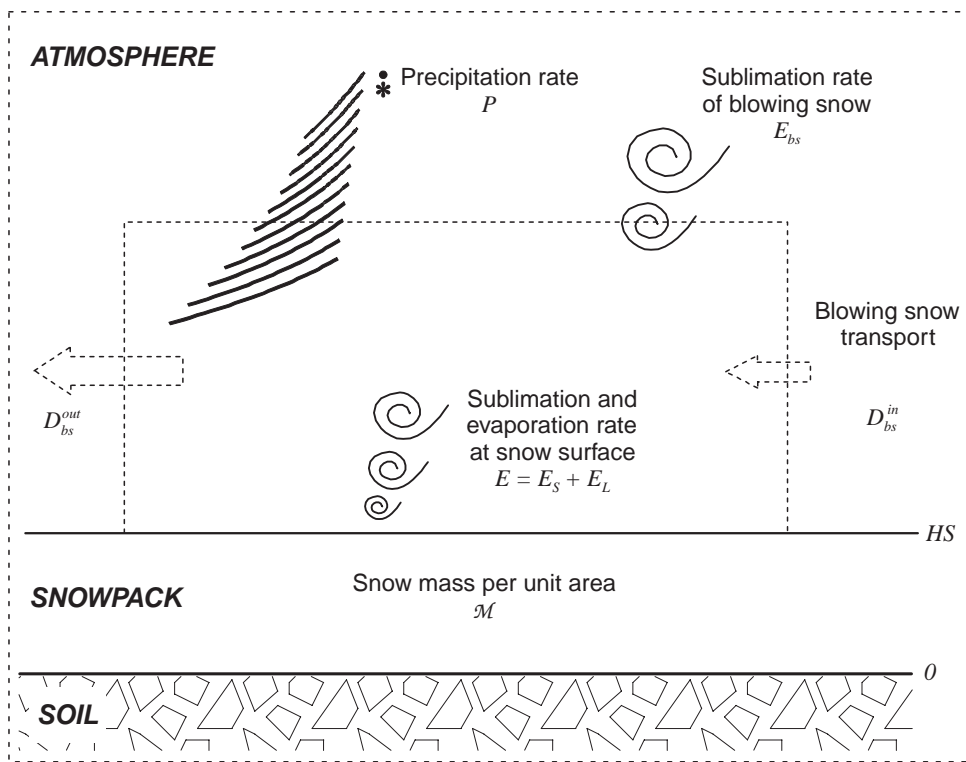


Figure 3.4. Mass balance with blowing snow.

Experimentally derived sublimation rates from mature evergreen forests range from 3 to about  $12 \text{ kg m}^{-2} \text{ d}^{-1}$  (Pomeroy *et al.*, 1998a; Nakai *et al.*, 1999) and can return 13–40% of seasonal snowfall to the atmosphere as sublimation from northern forests (Pomeroy and Gray, 1995; Pomeroy *et al.*, 1998a).

### 3.4.2 Blowing snow

Blowing snow fluxes occur over open snow surfaces with good exposure to wind and a supply of erodible snow (see Fig. 3.4). On large, relatively uniform surfaces such as ice sheets steady-state conditions may develop. However, on seasonal snow surfaces, exposed vegetation and larger scale topographic features disrupt steady-state conditions. At small scales (e.g. grass stalks, boulders) the features act as an additional surface roughness, and impede erosion or sometimes induce small depositions of wind-blown snow. At large scales (e.g. woodlands, valleys, mountain crests) the features can cause flow separation in the boundary layer and significantly reduce the shear stress on downwind surfaces, which may lead to the formation of large snowdrifts. The result is a strong heterogeneity to blowing snow fluxes

and a need to consider the landscape in calculating these fluxes. One important aspect of blowing snow is that it can dramatically increase latent heat transfer to the atmosphere via sublimation and that blowing snow transport and sublimation can control the mass balance of non-melting snow covers in open areas. Including blowing snow in the mass balance, Equation (3.4) may be rewritten as:

$$\frac{d\mathcal{M}}{dt} = P - \nabla \cdot D_{\text{bs}} - E_{\text{bs}} \pm E - R_{\text{runoff}}, \quad (3.31)$$

where  $D_{\text{bs}}$  is the horizontal blowing snow transport (with dimensions of mass per unit length per unit time) and  $E_{\text{bs}}$  is the rate of sublimation of blowing snow. Horizontal inhomogeneities in either the surface wind field or surface characteristics can generate corresponding inhomogeneities in snow transport leading to a divergence of  $D_{\text{bs}}$  and a redistribution of surface snow.

Blowing snow transport,  $D_{\text{bs}}$ , primarily occurs in two modes: saltation,  $D_{\text{salt}}$  and suspension,  $D_{\text{susp}}$ , thus:

$$D_{\text{bs}} = D_{\text{salt}} + D_{\text{susp}}. \quad (3.32)$$

Saltation is the mechanism by which snow particles are eroded from or deposited onto the snow surface and transported near to the surface. The process involves particles bouncing downstream and shattering new particles from the snow surface. Suspension occurs above the saltation layer and involves smaller particles lofted by turbulence to heights several tens of meters above the snow surface. At very low wind speeds saltation is the primary mode of transport, while at higher wind speeds suspension becomes predominant.

Steady-state saltation is generally considered to operate in a dynamic balance with atmospheric driving forces, where the atmospheric shear stress,  $\tau_{\text{atm}}$ , is partitioned into that applied to the non-erodible surface,  $\tau_{\text{n}}$ , that applied to the stationary erodible surface,  $\tau_{\text{s}}$ , and that applied to the saltating bed of snow particles,  $\tau_{\text{p}}$ . Thus:

$$\tau_{\text{atm}} = \tau_{\text{n}} + \tau_{\text{s}} + \tau_{\text{p}}. \quad (3.33)$$

Most blowing snow models (Pomeroy *et al.*, 1993; Pomeroy and Gray, 1995; Bintanja, 1998; Dery *et al.*, 1998; Liston and Sturm, 1998; Essery *et al.*, 1999; Pomeroy and Li, 2000) use a solution for the saltating mass flux,  $D_{\text{salt}}$ , derived and field-tested by Pomeroy and Gray (1990) where:

$$D_{\text{salt}} = \frac{a_5 u_{*t} \rho_a}{u_* g} (u_*^2 - u_{*n}^2 - u_{*t}^2) \quad (3.34)$$

and  $a_5$  is an experimentally determined ‘‘saltation efficiency’’ coefficient ( $0.68 \text{ m s}^{-1}$ ),  $u_*$  is the friction velocity,  $u_{*t}$  is the threshold friction velocity (that at the initiation or cessation of saltation),  $u_{*n}$  is the friction velocity applied to small-scale non-erodible elements. Li and Pomeroy (1997a) outline operational

techniques to calculate the threshold friction velocity from the meteorological history of the snowpack, while Pomeroy and Li (2000) discuss the influence of vegetation on  $u_{*n}$ . Doorschot (2002) and Doorschot and Lehning (2002) address the relative importance of aerodynamic entrainment compared to rebound and ejection during steady-state saltation, a topic which is still not fully resolved.

Suspended blowing snow particles are presumed to move downwind with the same speed as fluid points in the atmosphere, but are not lifted as effectively due to inertia and a significant terminal fall velocity. The downwind mass flux of suspended snow,  $D_{\text{susp}}$ , may be described as,

$$D_{\text{susp}} = \frac{u_*}{\kappa} \int_{h_*}^{z_b} c_{\text{susp}}(\zeta) \ln(\zeta/z_o) d\zeta, \quad (3.35)$$

where  $\kappa$  is von Kármán's constant,  $h_*$  is the lower boundary for suspended snow (upper boundary for saltating snow),  $z_b$  is the upper boundary for suspended snow,  $c_{\text{susp}}(\zeta)$  is the mass concentration of suspended snow at height  $\zeta = z - HS$  above the snow surface and  $z_o$  is the aerodynamic roughness length. Presuming steady-state, one-dimensional diffusion and in analogy to Fick's law, the instantaneous mass concentration may be found as

$$(w c_{\text{susp}})' = -\kappa_s(\zeta) \frac{\partial c_{\text{susp}}}{\partial \zeta}, \quad (3.36)$$

where  $w$  is the vertical particle velocity at height  $\zeta$  and  $\kappa_s(\zeta)$  is the turbulent diffusion coefficient for snow particles at height  $\zeta$ . For steady-state, non-advective conditions, this formulation can be solved to find a mass concentration profile as:

$$c_{\text{susp}}(\zeta + d\zeta) = c_{\text{susp}}(\zeta) \left( \frac{\zeta + d\zeta}{\zeta} \right)^{w_*(\zeta)}, \quad (3.37)$$

where  $w_*$  is a dimensionless vertical velocity. Pomeroy and Male (1992) experimentally derived expressions for  $h_*$  and  $w_*$ . Kind (1992) proposed an improved theoretical solution for  $c_{\text{susp}}(\zeta)$  assuming steady-state turbulent diffusion. This solution has been used in the Liston and Sturm (1998) model. Dery *et al.* (1998) considered non-steady-state diffusion formulations involving explicit calculation over the particle size spectrum, and the effects of sublimation in setting the upper boundary,  $z_b$ . Unfortunately, measurements that can describe the individual behaviors of  $\kappa_s$  and  $w$  are lacking, and hence there is considerable uncertainty in derivations of  $w_*$ .

Determination of the amount of sublimation during blowing snow is based on the work of Thorpe and Mason (1966) with modifications by Schmidt (1972) and Pomeroy (1989). The sublimation rate within a column of blowing snow,  $E_{\text{bs}}$ , is calculated with reference to the sublimation rate  $dm_p/dt$  of a single blowing snow

particle of mass  $m_p$ , the variation in mass concentration with height,  $c_{\text{susp}}(r_{\text{pt}}, z)$ , and the change in particle radius,  $r_{\text{pt}}(m_p)$ , as

$$E_{\text{bs}} = \int_0^{z_b} \int \frac{1}{m_p(r_{\text{pt}}, z)} \frac{dm_p}{dt} c_{\text{susp}}(r_{\text{pt}}, z) dz dr_{\text{pt}}. \quad (3.38)$$

The sublimation rate of a single blowing snow particle is,

$$\frac{dm_p}{dt} = 2r_{\text{pt}} D_a Sh (\rho_{v,a} - \rho_{v,\text{pt}}), \quad (3.39)$$

which is balanced by the convective heat transferred to the particle,

$$L_{\text{vi}} \left( \frac{dm_p}{dt} \right) = -2\pi r_{\text{pt}} k_a Nu (T_a - T_{o,\text{sp}}), \quad (3.40)$$

where  $D_a$  is the diffusion coefficient of water vapor in air ( $\text{m}^2 \text{s}^{-1}$ ),  $Sh$  is the Sherwood number,  $\rho_{v,a}$  is the water vapor density in ambient air and  $\rho_{v,\text{pt}}$  is that at the particle surface and  $k_a$  is the thermal conductivity of air ( $\text{W m}^{-1} \text{K}^{-1}$ ),  $Nu$  is the Nusselt number,  $T_{o,\text{sp}}$  is the ice sphere surface temperature (K) and  $T_a$  is the ambient air temperature (K). Lee (1975) found that both the Nusselt and Sherwood numbers can be related to the particle Reynolds number,  $N_{\text{Re}}$ , as

$$Nu = Sh = 1.79 + 0.606 N_{\text{Re}}^{0.5}. \quad (3.41)$$

Presuming that blowing snow particles are in thermodynamic equilibrium, Schmidt (1972) combined Equations (3.39) and (3.40) using the Clausius–Clapeyron equation to solve for  $dm/dt$ . The combined equation can be found in several later publications (Schmidt, 1991; Pomeroy *et al.*, 1993; Dery *et al.*, 1998).

One problem in applying sublimation equations is the difficulty in determining the fields of air temperature and humidity in the lowest meter of the atmosphere where the mass concentration of blowing snow is greatest. Thermodynamic models such as that of Dery *et al.* (1998) suggest that the atmosphere cools and approaches saturation near the snow surface during blowing snow. Measurements of these fields in extremely stable surface boundary layers over ice shelves support cold, humid conditions in this layer (King *et al.*, 1996); however, measurements above terrestrial snow surfaces during blowing snow often show a notable undersaturation of water vapor with respect to ice (Pomeroy and Li, 2000). Pomeroy and Essery (1999) measured sublimation fluxes during light blowing snow of up to  $60 \text{ W m}^{-2}$ ; these fluxes were far larger than those predicted from simple surface sublimation (approx  $10 \text{ W m}^{-2}$ ) and were well matched by the model predictions using the Prairie Blowing Snow Model driven by surface observations (Pomeroy and Li, 2000).

Attempts to scale up the calculations of blowing snow fluxes to heterogeneous terrain have been made by Pomeroy *et al.* (1993, 1997), Gauer (1998), Liston and Sturm (1998), Essery *et al.* (1999), Lehning *et al.* (2004), Bowling *et al.* (2004), and Essery and Pomeroy (2004). In all cases considerable difficulties are encountered in these attempts because of the development of non-steady-state conditions and flow convergence and divergence within the surface boundary layer over complex terrain. Typical small-scale features such as flow separation, recirculation and speed-up effects are indeed the driving mechanisms behind inhomogeneous snow distribution. For the simple case of scaling up blowing snow fluxes over heterogeneous snow covers on level, uniform terrain (Li and Pomeroy, 1997b; Pomeroy and Li, 2000), a cumulative normal probability distribution is used to weight fluxes by the probability of a blowing snow occurrence,  $P_{bs}$ . The formulation is based on an observed association between the probability of occurrence of blowing snow, the average hourly 10 m wind speed,  $u_{10}$ , average hourly air temperature,  $T_a$ , in °C and snow surface age,  $t_h$ , in hours where:

$$P_{bs}(u_{10}, T_a, t_h) = \frac{1}{\sqrt{2\pi}\delta} \int_0^{u_{10}} \exp\left[-\frac{(\bar{u} - u)^2}{2\delta^2}\right] du \quad (3.42)$$

and for dry snow, the mean wind speed is found as

$$\bar{u} = 11.2 + 0.365T_a + 0.00706T_a^2 + 0.9 \ln(t_h) \quad (3.43)$$

and the standard deviation of wind speed is found as

$$\delta = 4.3 + 0.145T_a + 0.00196T_a^2. \quad (3.44)$$

Note that  $\bar{u}$  and  $\delta$  are properties of the snow surface and affected by the meteorological history of the snowpack, whilst  $u$  depends on current wind speed. If the snow surface is wet or icy, then values can be assigned as  $\bar{u} = 21 \text{ m s}^{-1}$  and  $\delta = 7 \text{ m s}^{-1}$  based on observations in the Canadian Prairies (Li and Pomeroy, 1997b).

There are different conclusions among experimental and modeling studies regarding the importance of blowing snow fluxes to regional snow mass balance and surface fluxes. Bintanja (1998) suggests that blowing snow sublimation in the Antarctic varies from negligible in the interior to  $170 \text{ kg m}^{-2}$  near the coast and is therefore a major term in the mass balance of the Antarctic ice sheet. Dery and Yau (2002) used the re-analysis (ERA15) data of the European centre for medium-range weather forecasts (ECMWF) at a resolution of  $2.5^\circ$  to study the effects of surface sublimation and blowing snow on the surface mass balance of the largely forested Mackenzie River basin, Canada. They found that surface sublimation removes

29 kg m<sup>-2</sup> SWE per year, or about 7% of the annual precipitation of the largely subarctic Mackenzie Basin.

From blowing snow model results and measured areal snow mass balances, Pomeroy *et al.* (1997) as well as Liston and Sturm (1998) suggest that the percentage of annual snowfall that is sublimated via blowing snow from arctic surfaces is 20% in northern Canada and 9% to 22% in northern Alaska. The model of Essery *et al.* (1999) suggests annual sublimation losses from 25% to 47% of annual snowfall for northern Canada, depending upon surface vegetation and topography. In removing these large sublimation estimates from their blowing snow model, Essery *et al.* (1999) found that snow accumulation was grossly overestimated in deposition zones, whereas it was well estimated when sublimation was included. Despite the deficiencies in these relatively simple blowing snow models, it appears that sublimation estimates can reasonably match seasonal losses and that, in field situations, the humidity feedback effects in the lower surface boundary layer proposed by Dery *et al.* (1998) are not normally sufficient to significantly lower seasonal sublimation rates.

### 3.4.3 Accumulation in alpine topography

Both orography and wind strongly affect the spatial distribution of snow depth in mountainous regions. Föhn (1977, 1985) addressed the question of representative new snow depth measurements in mountainous terrain. Clearly, crests, wind- and leeward slopes as well as depressions have to be avoided. Even at the most suited level sites, the catch efficiency of precipitation gauges (60–80%) does not closely match the reliability of a snow board laid on the snow surface. Even so, Föhn (1977, 1985) states that precipitation gauges located in surrounding valley floors may help to extrapolate new snow depths over larger areas in wintertime; very often one has to rely on available weather forecast outputs as well. By combining the latter with statistical and climatic approaches, promising results have been obtained (Durand *et al.*, 1993; Raderschall, 1999).

Yet for many applications redistribution by wind on leeward slopes has to be taken into account. Föhn and Hächler (1978) give an empirical relation for a 35° steep leeward slope as:

$$HN_w = c_2 \bar{u}_{\text{crest}}^3, \quad \bar{u} \leq 20 \text{ m s}^{-1}, \quad (3.45)$$

where  $HN_w$  is the mean additional new snow (in m) deposited on the leeward slope over a time period of 24 h,  $c_2 = 0.8 \times 10^{-4}$  (s<sup>3</sup> m<sup>-2</sup>) is an empirical coefficient and  $\bar{u}_{\text{crest}}$  is the mean wind speed measured on the crest. Despite the complexity of both modeling and measurements, blowing and drifting snow in heterogeneous

terrain is currently a topic of strong interest (Pomeroy, 1991; Liston and Sturm, 1998; Pomeroy *et al.*, 1999c; Durand *et al.*, 2001; Michaux *et al.*, 2001). Modeling blowing snow over a steep alpine ridge, Gauer (2001) obtained a power relation for the simulated steady-state flux, decreasing from approximately 4 to 2 with increasing wind speed. The mass flux decrease with increasing wind speed further indicates that a saturation of snow transport occurs. Combining a saltation model (Doorschot and Lehning, 2002) with an analytical wind profile taking into account speed-up effects over a ridge, Doorschot *et al.* (2001) observed a similar trend. The latter authors also included preferential deposition of precipitation as a third mode of snow transport to the lee slope. Preferential deposition does not require any threshold value to be exceeded to occur and may thus be predominant under certain conditions in steep Alpine terrain.

Finally, on the scale of a few hundred to one thousand square kilometers, Föhn (1992) as well as Martin *et al.* (1994) studied the impact of climate on snow depth in alpine regions. Such compilations provide valuable information for governmental agencies, hydropower facilities, winter tourism, and flood mitigation.

### 3.5 Examples of energy and mass balances

The relative contribution of the different fluxes involved in the energy and mass balance of the snow cover strongly depends on the prevailing meteorological and topographical conditions as well as on vegetation. The examples presented are “typical” snow covers although they do not all formally correspond to a classification scheme as proposed by Sturm *et al.* (1995); neither are they exhaustive.

Sections 3.5.1–3.5.3 deal with daily averages over continuous snow covers, stressing the relative contribution of each flux as the season proceeds. Prevailing meteorological conditions are also shown. Table 3.2 emphasizes this time average approach summarizing means for chosen time periods. Sections 3.5.4 and 3.5.5 are process oriented, showing and discussing detailed balances over a few days’ time. Where conditions influencing the energy balance vary strongly, this latter approach is best suited to describing short time variations that are smeared out by averaging.

Note that the radiative components of the energy balance as well as the mass balance are usually measured *in situ*. The turbulent fluxes, however, are parameterized using a bulk transfer formulation (see e.g. Section 3.3, Equation 3.11). Remember that according to the sign convention introduced in Section 3.2, negative fluxes are associated with positive changes of the snowpack’s internal energy, i.e. with an energy gain. In Sections 3.5.1–3.5.3, mass fluxes are integrated over a time period of one day, with precipitations (accumulation) and runoff (ablation) having opposite signs.

Table 3.2 Detailed investigations of the energy balance over alpine snow covers and glaciers.

Surface	Location	Period	Surface fluxes <sup>a</sup>			$dH/dt^b$	Source
			$R_N^c$	$H_S$	$H_L$		
Melting snow cover	Weissfluhjoch, Switzerland (47° N)	May to Jun	-53.0 <sup>d</sup>	-0.8	0.1	53.7	1
	Finse, Norway (61° N)	15 d in May	-25.0	-21.4	-0.3	46.7	2
	Southern Alps, New Zealand (43° S)	Oct 28 to Nov 9	-20.0	-69.0	-31.0	120.0	3
	Sierra Nevada, USA. (37° N)	May Jun	-44.0 -93.0	-50.0 -92.0	54.0 71.0	40.0 114.0	4
Melting snow cover over glacier	Peyto Glacier, Canada (52° N)	14 d in Jul	-79.8	-87.0	-14.5	181.3	5
Over glacier under melting condition	Mt. Blanc area, French Alps (46° N)	23 d in Jul	-20.8	-5.0	4.9	20.9	6
	Urumqi Glacier N° 1, Tien Shan (42° N)	Jun to Aug	-54.0	-12.0	14.0	52.0	7

<sup>a</sup> Average surface fluxes in  $W m^{-2}$  over the given period.

<sup>b</sup>  $(dH/dt)$  is the net change rate of the snowpack's internal energy per unit area, which is the negative sum of net radiative ( $R_N$ ), sensible heat ( $H_S$ ) and latent heat ( $H_L$ ) fluxes, but neglecting advective and ground heat fluxes (see Equation 3.1).

<sup>c</sup> The net radiative flux ( $R_N$ ) is the sum of net shortwave radiation flux ( $S_N$ ) and net longwave radiation flux ( $L_N$ ).

<sup>d</sup>  $S_N = -79.0 W m^{-2}$ ;  $L_N = 26.0 W m^{-2}$

References: 1, Plüss (1997); 2, Harding (1986); 3, Moore and Owens (1984); 4, Marks and Dozier (1992); 5, Föhn (1973); 6, de la Casimière (1974); 7, Calanca and Heuberger (1990).

### 3.5.1 *High-elevation alpine snow cover*

*Christian Plüß, Charles Fierz, and Paul M. B. Föhn*

#### *Relevance and characteristics*

High alpine seasonal snow covers are present in mountainous areas around the world. The duration and spatial distribution of alpine snow covers is extremely variable and depends mainly on the geographical location, the climatic conditions, and the elevation of the mountain range. Alpine snow covers are of large economic and social importance in many areas, for example as a water resource for hydropower or as a base for tourism. In all alpine areas the snow cover is an important climate element because of its high albedo and low surface temperature. However, seasonal alpine snow covers may also cause natural hazards such as avalanches or flooding. The snow cover of the Alps – situated in the heart of densely populated Europe – meets all the above-mentioned issues and therefore considerable research effort has been spent towards its investigation.

The central part of the Alps is seasonally snow covered from about December to April above an altitude of 1000 m. The snow cover is highly variable in time and space because of both the complex topography and large differences in elevation within the mountain range. Wind influence as well as variable elevation, slope angles, and surface conditions lead to a highly structured snowpack being spatially inhomogeneous at scales as small as a slope, contrary to the Arctic, Antarctic, or prairie snowpack. Accordingly, the distribution of snow accumulation is very difficult to investigate (Elder *et al.*, 1989; Sturm *et al.*, 1995).

#### *Site*

The site of Weissfluhjoch lies in the eastern Swiss Alps near the town of Davos. The measurement site is located at a horizontal site in a southeasterly slope at an altitude of 2540 m a.s.l. (46.83° N, 9.81° E). On this well-equipped site, daily manual observations have been performed since 1936 and today most relevant nivo-meteorological parameters are measured automatically at a half-hourly time step (down- and up-welling shortwave and longwave radiation, air temperature, humidity, wind speed, snow surface temperature, snow depth). The snow cover lasts on average nine months (269 days), from mid-October to mid-July, and the mean snow depth reaches its maximum around mid-April (221 cm). The mean maximum snow water equivalent amounts to 857 mm w.e.

#### *Energy balance*

Energy balance investigations over an alpine snow cover were performed mainly in the European Alps and the North American Rocky Mountains. Many of these studies

were performed over snow-covered glaciers under melt conditions (see Tables 3.2 and 3.3). All these investigations show that, on a daily basis, net radiation is the primary energy source, while turbulent fluxes are generally of minor importance.

Along with the daily means of air temperature, wind, and albedo, the daily means of energy fluxes at the surface and mass balance at Weissfluhjoch (eastern Swiss Alps) are presented in Fig. 3.5. Using the aforementioned measured forcing data, the snow-cover model SNOWPACK (Bartelt and Lehning, 2002; Lehning *et al.*, 2002a, 2002b) computes the energy balance, allowing for the extracting of parameterized turbulent fluxes.

Despite the high albedo of the snow cover, the shortwave net radiation flux  $S_N$  is the dominant energy source for the snow cover during most of the investigation period. Longwave net radiation flux  $L_N$  is, in general, an energy loss and depends mainly on cloud conditions. During the ablation period, net radiative flux  $R_N$  is by far the dominant energy source for snowmelt. The magnitude of the turbulent fluxes of sensible and latent heat,  $H_S$  and  $H_L$ , respectively, are very small on average, but the daily mean values may exceed the magnitude of net radiative flux and are therefore not negligible for the investigation of short-term processes. At Weissfluhjoch, the small average magnitude of the turbulent fluxes is attributed firstly to the relatively small wind speed at this site and secondly to the frequent changes of the weather patterns, which lead to changes of the sign of these fluxes.

### *Modeling aspects*

The high variability of the alpine snow cover in space and time proves to be very difficult to model. Accumulation depends largely on wind influence and small-scale precipitation differences may lead to very inhomogeneous conditions. The energy fluxes at the snow surface are highly variable due to topographic influence on the radiation fluxes and due to high variability of the turbulent fluxes. Dozier (1980) presented a spatially distributed model for shortwave radiation, Plüss and Ohmura (1997) proposed a modeling approach for longwave radiation. For the turbulent fluxes only very simple models have been proposed so far, despite the fact that over melting snow, the turbulent fluxes may be of considerable importance (Olyphant and Isard, 1988).

For ablation estimation, hydrologic models (see Kirnbauer *et al.*, 1994) have proven to successfully model the spatial distribution of ablation. Fierz *et al.* (1997) showed that snow temperature profiles could be modeled on several aspects using a distributed energy balance model to drive a point snow-cover model.

Table 3.3 Energy balance over snow covers for selected time periods.

Type of snow cover	Location	Period	Surface fluxes <sup>a</sup>					$d\mathcal{H}/dt^b$
			$S_N$	$L_N$	$R_N^c$	$H_S$	$H_L$	
High Alpine	Weissfluhjoch, Switzerland (47° N)	Nov to Dec 95	-13.7	31.9	18.2	-19.7	5.0	-3.5
		Jan to Apr 96	-29.7	46.8	17.1	-19.4	7.5	-5.2
		May to Jun 96	-86.7	40.8	-45.8	-28.0	-2.5	76.3
Middle Alpine	Col de Porte, France (61° N)	Jan 95	-4.9	11.2	6.3	-6.1	-2.0	1.8
		Apr 95	-46.9	12.5	-34.4	-11.0	-4.1	49.5
		Jan to Apr 95	-21.8	14.7	-7.1	-7.7	-2.1	16.9
		Jan 94	-6.6	16.0	9.4	-7.0	-2.4	0.0
Snow-covered sea ice	High Arctic ice flow, North Pole 4, (>85° N)	Apr 94	-25.3	13.8	-11.5	-8.4	-2.5	22.4
		Jan to Apr 94	-22.0	17.4	-4.6	-9.9	-2.0	16.5
		May to Jun 56	-48.0	26.3	-21.7	-11.6	12.3	-2.2
		Jul to Aug 56	-36.7	-14.6	-22.1	2.9	8.4	10.8
		Sep to Oct 56	-2.5	13.4	10.9	-1.6	1.0	-10.3
		Nov to Dec 56	0.0	11.9	11.9	-9.3	1.3	-3.9
		Jan to Mar 57	-0.4	16.5	-16.1	-10.7	0.8	-6.2

<sup>a</sup> Average surface fluxes in  $W m^{-2}$  over the given period.

<sup>b</sup>  $(d\mathcal{H}/dt)$  is the net change rate of the snowpack's internal energy per unit area, which is the negative sum of net radiative ( $R_N$ ), sensible heat ( $H_S$ ) and latent heat ( $H_L$ ) fluxes, but neglecting advective and ground heat fluxes (see Equation 3.1).

<sup>c</sup> The net radiative flux ( $R_N$ ) is the sum of net shortwave radiation flux ( $S_N$ ) and net longwave radiation flux ( $L_N$ ).

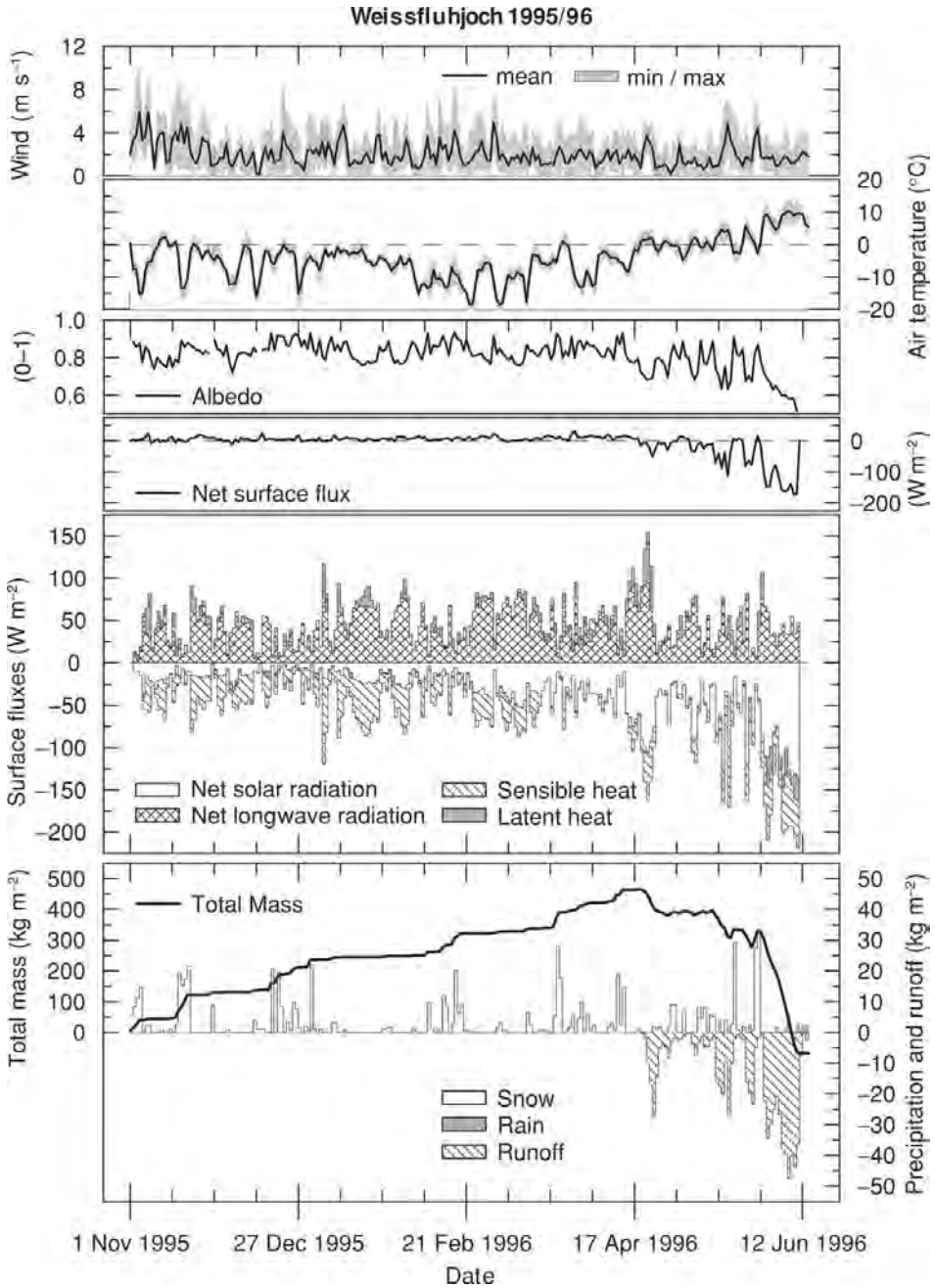


Figure 3.5. Daily means and, where appropriate, daily minima and maxima (shaded band) at Weissfluhjoch during the winter 1995/96. The snow cover was continuous from November 2, 1995 to June 11, 1996. Net surface flux is the sum of surface fluxes, which corresponds to the net negative change rate of the snowpack's internal energy per unit area ( $-dH/dt$ ) neglecting advective and ground heat fluxes (cf. Equation 3.1). Total mass is the accumulated difference of precipitations (snow and rain) to runoff, neglecting sublimation and evaporation (cf. Equation 3.4).

### 3.5.2 *Middle elevation alpine snow cover*

*Eric Martin*

#### *Relevance and characteristics*

Col de Porte is quite representative of middle elevation sites in a temperate alpine climate. Many ski resorts and hydropower stations in the Alps are located within the same elevation range.

The climate is wet (2000 mm w.e. yr<sup>-1</sup>) because it is situated in the western part of the European Alps. The mean winter temperature (December–February) is  $-1^{\circ}\text{C}$ . Rainfall events are common in winter. During the first part of the winter, the snowpack structure is highly variable; all grain types can be encountered. Because of regular rainfall events, a layer of wet grains topped by a layer of rounded grains constitutes a typical winter snowpack. Depth hoar is encountered only in cases of shallow snow cover and cold conditions. Surface hoar growth occurs several times in winter.

#### *Site*

At Col de Porte, at an altitude of 1320 m a.s.l., the snow cover lasts an average of five months, from the end of November to the beginning of May. The mean maximum snow depth is 130 cm at the beginning of March. Snowmelt events may occur at any time but ablation usually takes place after mid-March. The maximum snow water equivalent varies generally between 200 and 500 mm w.e.

Screening of shortwave radiation is important in December and January because of trees. At large scales, albedo is dependent on the presence of snow on branches but it may sometimes also be affected by the deposition of fragments of needles. Wind is generally light.

#### *Energy balance*

The site is equipped with shortwave and longwave radiation sensors. Air temperature, humidity, and wind speed are also measured at hourly time steps. Energy balance investigations are made using the snow model CROCUS (Brun *et al.*, 1989, 1992). Radiation terms are measured while the model calculates turbulent fluxes. Parameterization of the latter fluxes is discussed in Martin and Lejeune (1997).

Along with the daily means of air temperature, wind and albedo, the daily means of energy fluxes at the surface and mass balance at Col de Porte are presented in Figs. 3.6 and 3.7 for the winter seasons 93/94 and 94/95, respectively. Turbulent fluxes (sensible and latent heat) transfer heat from the atmosphere to the snow cover as the atmosphere is usually stable. March 1994 was very warm and snowmelt occurred throughout this month. On the contrary, the first part of April was cold and snowy before the final melting period. In 94/95, melting only occurred in April.

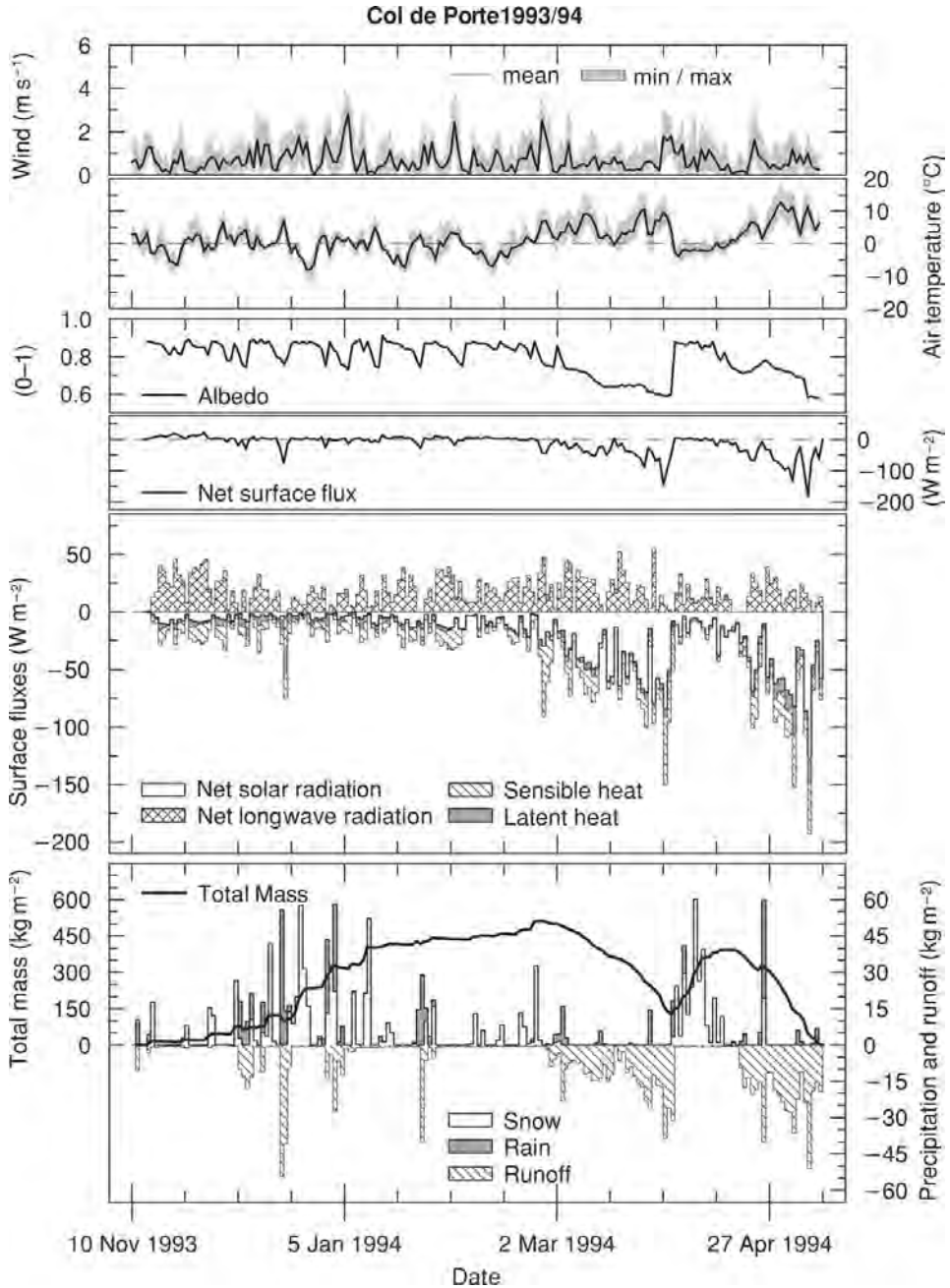


Figure 3.6. Daily means and, where appropriate, daily minima and maxima (shaded band) at Col de Porte during the winter 93/94. The snow cover was continuous from November 13, 1993 to May 5, 1994. Net surface flux is the sum of surface fluxes, which corresponds to the net negative change rate of the snowpack's internal energy per unit area ( $-dH/dt$ ) neglecting advective and ground heat fluxes (cf. Equation 3.1). Total mass is the accumulated difference of precipitations (snow and rain) to runoff, neglecting sublimation and evaporation (cf. Equation 3.4).

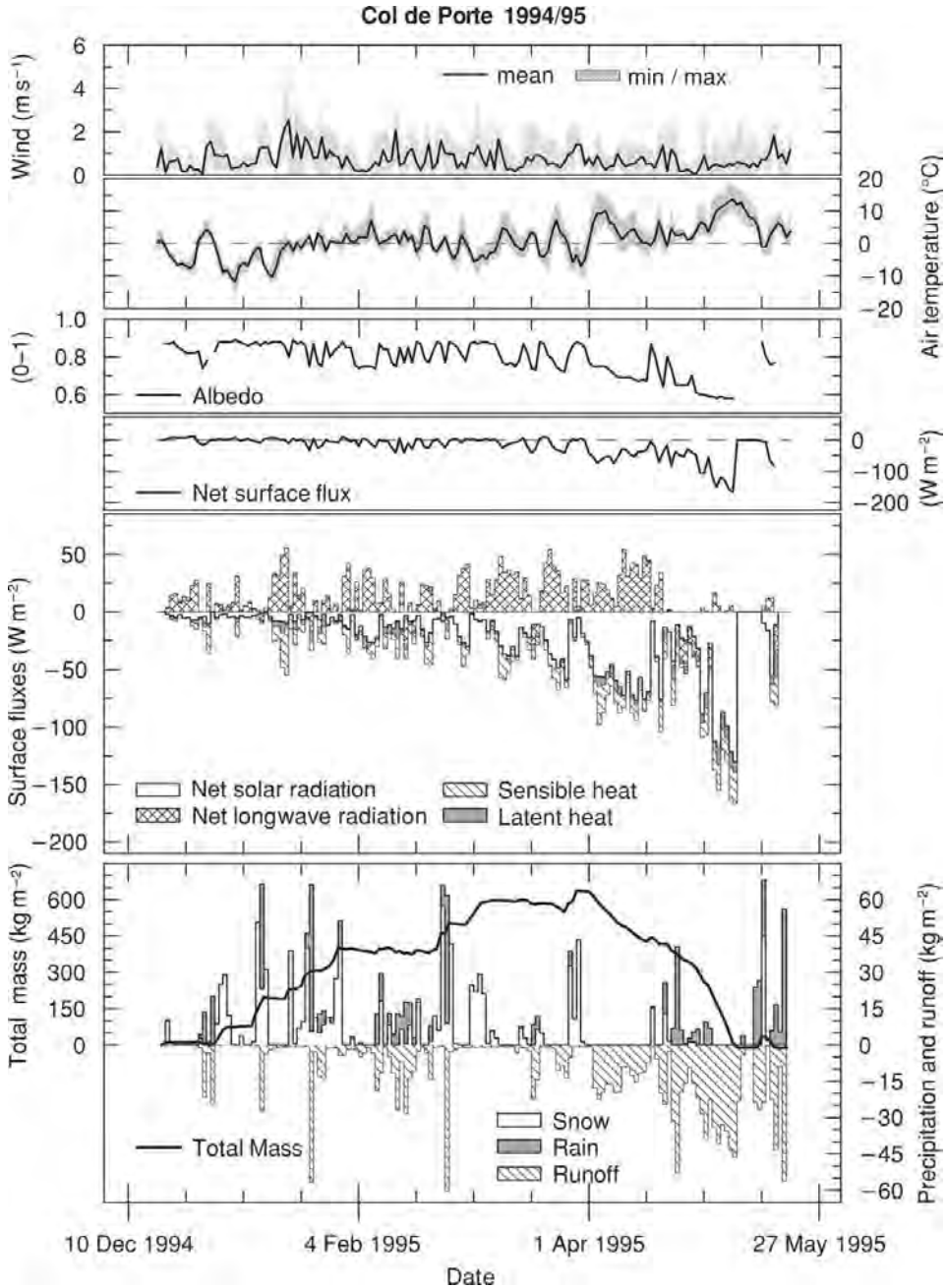


Figure 3.7. Daily means and, where appropriate, daily minima and maxima (shaded band) at Col de Porte during the winter 1994/95. The snow cover was continuous from December 31, 1994 to May 8, 1995. Net surface flux is the sum of surface fluxes, which corresponds to the net negative change rate of the snowpack's internal energy per unit area ( $-dH/dt$ ) neglecting advective and ground heat fluxes (cf. Equation 3.1). Total mass is the accumulated difference of precipitations (snow and rain) to runoff, neglecting sublimation and evaporation (cf. Equation 3.4).

The magnitude of net shortwave radiation is large during the melting period (March 94 and April 95). The variations of the net longwave radiation are more complex.

#### *Modeling aspects*

Turbulent fluxes are probably the most difficult factor to take into account at this site because of the complex topography. All types of snowpack can be encountered at this site: cold or completely wet even in winter, which induces difficulties in modeling the structure and layer texture of the snowpack.

### **3.5.3 Snow-covered sea ice on a high arctic ice flow**

*Rachel E. Jordan*

#### *Relevance and characteristics*

Between 1937 and 1991, Russian scientists embarked on 31 “North Pole” field experiments within the Arctic Ocean. With the recent relaxing of East–West relations, the extensive set of meteorological, oceanographic and ice flow data from these expeditions has been made available to Western scientists on a CD-ROM (National Snow and Ice Data Center, 1996). There is now a general consensus that energy exchange over the polar ice caps is of critical importance to long-term climatological change. A comparison of historical data with that from the recent SHEBA expedition (Persson *et al.*, 2002; Uttal *et al.*, 2002) may reveal emerging trends in the surface energy balance of the Arctic Ocean.

#### *Site*

The Russian drifting station North Pole 4 (NP-4) was within 5° latitude of the North Pole from April 1956 until April 1957. Instrumentation at the NP-4 site is described by Kucherov and Sternzat (1959), Marshunova and Mishin (1994), and Jordan *et al.* (1999). The NP-4 site was characterized by high winds, fine-grained, dense snow, and a relatively shallow snowpack. Spring, summer, and winter seasons had distinct characteristics. Much of the snow was lost through melting during the summer and melt ponds formed in the sea ice, causing extreme variability in albedo. Cloud cover was heavy over the melting snow and the air temperature remained near 0 °C. In contrast, the amplitude of temperature swings associated with the passing of synoptic systems was up to 40 °C in winter (see Fig. 3.8).

#### *Energy balance*

Energy balance studies over arctic ice flows include works by Nazintsev (1963, 1964), Maykut (1982), Ebert and Curry (1993), Radionov *et al.* (1996), Lindsay (1998), and Uttal *et al.* (2002). Jordan *et al.* (1999) describe in detail the NP-4 data presented here in Fig. 3.8.

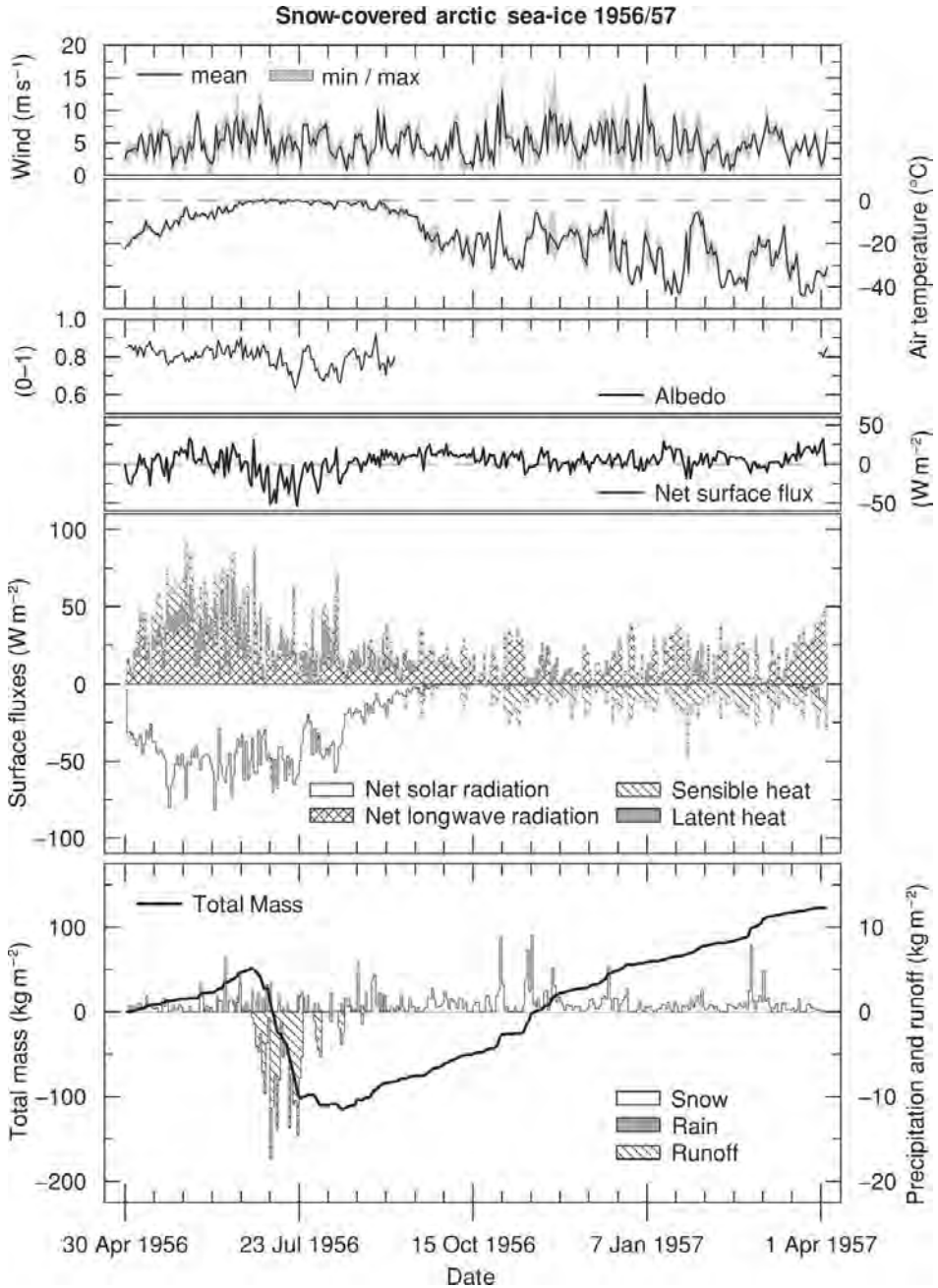


Figure 3.8. Daily means and, where appropriate, daily minima and maxima (shaded band) on snow-covered sea ice on a high arctic ice flow from April 30, 1956 to April 3, 1957. Net surface flux is the sum of surface fluxes, which corresponds to the net negative change rate of the snowpack's internal energy per unit area ( $-d\mathcal{H}/dt$ ) neglecting advective fluxes and heat flux from the sea ice (cf. Equation 3.1). Total mass is the accumulated difference of precipitations (snow and rain) to runoff, neglecting sublimation and evaporation (cf. Equation 3.4).

Net shortwave radiation was the dominant energy flux to the snowpack during the late spring and summer. During these seasons at NP-4, the turbulent fluxes were close in magnitude and predominantly upwards, thus cooling the surface. Figure 3.8 shows a positive radiation balance after mid-September and simultaneously the appearance of downward spikes in the sensible heat flux, which increase in magnitude over the winter. The largest longwave radiation losses occurred under cloudless skies and were primarily compensated by sensible heat exchange. Latent heat fluxes were predominantly upward or evaporative. The magnitude of latent heat was small during the winter because saturation vapor pressure decreases exponentially with temperature.

Figure 3.8 shows a high snow albedo between 0.8–0.9 for new snow and a low albedo of 0.65 for older snow, near the value for bare ice. Snow cover persisted throughout the summer at this location, with depths ranging between 3 and 8 cm. About one-half of summer precipitation fell as snow and the increases in albedo reflect this in Fig. 3.8. The 1997–1998 SHEBA expedition, by contrast, reported loss of snow cover by early August. The remaining surface mix of bare ice and melt ponds had a much lower albedo than snow. Such dramatic alterations in albedo lead to an ice albedo feedback (Perovich *et al.*, 2002), which plays a key role in the energy budget of the high Arctic.

#### *Modeling aspects*

High arctic sites are subject to blowing and drifting snow and exhibit considerable variability in snow depth. Thus, the wind transport of snow must be considered to build realistic snow covers. Precipitation measurements reported here are corrected for wind effects, evaporation, and wetting error (Yang, 1995; Jordan *et al.*, 1999). Because arctic snow is fine-grained and packed by wind, polar snowpacks are much denser than their temperate counterparts. The density of newly fallen snow should therefore be around 150–300 kg m<sup>-3</sup> and increase with wind speed.

Sturm *et al.* (2002) infer an effective thermal conductivity of 0.33 W m<sup>-1</sup> K<sup>-1</sup> from snow temperature profiles at SHEBA, which is higher than that for temperate snow and also higher than recent field measurements by Sturm *et al.* (1997, 2002). Sturm *et al.* (2002) conclude that mechanisms other than one-dimensional conduction may enhance the heat exchange within the polar snowpack. Jordan *et al.* (2003) suggest that high winds may induce wind ventilation in the upper 10–20 cm of the snowpack and thereby increase its effective thermal conductivity.

Persistent radiative losses in winter lead to periods when the standard stability correction for stable atmospheres can shut down sensible heat exchange. To avoid unrealistically low surface temperature predictions, Jordan *et al.* (1999) therefore replaced the usual log–linear stability function with one that maintains a minimal turbulent exchange.

### 3.5.4 Canadian prairies

John W. Pomeroy and Donald M. Gray

#### *Relevance and characteristics*

“Prairie” snow seasonally covers northern continental grain-growing and grassland regions of North America, Europe, and Asia. These snow covers impact both the social and the economic aspects of the region because: a large proportion of the population lives in rural districts, grain and livestock exports are globally important food supplies, the region experiences long and severe winters and summer water deficits, and agriculture and industry rely on long distance transport by road and rail (Steppuhn, 1981).

Although snowfall only comprises about one-third to one-half of annual precipitation, snowmelt runoff often exceeds 90% of annual streamflow (Gray, 1970). Spring floods caused by prairie snowmelt water are the most economically destructive natural phenomena in the U.S.A. and Canada and defensive measures such as large “ring-dikes” are used to protect major cities such as Winnipeg, Manitoba.

On the prairies, blowing snow erosion and sublimation may result in increased water deficits, termed “northern desertification” in Russia (Dyunin *et al.*, 1991), which may be enhanced by the suppression and removal of natural vegetation. In many areas, blowing snow storms result in winter restrictions on transportation and a specialized design of infrastructure to minimize snow removal costs and snow load damage (Tabler and Schmidt, 1986.)

Prairie snow covers persist from November to April. They are generally cold, dry, and wind-packed. Blowing snow causes redistribution several times during a winter season and results in dense (generally greater than  $250 \text{ kg m}^{-3}$ ), crusted and variable (coefficient of variation of SWE 0.3–0.58) snow covers (Pomeroy *et al.*, 1998b). Snow accumulation is very sensitive to vegetation cover and topography, and the depths in sheltered sites can be five or six times that on exposed sites (Steppuhn and Dyck, 1974; Pomeroy *et al.*, 1993). In early spring the energy for melting snow is largely derived from shortwave radiation and as melt progresses the magnitude of net radiative flux generally increases due to the increase in magnitude of incoming shortwave flux and the decrease in areal albedo due to the decreases in snow depth and in snow-covered area (O’Neill and Gray, 1973). Advection of sensible heat from bare ground to snow has been shown to play an important role in the melting of a patchy snow cover (Shook and Gray, 1997). As a result, areal melt rates are greatest when the snow-covered area is between 40% and 60% (Shook, 1995). Ground heat flux is negligible during melt because of the infiltration of meltwater into frozen soils, which leads to the release of latent heat upon freezing and very small temperature gradients near the soil surface (Zhao *et al.*, 1997; Pomeroy *et al.*, 1998b).

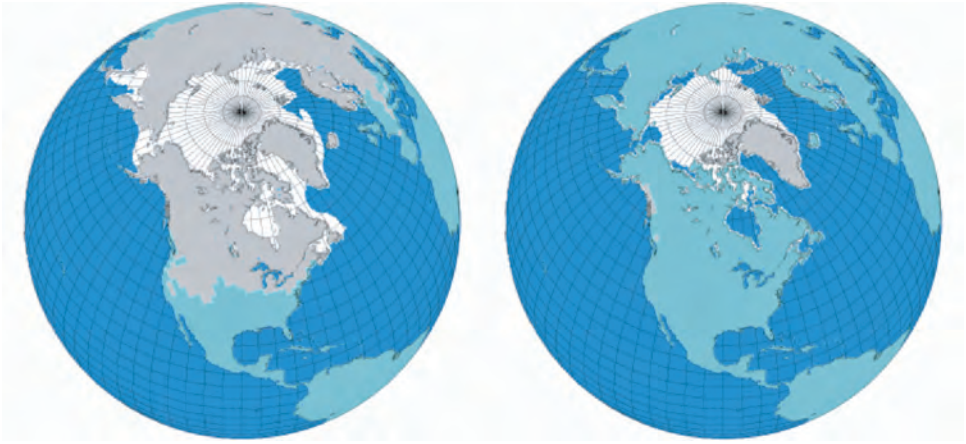
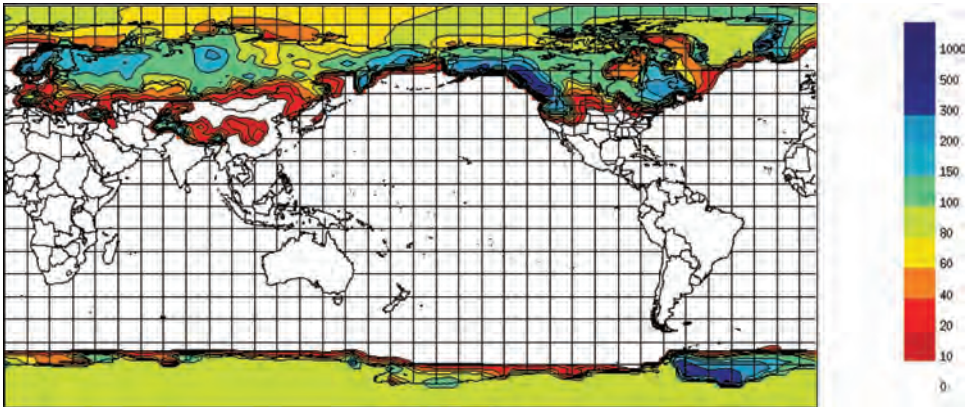


Plate 1.2. Mean seasonal variation in snow (gray) and sea-ice cover (white) between February (left) and August (right) as derived from satellite data. Data from NSIDC “Weekly Snow Cover and Sea Ice Extent,” CD-ROM, NSIDC, 1996.

(a)



(b)

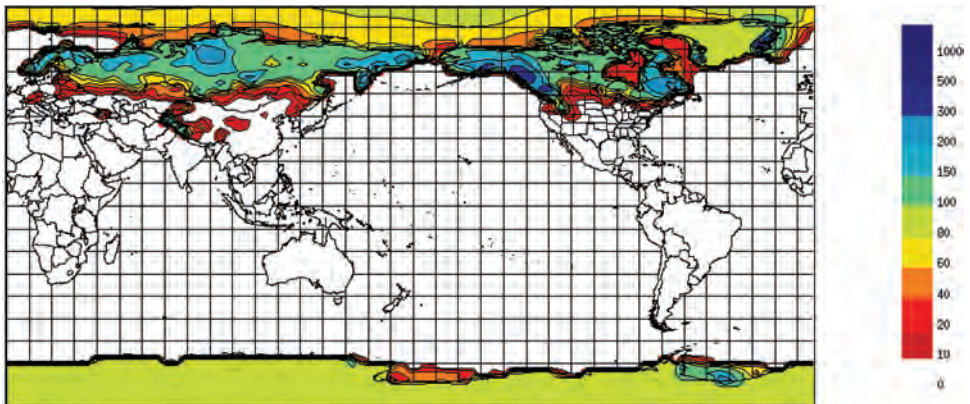


Plate 1.4. Comparison of mean March winter SWE (mm) simulated by the Canadian coupled global climate model (CGCM3) for the 1981–2000 “current climate” period (a) with simulated mean SWE for the 2081–2100 period (b) based on the SRES A2 emission scenario. Data courtesy of the Canadian centre for climate modeling and analysis.

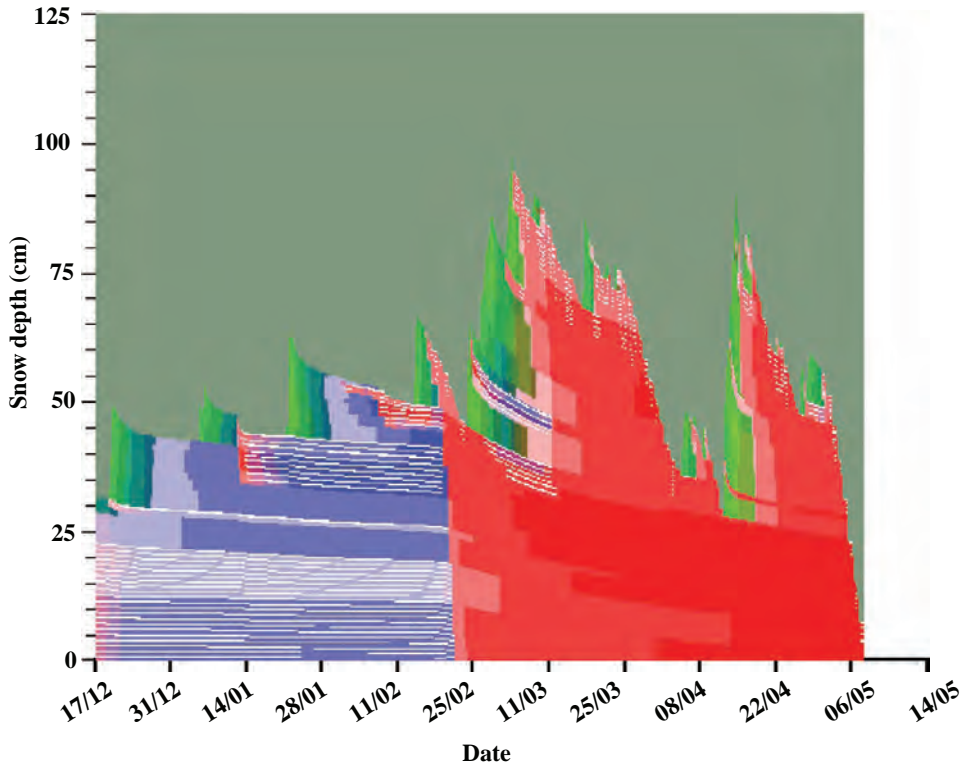


Plate 4.1. Simulation of temporal evolution of snowpack layering at Col de Porte during winter 1998/99. Each color represents a snow type (see Brun *et al.*, 1992).

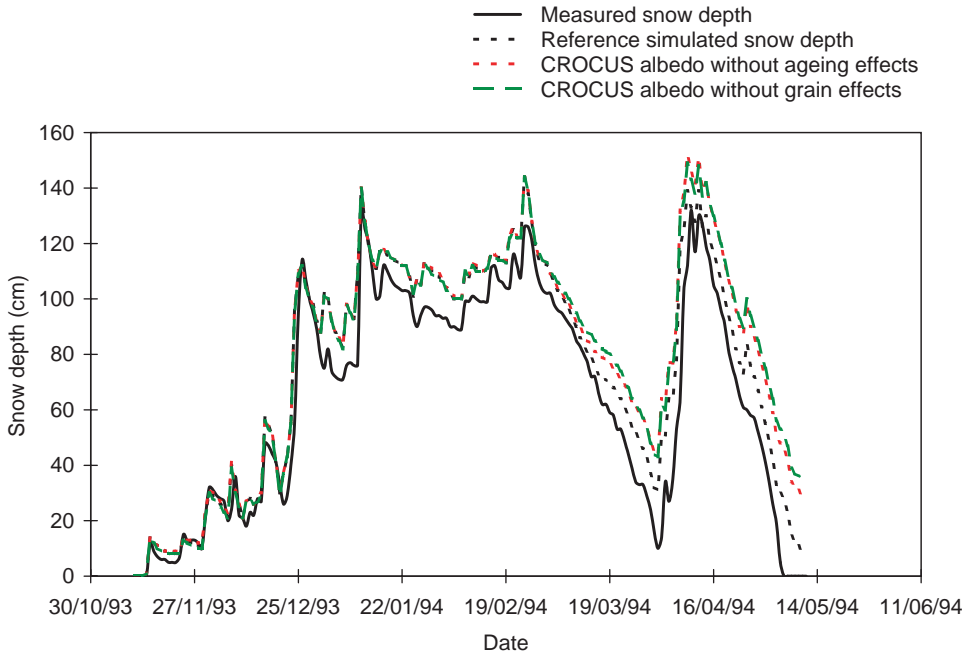


Plate 4.2. Sensibility to ageing and grain size in albedo calculation on snow depth simulations.

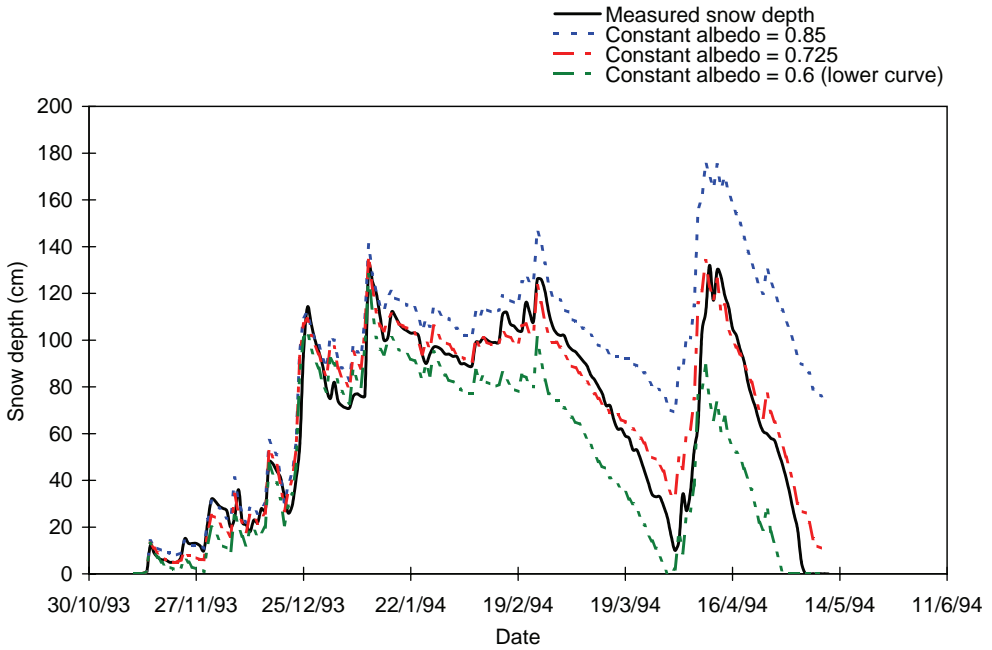


Plate 4.3. Sensibility to albedo on snow depth simulations.

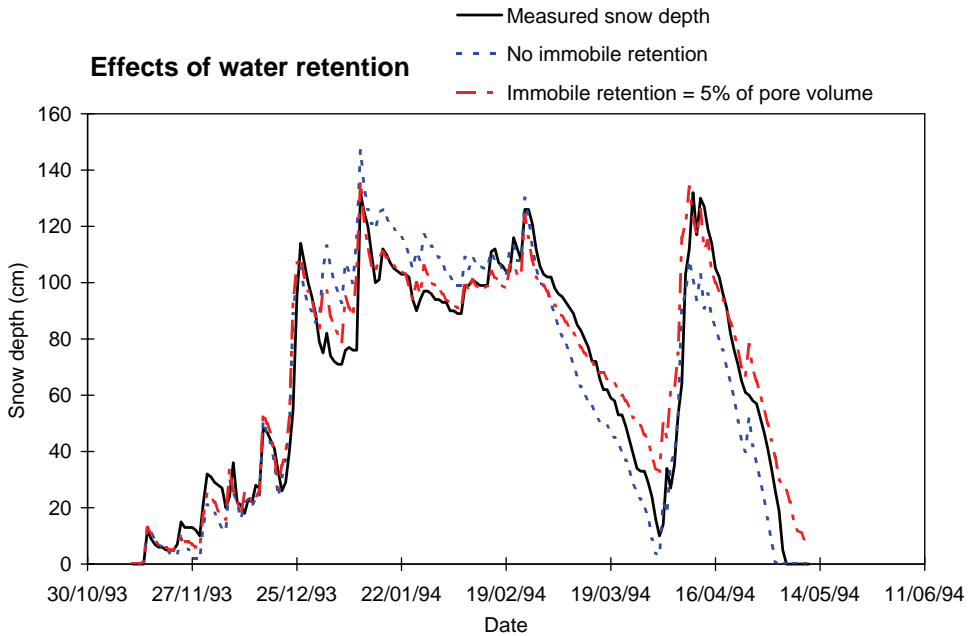


Plate 4.4. Sensibility to water retention on snow depth simulations.

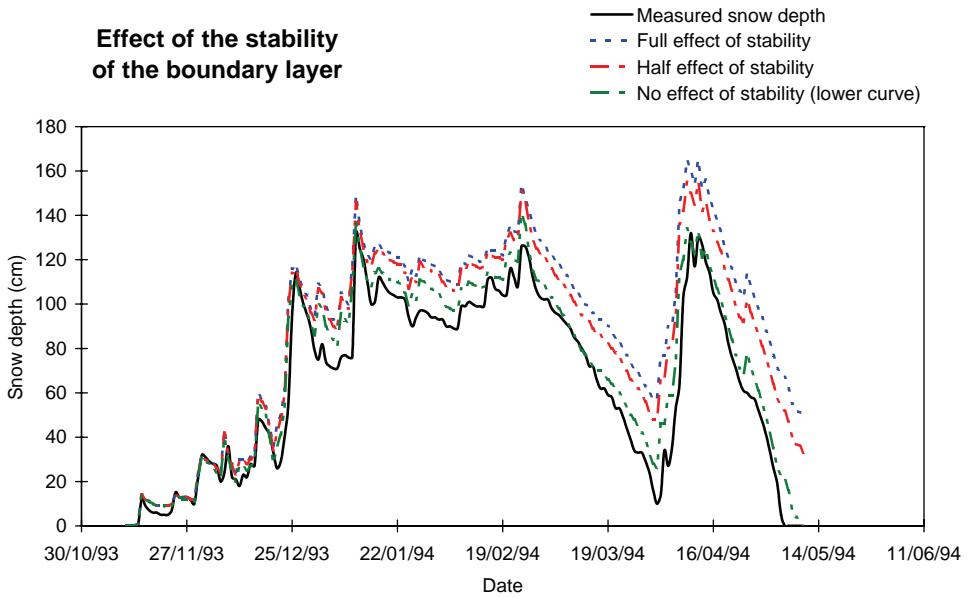


Plate 4.5. Sensibility to the stability of the boundary layer on snow depth simulations.

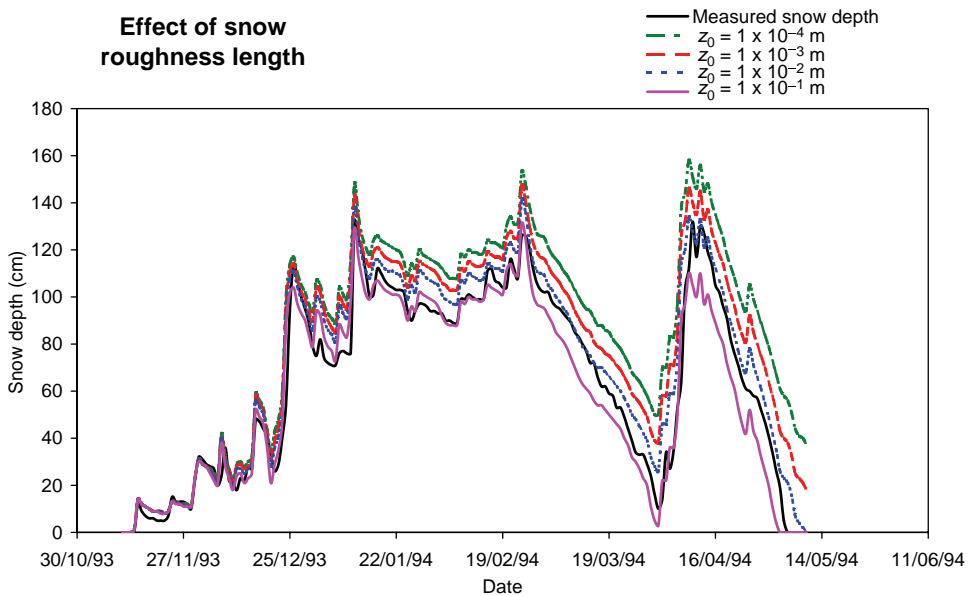


Plate 4.6. Sensibility to snow length roughness on snow depth simulations.

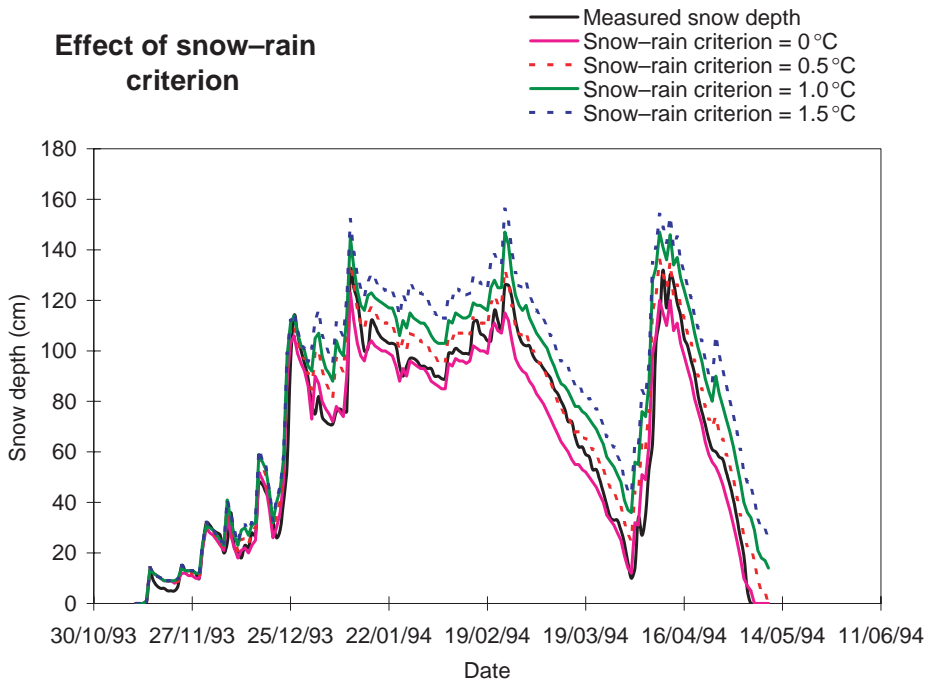


Plate 4.7. Sensibility to snow-rain criterion on snow depth simulations.

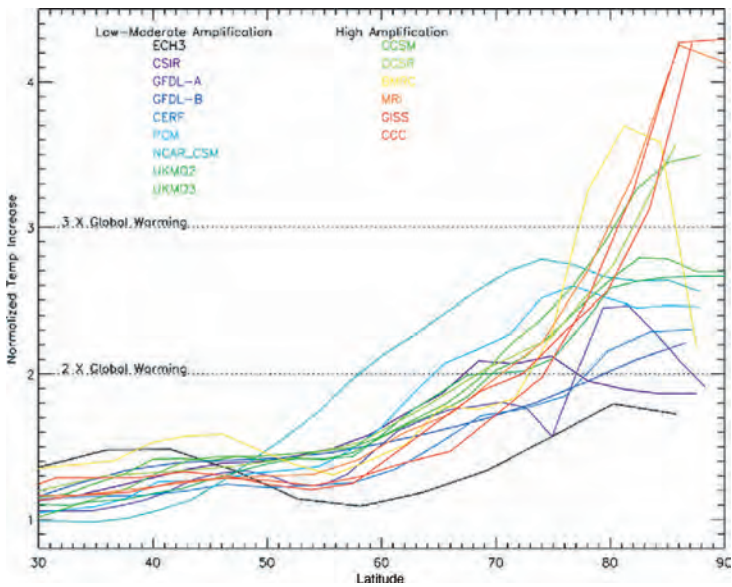


Plate 4.14. Surface air temperature change in 15 coupled GCMs that have doubled atmospheric CO<sub>2</sub> concentrations. All models show “polar amplification” and enhanced warming in the Arctic compared to tropical latitudes. Taken from Holland and Bitz (2003).

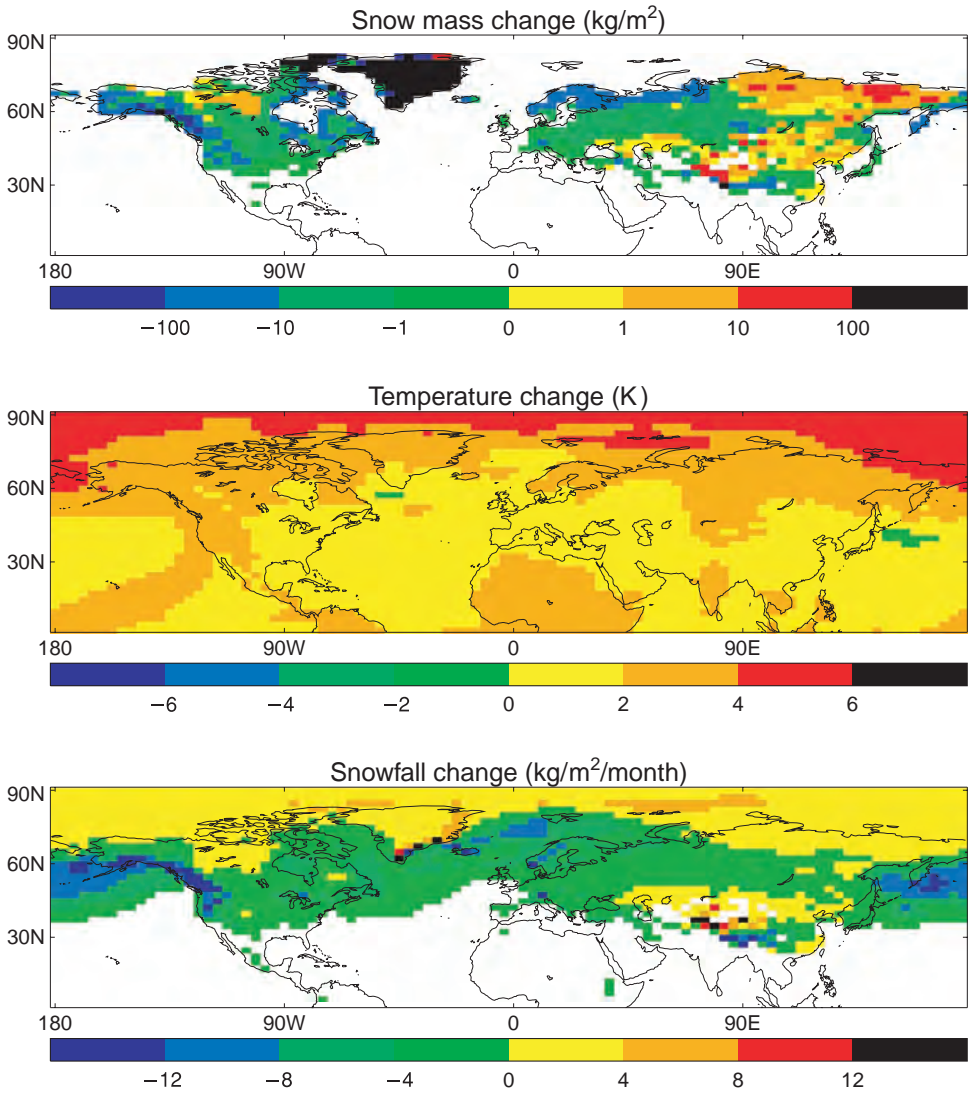


Plate 4.19. Differences between 2030–2050 averages from the climate-change simulation and 130-year averages from the control of the Hadley GCM for (a) snow mass (b) temperature and (c) snowfall. Taken from Essery (1997).

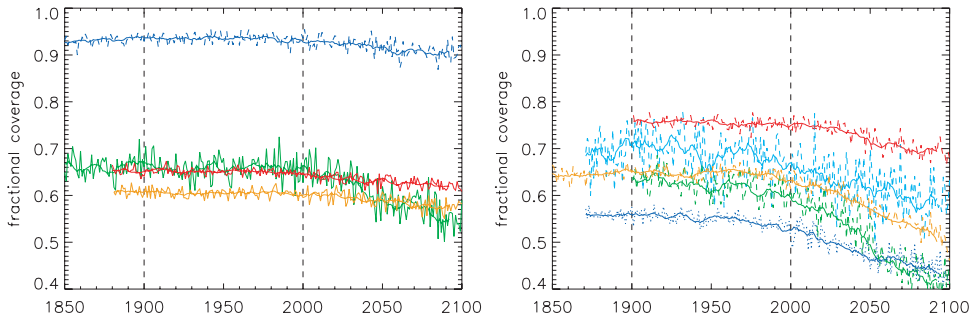


Plate 4.20. Annual time series (thin line), overlaid with nine-year running means (thick line), of ensemble-mean January North American snow cover extent, including both twentieth century and twenty-first century scenarios, for nine available coupled atmosphere-ocean GCMs. Taken from Frei and Gong (2005).

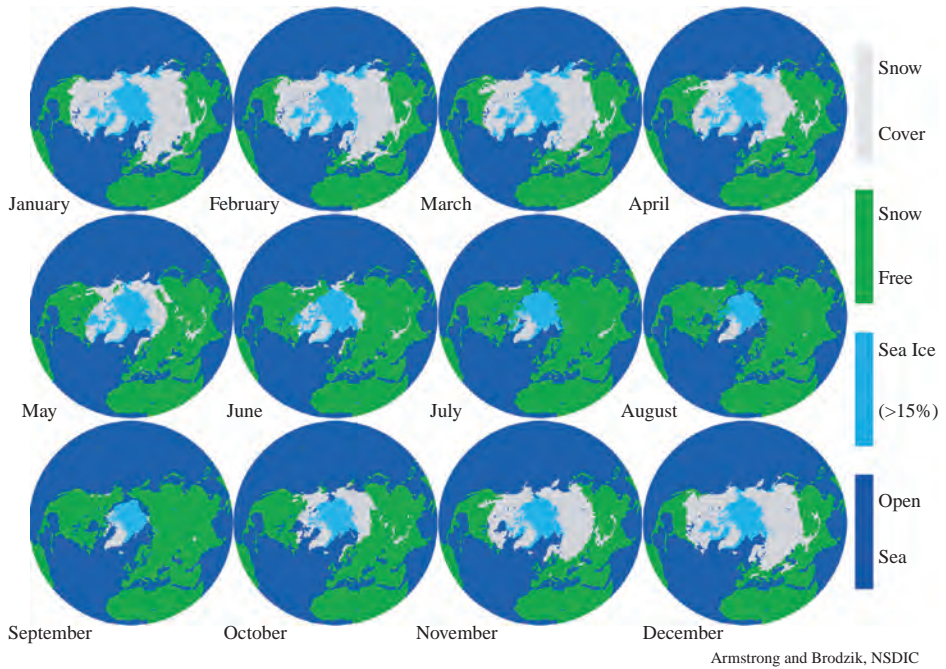


Plate 5.2. Monthly Northern Hemisphere snow cover (1966–2005) and sea ice extent (1978–2005) climatologies (Source: NSIDC *Northern Hemisphere EASE-Grid Weekly Snow Cover and Sea Ice Extent Version 3, 2005*).

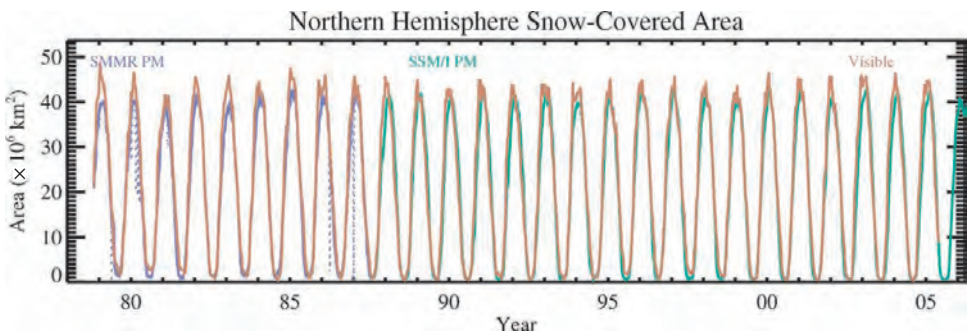


Plate 5.3. Northern Hemisphere monthly SCA, 1978–2005, from NOAA snow charts (orange) and microwave satellite (purple/green) data sets.

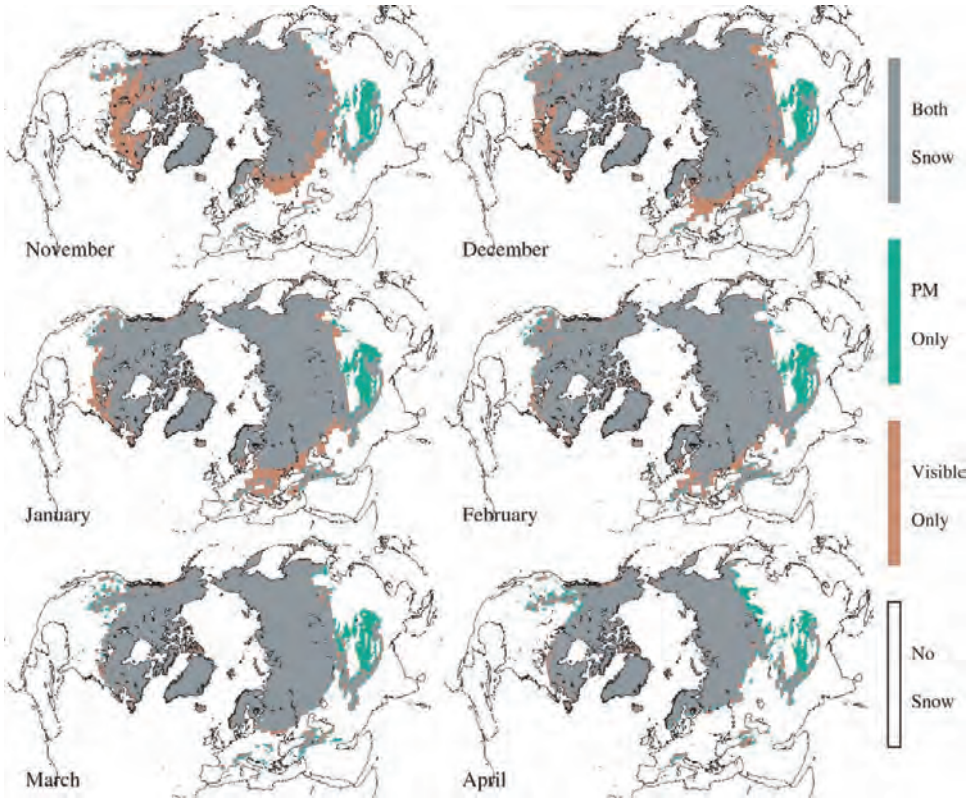


Plate 5.4. Comparison of mean monthly Northern Hemisphere snow extent derived from visible and passive microwave satellite data, 1978–2005 (50% or more of the weeks in the particular month over the total time period classified as snow covered).

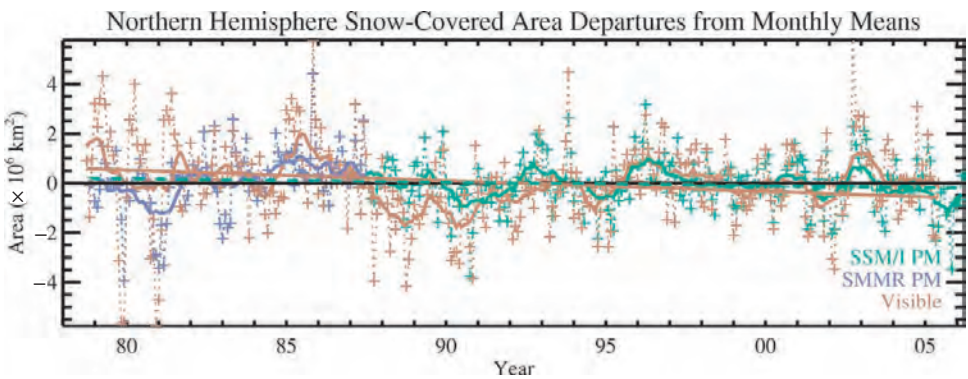


Plate 5.5. Northern Hemisphere SCA departures from monthly means, 1978–2005, from NOAA snow charts (orange) and microwave satellite (purple/green) data sets. The NOAA time series for this period exhibits a significant decreasing trend of  $-2.0\%$  per decade (solid orange line); the microwave snow-cover time series exhibits a decreasing trend of  $-0.7\%$  per decade that is not significant at a 90% level (dashed green line).

### Site

Kernen Farm (500 m a.s.l.) is east of the City of Saskatoon (52° N, 107° W) in the central southern half of the Province of Saskatchewan, Canada. The farm is situated on an open, flat, lacustrine plain, which is cropped to cereal grains and pulse crops under the practice of dryland farming (Shook and Gray, 1996). Trees are limited to farmyards, which are located several kilometers distant from the site. The climate is subhumid and typical of northern prairies with cold winters and continuous snow cover from late November to early April.

Experiments were conducted in December 1998 and March 1999 at level sites with continuous snow cover on fields of uniform short vegetation or fallow. Energy balance and related parameters were measured and recorded half-hourly using eddy correlation equipment (Gill Instruments “Solent” or Campbell Scientific “CSAT” sonic anemometers, Campbell Scientific “Krypton” hygrometers, fine wire thermocouple controlled by a datalogger for covariance calculation), Radiation and Energy Balance System “REBS” net radiometers and ground heat flux plates, “NRG40” cup anemometer, “Everest” infrared thermometer, “Vaisala” HMP35CF platinum resistance thermometers, Campbell Scientific “SR-50” ultrasonic snow depth gauge and University of Saskatchewan blowing snow particle counters (Brown and Pomeroy, 1989; Shook and Gray, 1997; Pomeroy *et al.*, 1998b, 1999b). During the measurement periods, the sites were frequently manned, which provided a high confidence in the observations.

### Energy balance

Two energy balances and related measurements are shown in Figs. 3.9 and 3.10. As stated previously, negative values indicate downward fluxes. Figure 3.9 shows fluxes during an early winter snow accumulation period with blowing snow, Fig. 3.10 shows fluxes during a snow warming and melt sequence in spring. The snow accumulation period (Fig. 3.9) shows a characteristic prairie weather pattern of highly variable meteorology associated with the passage of frontal systems.

On 17 December the air temperature warmed to slightly above freezing, then dropped dramatically with strong winds to below  $-20^{\circ}\text{C}$  in about 12 hours. During this cooling period snowfall and blowing snow were recorded and the lower surface boundary layer remained well mixed. Over the next two days the temperature dropped below  $-30^{\circ}\text{C}$  (by 20 December) with lower wind speeds and a stable lower surface boundary layer forming. During short periods around mid-day, the magnitude of net radiation was small but negative (peak  $-20$  to  $-90\text{ W m}^{-2}$ ), however at other times it was positive, reaching  $40\text{ W m}^{-2}$ , while staying smaller than  $10\text{ W m}^{-2}$  during cloudy nights. Turbulent fluxes are enhanced over that expected from smooth snow covers because of exposed vegetation (snow depth  $<10\text{ cm}$ ,

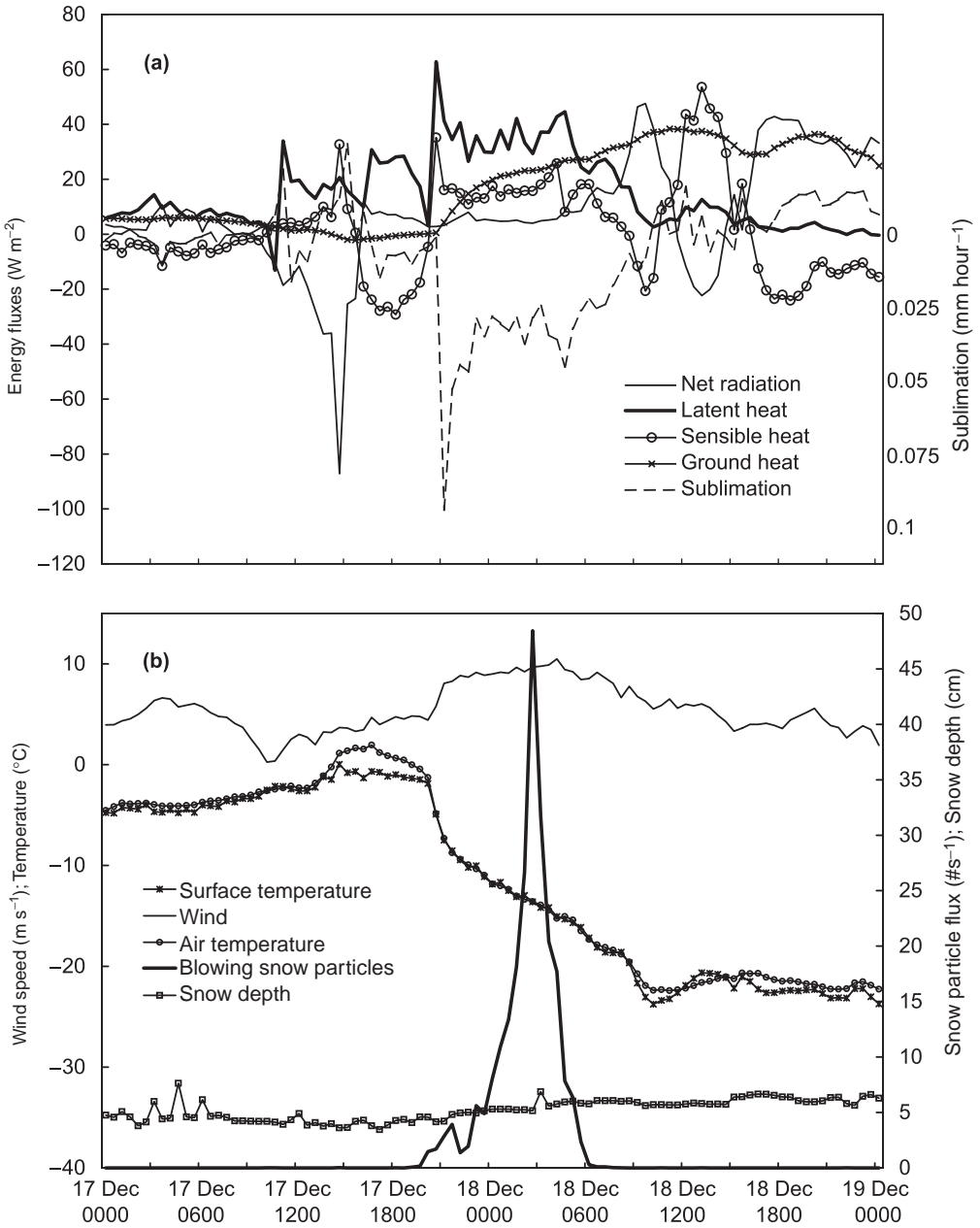


Figure 3.9. Direct measurements made during a snow accumulation period with blowing snow in December, 1998, Kernan Farm, Saskatoon, Saskatchewan, Canada. (a) Fluxes of net radiation, latent heat, and sensible heat, measured 1 m (net radiation) and 2 m (turbulent fluxes) above the snow cover, as well as ground heat flux measured 5 cm into the soil and (b) snow surface temperature, air temperature, and wind speed measured 1.3 m above the snow surface as well as blowing snow particle flux (measured 0.2 m above the snow surface) and snow depth.

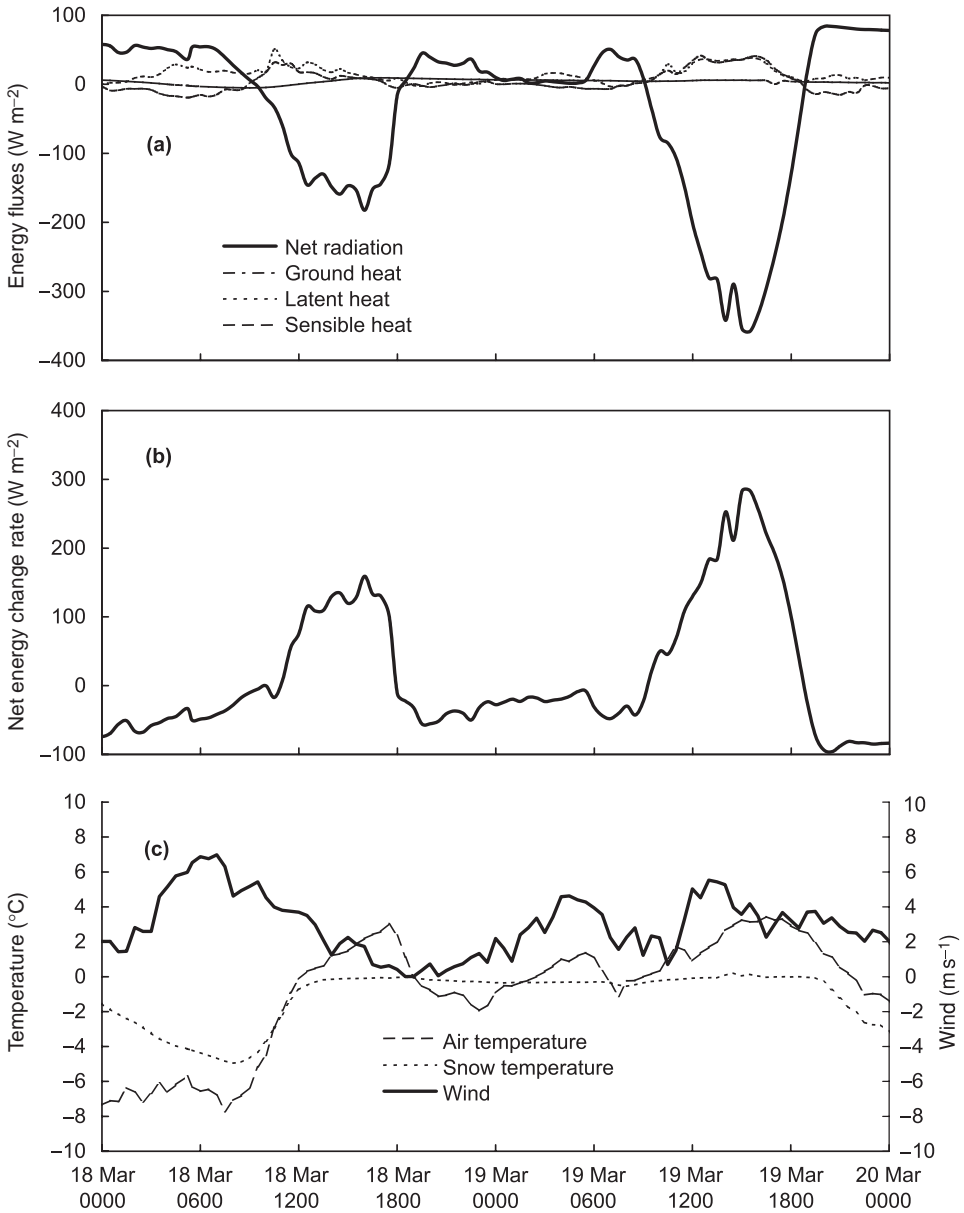


Figure 3.10. Direct measurements made during a snowmelt period in March, 1999, Kernen Farm, Saskatoon, Saskatchewan, Canada. (a) Fluxes of net radiation, latent heat, and sensible heat, measured 1 m (net radiation) and 2 m (turbulent fluxes) above the snow cover, as well as ground heat flux measured 5 cm into the soil, (b) net change rate of the snowpack's internal energy per unit area ( $dH/dt$ ). Positive values correspond to either warming or melting (cf. Equation 3.2), and (c) snow temperature at mid-pack depth as well as air temperature and wind speed measured 1.3 m above the snow surface.

patchy grass height approximately 25 cm) and are strongly affected by the occurrence of blowing snow. During the blowing snow event from 17 to 18 December, latent heat fluxes peak at  $60 \text{ W m}^{-2}$  and become small or negligible after that.

Sensible heat flux peaks at up to  $50 \text{ W m}^{-2}$  during cold, relatively calm, negative radiation periods (18–20 December). During cold, relatively calm, positive radiation periods, sensible heat is generally slightly negative, with peak values at  $-30 \text{ W m}^{-2}$  but most often not lower than  $-20 \text{ W m}^{-2}$ . A notable flux in this early winter period is the consistently positive ground heat flux into the snowpack, which becomes prominent ( $30\text{--}40 \text{ W m}^{-2}$ ) as cooling of snow and air proceeds (18–20 December). The blowing snow event did not result in a large increase in snow depth but density increased from near 100 to  $140 \text{ kg m}^{-3}$  due to the impact of saltating snow particles and subsequent sintering.

An exemplary snowmelt period (Fig. 3.10) occurred in March 1999 over a smooth, continuous snow cover (average depth = 14.5 cm, density =  $330 \text{ kg m}^{-3}$ ). Internal temperatures show that the snowpack warmed from  $-5 \text{ }^\circ\text{C}$  on 18 March to isothermal conditions as temperatures reached nearly  $0 \text{ }^\circ\text{C}$  on 19 March. The magnitude of daytime net radiation was large but negative, peaking at  $-182 \text{ W m}^{-2}$  on 18 March (cloudy) and  $-360 \text{ W m}^{-2}$  on 19 March (mostly clear). The preceding melt was a small blowing snow event (wind speed peak  $7 \text{ m s}^{-1}$ ) early on 18 March. The largest latent heat fluxes of the period ( $50 \text{ W m}^{-2}$ ) occurred during this event. The magnitude ( $<6 \text{ W m}^{-2}$ ) of the ground heat flux was quite small on both days, becoming slightly negative and thus directed to the soil as the snowpack warmed. Despite wind speeds of up to  $5.5 \text{ m s}^{-1}$ , turbulent fluxes during the melt were small and similar in size (peak  $40 \text{ W m}^{-2}$ ), much smaller than the magnitude of net radiation. The net energy change rate shows a large positive input to the snowpack on both days (see Equation 3.1). On 18 March warming snow temperatures suggest that this positive input increased the internal energy of the snowpack while constant internal temperatures on 19 March imply that most went into snowmelt (see Equation 3.2). This melt period was ephemeral and the snowpack returned to subfreezing conditions at the end of 19 March.

### *Modeling aspects*

Relatively uniform, level prairie snow covers should be one of the most successful types of snow for physical models; however, the complexity of prairie snow phenomena have resulted in several modeling challenges towards which long-term process research has been directed (Male and Gray, 1975, 1981; Pomeroy *et al.*, 1998b). Shook and Gray (1994) described the variation of depth and density and the influence of covariance between these properties in determining areal snow mass. Granger and Male (1978) measured the turbulent exchange over melting prairie snow and derived stability corrections for eddy diffusivities for water vapor and

heat with respect to momentum transfer; these corrections dampened the turbulent exchange from the normal log-linear formulations (e.g. Webb, 1970). Shook (1993, 1995) studied the depletion of the snow-covered area during melt and showed that changes in areal albedo can be adequately explained by the decrease in the snow-covered area and the assumption that albedo does not change significantly during melt. Shook (1995) found that the advection of sensible heat could contribute substantial melt energy when snow cover was incomplete. Pomeroy *et al.* (1998b) examined the performance of certain land surface schemes for prairie snowmelt and found that turbulent fluxes and ground heat flux were generally overestimated.

### 3.5.5 Boreal forest

*John W. Pomeroy and Richard J. Harding*

#### *Relevance and characteristics*

The boreal forest in winter is a complex mosaic of land surface types varying from closed coniferous canopies, mixed-wood deciduous forests, sparsely vegetated areas (clearings, wetlands, clear-cuts, burns) to ice and snow-covered lakes. At roughly 20% of the earth's land area, the boreal forest is the largest terrestrial type of land cover and extends in a circumpolar band across North America, Europe, and Asia. Canada, Russia, and the Scandinavian countries are dominated by boreal forest, although in most cases it lies to the north of major population centers. Economic activities in the boreal forest center on forest harvesting, tourism, and mining, yet many boreal forests retain an indigenous aboriginal population whose members conduct aspects of a traditional hunting, fishing, and gathering lifestyle. The large number of lakes and rivers (up to 40% of some boreal regions are covered by water) promote fishing and water transport that has been fundamental to the development of northern Canada and Siberia. Recent environmental concerns focus on the extensive clearcutting of boreal forest in Canada and Russia, episodic acidic precipitation (including snow) from anthropogenic pollution, and the apprehension that climate warming will result in a major northward shift in the boreal climate zone and loss of forest lands in the southern boreal forest.

One distinction of the boreal forest in comparison to more temperate forests is its long snow-covered period and cold winter temperatures (Harding and Pomeroy, 1996). The depth, density, and duration of snow cover is ecologically important to mammals and various microbial life-forms in this forest; in some cases the snow cover provides a thermally moderated habitat, in others a means of avoiding predators (Jones *et al.*, 2001). Boreal forest productivity and carbon cycling are strongly influenced by the supply of available nitrogen and soil moisture. Snow influences productivity and carbon cycling by providing, upon melt and

infiltration, a significant portion of the annual water and inorganic nitrogen input (Pomeroy *et al.*, 1999a). The global boreal forest exerts a strong control on climate and because of its low winter albedo, its removal and the resulting higher albedo in spring might result in a cooling of the Northern Hemisphere (Thomas and Rowntree, 1992). Snowmelt provides 40–60% of annual streamflow from boreal forests, with increases in snowmelt runoff of 24–75% when forest cover is removed (Hetherington, 1987).

Boreal forest snow covers are strongly influenced by the forest canopy, its interception of snow and radiation and dampening of wind speed and mixing above the snowpack's surface. Pomeroy *et al.* (1998a) observed in a mixed range of boreal forest cover types that 20–65% of cumulative snowfall was intercepted in early winter, and 10–45% of snowfall sublimated over the season. Leaf area strongly controls interception efficiency (Hedstrom and Pomeroy, 1998) and clearcutting or conversion of coniferous stands to deciduous species reduces interception to insignificant levels (Pomeroy and Granger, 1997). The energetics of intercepted snow in the boreal forest have been studied by Nakai *et al.* (1993, 1994, 1999), Lundberg and Halldin (1994), Harding and Pomeroy (1996), Pomeroy and Dion (1996), Pomeroy *et al.* (1998a) and Parviainen and Pomeroy (2000). These studies show that the albedo of snow-covered forest canopies is low ( $<0.2$ ), that sublimation rates up to  $3 \text{ kg m}^{-2} \text{ d}^{-1}$  are possible from snow-covered canopies and that the direction and magnitude of sensible and latent heat fluxes are influenced by the presence of snow in the canopy because it represents a “wetter,” cooler surface than a snow-free canopy. Parviainen and Pomeroy (2000) suggest that sublimation is driven by local-scale advection of sensible heat from exposed branches heated in the sun to intercepted snow clumps and that the efficiency of this advection is related to the fractal geometry of intercepted snow clumps (Pomeroy and Schmidt, 1993).

Studies of snow under the canopy have been directed towards snow accumulation and melt prediction. Boreal forest snow covers have relatively low coefficients of variation of snow water equivalent (0.04–0.14) and maximum densities near  $200 \text{ kg m}^{-3}$  (Pomeroy *et al.*, 1998b). At small scales, the snow water equivalent generally decreases with distance from coniferous tree stems (Woo and Steer, 1986; Jones, 1987; Sturm, 1992) and at stand scales it decreases with increasing canopy density (Kuz'min, 1960; Pomeroy and Gray, 1995). The forest cover attenuates the magnitude of incoming shortwave radiation and large-scale advection of warm air, reducing the “connectivity” between subcanopy snow and the atmosphere. Ni *et al.* (1997) and Pomeroy and Dion (1996) have measured and modeled winter subcanopy radiation and found its magnitude greatly reduced from the above canopy values and strongly dependent on solar zenith angle, leaf area, and needle orientation. Typically, subcanopy net radiation in a mature conifer stand is one-tenth that

above the canopy at the time of snowmelt. Davis *et al.* (1997), Hardy *et al.* (1997a, b), and Metcalfe and Buttle (1995, 1998) have measured and modeled snow ablation under boreal forest canopies and conclude that though the magnitude of net radiation is strongly reduced in forests and decreases with increasing canopy density, it still comprises the largest component of the energy balance because the subcanopy snow albedo drops substantially during melt as forest leaf litter and debris in the snowpack are exposed and because subcanopy turbulent fluxes are extremely small in magnitude and usually of the opposite direction. Faria *et al.* (2000) suggest that because subcanopy snowmelt energy and the pre-melt snow water equivalent have a spatial covariance, depletion of the snow-covered area is accelerated as the covariance increases. Pomeroy and Granger (1997) compared melt rates in various forest types and found that melt timing was accelerated three-fold in a clear-cut compared to under a mature boreal forest canopy because the net melt energy was up to four times greater in the clear-cut.

#### Site

Beartrap Creek (550 m a.s.l.) is a research basin, located at 54° N, 106° W, near the village of Waskesiu Lake, in Prince Albert National Park, Saskatchewan, Canada. The site has been the subject of intense investigations of boreal forest hydrology and climate under the Mackenzie global energy and water cycle experiment (MAGS), Prince Albert model forest hydrology study, and boreal ecosystem-atmosphere study (BOREAS). The region has a subhumid continental climate with six months of snow cover during a cold dry winter that experiences few melt events until April. Mean annual precipitation is 463 mm w.e. of which 33% occurs as winter snowfall. Topography is rolling with 700 m of local relief. Forest cover is typical of mature southern boreal forest: pine and mixed stands of aspen and white spruce on uplands, spruce, larch, and open muskeg in lowlands and about 15% covered by lakes.

The site studied is a mature, slightly open jack pine (*Pinus banksiana*) stand, 16–22 m tall with a winter leaf and stem area index of  $2.2 \text{ m}^2 \text{ m}^{-2}$  and canopy coverage of 82%. The fetch is level and uniform for about 100 m. Experiments were conducted in March, 1994 and 1996, using a canopy access tower (27 m). At the tower top two eddy correlation flux systems were installed, an Institute of Hydrology “Hydra” system for sensible and latent heat and a Gill Instruments “Solent” 3-axis sonic anemometer (Harding and Pomeroy, 1996). Above canopy net radiation and ground heat flux were measured using radiation and energy balance systems “REBS” net radiometers and heat flux plates and below canopy net radiation was measured using a Delta “T” tube net radiometer. Above canopy wind speed was measured using an RM Young propeller anemometer and temperature using a Vaisala HMP35CF hygro-thermometer. The intercepted snow load

was measured using a suspended full size pine tree, which was weighed with an in-line force transducer (Hedstrom and Pomeroy, 1998). Weight of snow on the tree (kg) was converted to an areal mass ( $\text{kg m}^{-2}$ ) using an empirical conversion developed from comparing event-based snow interception on the single tree to areal interception determined from above canopy snowfall measurements and changes in snow accumulation along a line of 25 snow survey points in subfreezing conditions.

### *Energy balance*

Two sets of energy balance and related surface conditions are shown. Figure 3.11 shows sensible and latent heat flux measurements made with a Hydra and checked against a Solent sonic anemometer along with net radiation above the canopy over a five day period in late March 1994. Fresh snowfall resulted in an initial intercepted load of about  $4.5 \text{ kg m}^{-2}$  on 27 March which then sublimated in temperatures ranging from  $-13$  to  $0^\circ\text{C}$  until the end of 29 March, when above freezing temperatures ( $5^\circ\text{C}$ ) resulted in melt and the unloading of any remaining snow.

Daily maximum temperatures then increased dramatically to  $17^\circ\text{C}$  on 31 March resulting in some early melt under the canopy. Four days had high net radiation inputs, i.e. negative peaks ranging from  $-450$  to  $-500 \text{ W m}^{-2}$ , while 28 March was overcast with a peak net radiation of only  $-100 \text{ W m}^{-2}$ . When snow was in the canopy (27–29 March), daytime latent heat fluxes were directed away from the surface at approximately one-half the magnitude of net radiation. Sensible heat fluxes over the snow-covered canopy were similar in magnitude and direction to latent fluxes on the high-insolation days (27 and 29 March) but negligible on 28 March when low insolation resulted in minimal canopy heating. When the canopy snow load ablated (30 March), the daytime magnitude of sensible heat flux remained half that of net radiation but latent heat became negligible early in the day and directed downward later in the day. On the 31 March sensible heat behavior was unchanged but latent heat became directed upward at one-half the magnitude of sensible heat. This may reflect evaporation from melting snow beneath the canopy or, more likely given the magnitude, transpiration from the pine canopy induced by extraordinarily warm temperatures. The weighed tree did show some weight loss in this period reflecting desiccation due to evapotranspiration.

Figure 3.12 shows a consistently subfreezing sequence from the same site on 16–18 March 1996. A Solent sonic anemometer measured sensible heat fluxes (not latent) and the ablation rate of intercepted snow was measured using the weighed tree. The ablation rate was converted to equivalent energy units (flux) as if all the energy was consumed for phase change to vapor (a reasonable assumption given the  $-15$  to  $-1^\circ\text{C}$  air temperatures).

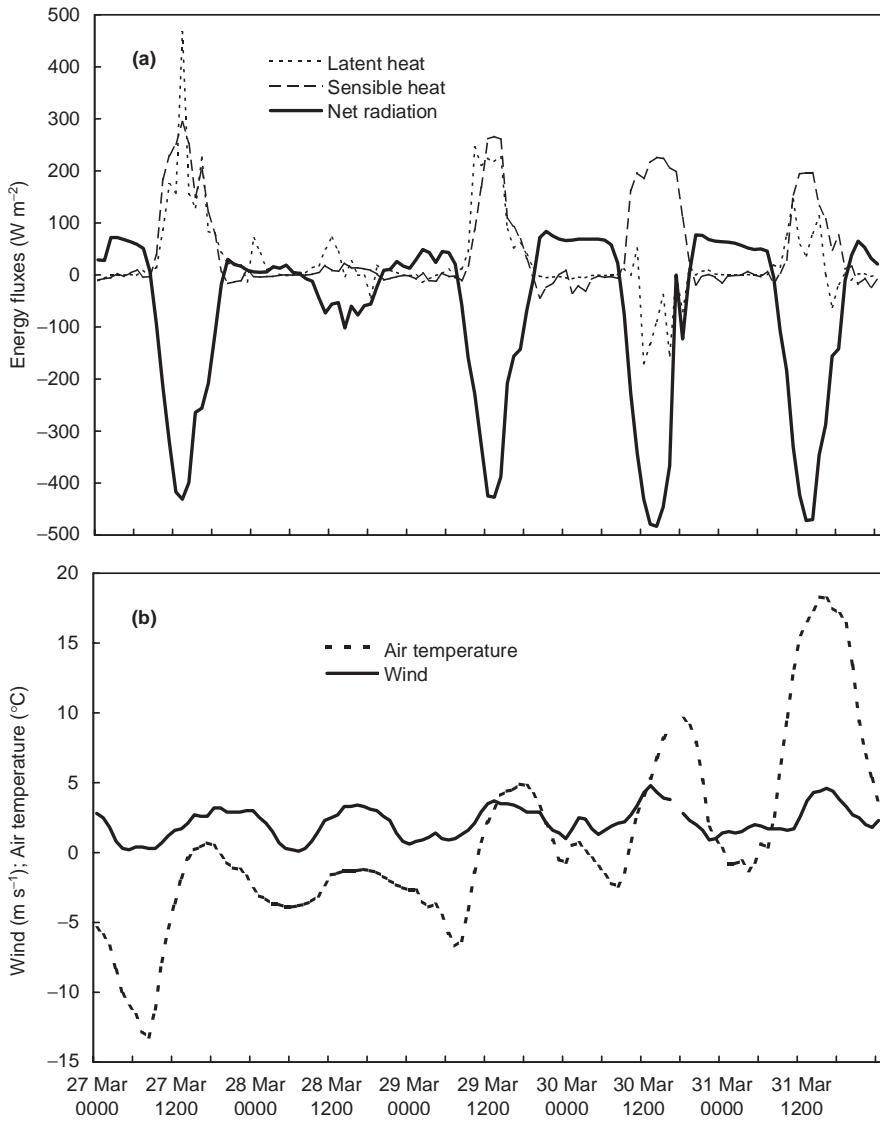


Figure 3.11. Fluxes and climate measured above a jack pine stand in the southern boreal forest of Saskatchewan, Canada, March, 1994. (a) Latent heat, sensible heat, and net radiation fluxes measured five meters above an initially snow-covered canopy and (b) air temperature and wind speed measured five meters above the canopy.

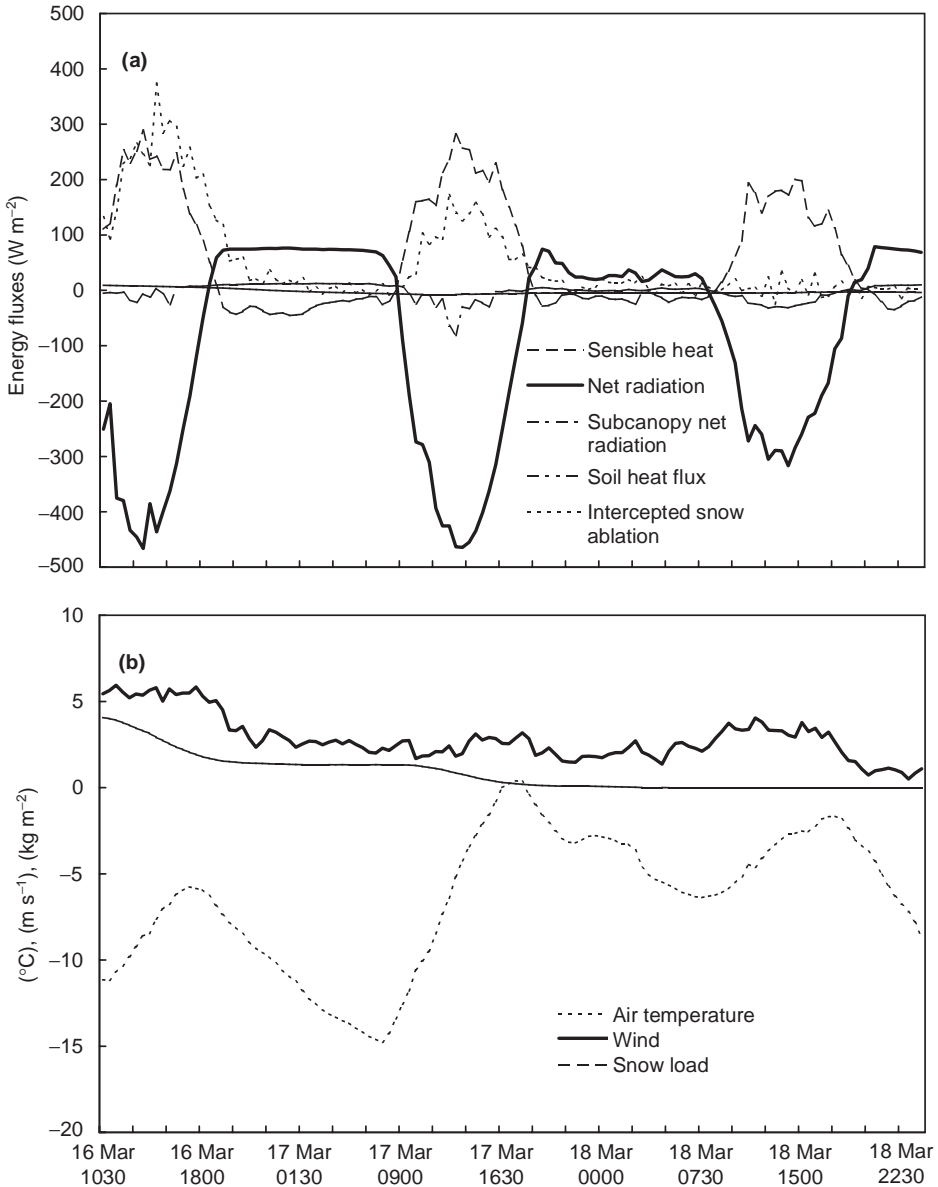


Figure 3.12. Fluxes about a boreal jack pine canopy, Saskatchewan, Canada, March, 1996. (a) Sensible heat, net radiation, subcanopy net radiation, ground heat flux, and estimated latent heat flux from intercepted snow ablation. Above canopy fluxes were measured 5 m above the canopy, below canopy radiation 1 m above the snow cover and ground heat flux 5 cm into the soil. Intercepted snow ablation was measured using a weighed, suspended full-size jack pine tree. (b) Air temperature and wind speed measured 5 m above the pine canopy. Intercepted snow load measured using a weighed, suspended pine tree.

Subcanopy net radiation and ground heat flux were also measured. An initial snow load of  $4.2 \text{ kg m}^{-2}$  ablated to  $1.5 \text{ kg m}^{-2}$  at the end of 16 March (strong winds, cold temperatures, and high insolation) and completely ablated by the end of 17 March. In this case sensible heat flux showed similar behavior to that in Fig. 3.11, at about one-half the magnitude of net radiation when the canopy is snow covered, increasing to three-quarters when snow free. Latent heat flux estimated from ablation equaled the sensible heat magnitude on the first (most snow-covered) day, then dropped to one-half the sensible magnitude on the second day and became negligible on the third day (snow-free canopy). Subcanopy net radiation was never more than one-tenth that of above canopy values, but remained slightly positive on 16 March when fresh snow covered the canopy and, along with a cool air mass, suppressed canopy temperatures and therefore downward longwave radiation. Ground heat fluxes were extremely small in magnitude and slowly fluctuated around zero.

#### *Modeling aspects*

The snow-covered canopy represents a separate snow layer that warrants its own mass and energy balance but is not represented by many land surface schemes (Essery, 1997). For instance, the ECMWF model recently used a routine that set the boreal forest canopy albedo to a high value (0.8) after a snowfall. When corrected to a much lower and appropriate value, air temperature predictions improved dramatically over the boreal region (Betts and Ball, 1997). CLASS and SiB are exceptions that do consider canopy snow, but calculate the snow interception process in a similar manner to rainfall and therefore underestimate intercepted load by an order of magnitude for large snowfalls (Pomeroy *et al.*, 1998b). The interception models of Calder (1990) and Hedstrom and Pomeroy (1998) provide possible corrections to these schemes. Turbulent fluxes above a snow-covered canopy can be calculated using a resistance scheme with resistance set at 10 times the value of a rain-wetted canopy (Lundberg *et al.*, 1998) or by varying the ratio of bulk transfer coefficients with snow load (Nakai *et al.*, 1999). Parviainen and Pomeroy (2000) modeled the Beartrap Creek pine site using a nested control volume approach in which an energy and mass balance was conducted for an intercepted snow control volume, using the Reynolds number to calculate turbulent transfer between the intercepted snow and the atmosphere. The CLASS land surface scheme was then coupled to this small-scale calculation to calculate turbulent transfer between the canopy and atmosphere. Using a geometric radiative transfer model (GORT) to calculate subcanopy radiation (Ni *et al.*, 1997) and SNTHERM to calculate snow-pack heat fluxes, snowmelt modeling was successful when snow surface albedo was reduced during melt and turbulent heat fluxes were given small values (Hardy *et al.*, 1997b).

## References

- Ambach, W. (1974). The influence of cloudiness on the net radiation balance of a snow surface with high albedo. *J. Glaciol.*, **13**(67), 73–84.
- Andreas, E. L. (1989). A physical bound on the Bowen ratio. *J. Appl. Meteorol.*, **28**(11), 1252–1254.
- Andreas, E. L. and Cash, B. A. (1996). A new formulation for the Bowen ratio over saturated surfaces. *J. Appl. Meteorol.*, **35**(8), 1279–1289.
- Bartelt, P. and Lehning, M. (2002). A physical SNOWPACK model for the Swiss avalanche warning; Part I: numerical model. *Cold Reg. Sci. Technol.*, **35**(3), 123–145.
- Beljaars, A. C. M. and Holtslag, A. A. M. (1991). Flux parametrization and land surfaces in atmospheric models. *J. Appl. Meteorol.*, **30**, 327–341.
- Betts, A. K. and Ball, J. H. (1997). Albedo over the boreal forest. *J. Geophys. Res.*, **102**(D24), 28 901–28 909.
- Bintanja, R. (1998). The contribution of snowdrift sublimation to the surface mass balance of Antarctica. *Ann. Glaciol.*, **27**, 251–259.
- Bintanja, R. and van den Broeke, M. R. (1995). Momentum and scalar transfer coefficients over aerodynamically smooth Antarctic surfaces. *Bound.-Lay. Meteorol.*, **74**, 89–111.
- Bintanja, R. and van den Broeke, M. R. (1996). The influence of clouds on the radiation budget of ice and snow surfaces in Antarctica and Greenland in summer. *Int. J. Climatol.*, **16**, 1281–1296.
- Bowling, L. C., Pomeroy, J. W., and Lettenmaier, D. P. (2004). Parameterisation of the sublimation of blowing snow in a macroscale hydrology model. *J. Hydrometeorol.*, **5**, 745–762.
- Brown, T. and Pomeroy, J. W. (1989). A blowing snow particle detector. *Cold Reg. Sci. Technol.*, **16**, 167–174.
- Brun, E., David, P., Sudul, M., and Brunot, G. (1992). A numerical model to simulate snow-cover stratigraphy for operational avalanche forecasting. *J. Glaciol.*, **38**(128), 13–22.
- Brun, E., Martin, E., Simon, V., Gendre, C., and Coléou, C. (1989). An energy and mass model of snow cover suitable for operational avalanche forecasting. *J. Glaciol.*, **35**(121), 333–342.
- Brutsaert, W. (1975). On a derivable formula for long wave radiation from clear skies. *Water Resources Res.*, **11**, 742–744.
- Calanca, P. and Heuberger, R. (1990). *Glacial Climate Research in the Tianshan* (ed. Ohmura, A. *et al.*). Zürcher Geographische Schriften (ZGS), Heft 38. Zürich: Swiss Federal Institute of Technology ETHZ, pp. 60–72.
- Calder, I. R. (1990). *Evaporation in the Uplands*. Chichester: Wiley, p. 144.
- Chamberlain, A. C. (1983). Roughness length of sea, sand and snow. *Bound.-Lay. Meteorol.*, **25**, 405–409.
- Claussen, M. (1991). Local advection processes in the surface layer of the marginal ice zone. *Bound.-Lay. Meteorol.*, **54**, 1–27.
- Davis, R. E., Hardy, J. P., Ni, W., *et al.* (1997). Variation of snow cover ablation in the boreal forest: a sensitivity study on the effects of conifer canopy. *J. Geophys. Res.*, **102**(D24), 29 389–29 398.
- de la Casinière, A. C. (1974). Heat exchange over a melting snow surface. *J. Glaciol.*, **13**, 55–72.
- Dery, S. J. and Yau, M. K. (2002). Large-scale mass balance effects of blowing snow and surface sublimation. *J. Geophys. Res.*, **107**(D23), 4679.

- Dery, S. J., Taylor, P. A., and Xiao, J. (1998). The thermodynamic effects of sublimating blowing snow in the atmospheric boundary layer. *Bound.-Lay. Meteorol.*, **89**, 251–283.
- Doorschot, J. (2002). Mass transport of drifting snow in high alpine environments. Ph.D. Thesis, Swiss Federal Institute of Technology ETHZ, Zürich. <http://e-collection.ethbib.ethz.ch/show?type=diss&nr=14515>
- Doorschot, J. and Lehning, M. (2002). Equilibrium saltation: mass fluxes, aerodynamic entrainment, and dependence on grain properties. *Bound.-Lay. Meteorol.*, **104**, 111–130.
- Doorschot, J., Raderschall, N., and Lehning, M. (2001). Measurement and one-dimensional model calculations of snow transport over a mountain ridge. *Ann. Glaciol.*, **32**, 153–158.
- Dozier, J. (1980). A clear sky spectral solar radiation model for snow-covered mountainous terrain. *Water Resources Res.*, **16**, 709–718.
- Durand, Y., Brun, E., Mérindol, L., *et al.* (1993). A meteorological estimation of relevant parameters for snow models. *Ann. Glaciol.*, **18**, 65–71.
- Durand, Y., Guyomarc'h, G., and Mérindol, L. (2001). Numerical experiments of wind transport over a mountainous instrumented site: I. Regional scale. *Ann. Glaciol.*, **32**, 187–194.
- Dyunin, A. K., Kvon, Ya. D., Zhilin A. M., and Komorov, A. A. (1991). Effect of snow drifting on large-scale aridization. In *Glaciers–Ocean–Atmosphere Interactions* (ed. Kotlyakov, V. M., Ushakov, A., and Glasovsky, A.). IAHS Publication No. 208. Wallingford: IAHS Press, pp. 489–494.
- Ebert, E. E. and Curry, J. A. (1993). An intermediate one-dimensional thermodynamic sea ice model for investigating ice–atmosphere interactions. *J. Geophys. Res.*, **98**(C6), 10 085–10 109.
- Elder, K., Dozier, J., and Michaelsen, J. (1989). Spatial and temporal variation of net snow accumulation in a small alpine watershed. Emerald Lake basin, Sierra Nevada, California, U.S.A. *Ann. Glaciol.*, **13**, 56–63.
- Essery, R. (1997). Modelling fluxes of momentum, sensible heat and latent heat over heterogeneous snow cover. *Q. J. Roy. Meteorol. Soc.*, **123**, 1867–1883.
- Essery, R., Li, L. and Pomeroy, J. W. (1999). A distributed model of blowing snow over complex terrain. *Hydrol. Process.*, **13**(14–15), 2423–2438.
- Essery, R. and Pomeroy, J. W. (2004). Vegetation and topographic control of wind-blown snow distributions in distributed and aggregated simulations for an Arctic tundra basin. *J. Hydrometeorol.*, **5**, 734–744.
- Faria, D. A., Pomeroy, J. W., and Essery, R. L. H. (2000). Effect of covariance between ablation and snow water equivalent on depletion of snow-covered area in a forest. *Hydrol. Process.*, **14**(15), 2683–2695.
- Fierz, C., Plüss, C., and Martin, E. (1997). Modelling the snow cover in complex alpine topography. *Ann. Glaciol.*, **25**, 312–316.
- Föhn, P. M. B. (1973). Short term snow melt and ablation derived from heat- and mass-balance measurements. *J. Glaciol.*, **12**(65), 275–289.
- Föhn, P. M. B. (1977). Representativeness of precipitation measurements in mountainous areas. In *Proc. Joint Scientific Meeting on Mountain Meteorology and Biometeorology AMS, SGBB, SSG*, Interlaken, Switzerland, 10–14 June 1976 (ed. Primault, B.). Geneva: Blanc et Wittwer, pp. 61–71.
- Föhn, P. M. B. (1985). Besonderheiten des Schneeniederschlages. In *Der Niederschlag in der Schweiz*. Beitr. Geol. Schweiz – Hydrol., vol. 31, Bern: Kümmerly und Frey, pp. 87–96.

- Föhn, P. M. B. (1992). Climatic change, snow cover and avalanches. In *Greenhouse-Impact on Cold-Climate Ecosystems and Landscape* (ed. Boer, M. and Koster, E.). Catena supplement 22. Cremlingen-Destedt: Catena, pp. 11–21.
- Föhn, P. and Hächler, P. (1978). Prédiction de grosses avalanches au moyen d'un modèle déterministe-statistique. In *Comptes Rendues de la Deuxième Rencontre Internationale sur la Neige et les Avalanches*, Grenoble, France, 12–14 avril 1978. Grenoble: Association Nationale pour l'Etude de la Neige et des Avalanches (ANENA), pp. 151–165.
- Gardiner, B. G. (1987). Solar radiation transmitted to the ground through cloud in relation to surface albedo. *J. Geophys. Res.*, **92**(D4), 4010–4018.
- Garratt, J. R. (1992). *The Atmospheric Boundary Layer*. Cambridge: Cambridge University Press.
- Gauer, P. (1998). Blowing and drifting snow in alpine terrain: Numerical simulation and related field measurements. *Ann. Glaciol.*, **26**, 174–178.
- Gauer, P. (2001). Numerical modeling of blowing and drifting snow in Alpine terrain. *J. Glaciol.*, **47**(156), 97–110.
- Grainger, M. E. and Lister, H. (1966). Wind speed, stability and eddy viscosity over melting ice surfaces. *J. Glaciol.*, **6**(43), 101–127.
- Granger, R. J. and Male, D. H. (1978). Melting of a prairie snowpack. *J. Appl. Meteorol.*, **17**, 1833–1842.
- Gray, D. M. (ed.). (1970). *Handbook on the Principles of Hydrology*. Ottawa: Canadian National Committee for the International Hydrological Decade.
- Harding, R. J. (1986). Exchanges of energy and mass associated with a melting snow pack. In *Modelling Snowmelt-Induced Processes* (ed. Morris, E. M.). IAHS Publication No. 155. Wallingford: IAHS Press, pp. 3–15.
- Harding, R. J. and Pomeroy, J. W. (1996). The energy balance of the winter boreal landscape. *J. Climate*, **9**, 2778–2787.
- Hardy, J. P., Davis, R. E., Jordan, R., *et al.* (1997a). Snow ablation modelling at the stand scale in a boreal jack pine forest. *J. Geophys. Res.*, **102**(D24), 29 397–29 406.
- Hardy, J. P., Davis, R. E., Jordan, R., Li, X., and Woodcock, C. (1997b). Snow ablation modelling in conifer and deciduous stands of the boreal forest. *Proc. Western Snow Conf.*, **65**, 114–124.
- Hedstrom, N. R. and Pomeroy, J. W. (1998). Accumulation of intercepted snow in the boreal forest: measurements and modelling. *Hydrol. Process.*, **12**, 1611–1625.
- Heinemann, G. (1989). Über die Rauigkeitslänge  $z_0$  der Schneeoberfläche des Filchner-Ronne Schelfeises. *Polarforschung*, **59**, 17–24.
- Hetherington, E. D. (1987). The importance of forests in the hydrological regime. *Can. Bull. Fish. Aquatic Sci.*, **215**, 179–211.
- Inoue, J. (1989). Surface drag over the snow surface of the Antarctic Plateau. 1. Factors controlling surface drag over the katabatic wind region. *J. Geophys. Res.*, **94**(D2), 2207–2217.
- Iqbal, M. (1983). *An Introduction to Solar Radiation*. Toronto: Academic Press.
- Joffre, S. M. (1982). Momentum and heat transfers in the surface layer over a frozen sea. *Bound.-Lay. Meteorol.*, **24**, 211–229.
- Jones, H. G. (1987). Chemical dynamics of snowcover and snowmelt in a boreal forest. In *Seasonal Snowcovers: Physics, Chemistry, Hydrology* (ed. Jones, H. G. and Orville-Thomas, W. J.). *NATO ASI Series C*, vol. 211. Dordrecht: Reidel Publishing, pp. 531–574.

- Jones, H. G., Pomeroy, J. W., Walker, D. A., and Hoham, R. (eds.). (2001). *Snow Ecology: an Interdisciplinary Examination of Snow-Covered Ecosystems*. Cambridge: Cambridge University Press.
- Jordan, R. E., Andreas, E. L., Fairall, C. W., *et al.* (2003). Modeling surface exchange and heat transfer for the shallow snow cover at SHEBA. In *Seventh Conference on Polar Meteorology and Oceanography*, Hyannis, MA (CD-ROM of preprints). Washington, DC: American Meteorological Society.
- Jordan, R. E., Andreas, E. L., and Makshtas, A. S. (1999). The heat-budget of snow-covered sea ice at North-pole 4. *J. Geophys. Res.*, **104**(D4), 7785–7806.
- Key, J. R., Silcox, R. A., and Stone, R. S. (1996). Evaluation of surface radiative flux parameterizations for use in sea ice models. *J. Geophys. Res.*, **101**(C2), 3839–3849.
- Kind, R. J. 1992. One-dimensional aeolian suspension above beds of loose particles – a new concentration-profile equation. *Atmos. Environ.*, **26A**, 927–931.
- King, J. C. 1990. Some measurements of turbulence over an Antarctic ice shelf. *Q. J. Roy. Meteor. Soc.*, **116**, 379–400.
- King, J. C. and Anderson, P. S. (1994). Heat and water vapour fluxes and scalar roughness lengths over an Antarctic ice shelf. *Bound.-Lay. Meteorol.*, **69**, 101–121.
- King, J. C., Anderson, P. S., Smith, M. C., and Mobbs, S. D. (1996). The surface energy and mass balance at Halley, Antarctica, during winter. *J. Geophys. Res.*, **101**(D14), 19 119–19 128.
- King, J. C. and Connolley, W. M. (1997). Validation of the surface energy balance over the Antarctic ice sheets in the U.K. Meteorological Office Unified Climate Model. *J. Climate*, **10**, 1273–1287.
- Kirnbauer, R., Blöschl, G., and Gutknecht, D. (1994). Entering the era of distributed snow models. *Nordic Hydrol.*, **25**, 1–24.
- Kondo, J. and Yamazawa, H. (1986). Bulk transfer coefficient over a snow surface. *Bound.-Lay. Meteorol.*, **34**, 123–135.
- König, G. (1985). Roughness length of an Antarctic ice shelf. *Polarforschung*, **55**, 27–32.
- König-Langlo, G. and Augstein, E. (1994). Parameterization of the downward longwave radiation at the Earth's surface in polar regions. *Meteorol. Z.*, **3**, 343–347.
- Konstantinov, A. R. (1966). *Isparenie v Prirode*. Leningrad: Gidrometeoizdat. Published 1968 as *Evaporation in Nature*. (English translation by Israel Programme for Scientific Translation, Jerusalem.)
- Konzelmann, T., van de Wal, R., Greuell, W., *et al.* (1994). Parameterization of global and longwave incoming radiation for the Greenland ice sheet. *Global Planet. Change*, **9**, 143–164.
- Kucherov, N. V. and Sternzat, M. S. (1959). The apparatus and method of investigations at stations North Pole 4 and North Pole 5. *Trudy. Arkt. Antarkt. Nauchno-Issl. Inst.*, **226**, 5–18. (In Russian; English translation available from the CRREL Library.)
- Kuz'min, P. P. (1960). *Formirovanie Snezhnogo Pokrova I Metody Opredeleniya Snegozasasov*, Leningrad. Published 1963 as *Snow Cover and Snow Reserves*. Washington, DC: National Science Foundation. (English translation by Israel Programme for Scientific Translation, Jerusalem.)
- Lee, L. W. (1975). Sublimation of snow in a turbulent atmosphere. Ph.D. Thesis, University of Wyoming, Laramie, WY.
- Lehning, M., Bartelt, P., Bethke, S., *et al.* (2004). Review of SNOWPACK and Alpine3D applications. In *Snow Engineering*, vol. V. (ed. Bartelt, P., Adams, E. E., Christen, M., Sack, R. L., and Sato, A.). Leiden: Balkema Publishers, pp. 299–307.

- Lehning, M., Bartelt, P., Brown, B., and Fierz, C. (2002a). A physical SNOWPACK model for the Swiss avalanche warning; Part III: Meteorological forcing, thin layer formation and evaluation. *Cold Reg. Sci. Technol.*, **35**(3), 169–184.
- Lehning, M., Bartelt, P., Brown, B., Fierz, C., and Satyawali, P. (2002b). A physical SNOWPACK model for the Swiss avalanche warning; Part II: Snow microstructure. *Cold Reg. Sci. Technol.*, **35**(3), 147–167.
- Li, L. and Pomeroy, J. W. (1997a). Estimates of threshold wind speeds for snow transport using meteorological data. *J. Appl. Meteorol.*, **36**, 205–213.
- Li, L. and Pomeroy, J. W. (1997b). Probability of occurrence of blowing snow. *J. Geophys. Res.*, **102**(D18), 21 955–21 964.
- Lindsay, R. W. (1998). Temporal variability of the energy balance of thick Arctic pack ice. *J. Climate*, **11**, 313–333.
- Liston, G. E. (1995). Local advection of momentum, heat and moisture during the melt of patchy snow covers. *J. Appl. Meteorol.*, **34**, 1705–1715.
- Liston, G. E. and Sturm, M. (1998). A snow-transport model for complex terrain. *J. Glaciol.*, **44**(148), 498–516.
- Lundberg, A., Calder, I., and Harding, R. (1998). Evaporation of intercepted snow: measurements and modelling. *J. Hydrol.*, **206**, 151–163.
- Lundberg, A. and Halldin, S. (1994). Evaporation of intercepted snow – an analysis of governing factors. *Water Resources Res.*, **30**, 2587–2598.
- Male, D. H. and Gray, D. M. (1975). Problems in developing a physically-based snowmelt model. *Can. J. Civil Eng.*, **2**, 474–488.
- Male, D. H. and Gray, D. M. (1981). Snowcover ablation and runoff. In *Handbook of Snow: Principles, Processes, Management and Use* (ed. Gray, D. M. and Male, D. H.). Toronto: Pergamon Press, pp. 360–436.
- Marks, D. and Dozier, J. (1992). Climate and energy exchange at the snow surface in the Alpine region of the Sierra Nevada. 2. Snow cover energy balance. *Water Resources Res.*, **28**, 3042–3054.
- Marsh, P. and Pomeroy, J. W. (1996). Meltwater fluxes at an Arctic forest tundra site. *Hydrol. Process.*, **10**, 1383–1400.
- Marsh, P., Pomeroy, J. W., and Neumann, N. (1997). Sensible heat flux and local advection over a heterogeneous landscape at an Arctic tundra site during snowmelt. *Ann. Glaciol.*, **25**, 132–136.
- Marshunova, M. S. and Mishin, A. A. (1994). Handbook of the radiation regime of the Arctic Basin (Results from the drift stations). *Technical Report APL-UW TR 9413*. Seattle, WA: Applied Physics Laboratory, University of Washington.
- Martin, E., Brun, E., and Durand, Y. (1994). Sensitivity of the French Alps snow cover to the variation of climatic variables. *Ann. Geophys.*, **12**, 469–477.
- Martin, E. and Lejeune, Y. (1997). Investigations on turbulent fluxes above the snow surface. *Ann. Glaciol.*, **26**, 179–183.
- Marty, C. (2000). Surface radiation, cloud forcing and greenhouse effect in the Alps. Ph.D. Thesis, Swiss Federal Institute of Technology ETHZ, Zürich. <http://e-collection.ethbib.ethz.ch/cgi-bin/show.pl?type=diss&nr=13609>
- Maykut, G. A. (1982). Large-scale heat exchange and ice production in the central Arctic. *J. Geophys. Res.*, **87**(C10), 7971–7984.
- Metcalfe, R. A. and Buttle J. M. (1995). Controls of canopy structure on snowmelt rates in the boreal forest. *Proc. Eastern Snow Conf.*, **52**, 249–257.
- Metcalfe, R. A. and Buttle, J. M. (1998). A statistical model of spatially distributed snowmelt rates in a boreal forest basin. *Hydrol. Process.*, **12**, 1701–1722.

- Michaux, J. L., Naaim-Bouvet, F., and Naaim, M. (2001). Drifting snow studies over a mountainous instrumented site: measurements and numerical model. *Ann. Glaciol.*, **32**, 175–181.
- Moore, R. D. and Owens, I. F. (1984). Controls on advective snowmelt in a maritime alpine basin. *J. Appl. Meteorol.*, **23**, 135–142.
- Morris, E. M. (1989). Turbulent transfer over snow and ice. *J. Hydrol.*, **105**, 205–223.
- Morris, E. M., Anderson, P. S., Bader, H.-P., Weilenman, P., and Blight, C. (1994). Modelling mass and energy exchange over polar snow using the DAISY model. In *Snow and Ice Covers: Interactions with the Atmosphere and Ecosystems* (ed. Jones, H. G., Davies, T. D., Ohmura, A., and Morris, E. M.). IAHS Publication No. 223. Wallingford: IAHS Press, pp. 53–60.
- Nakai, Y., Kitahara, H., Sakamoto, T., Saito, T., and Terajima, T. (1993). Evaporation of snow intercepted by forest canopies. *J. Jpn. Forest Soc.*, **75**, 191–200.
- Nakai, Y., Sakamoto, T., Terajima, T., Kitahara, H., and Saito, T. (1994). Snow interception by forest canopies: weighing a conifer tree with meteorological observation and analysis with Penman–Monteith formula. In *Snow and Ice Covers: Interactions with the Atmosphere and Ecosystems* (ed. Jones, H. G., Davies, T. D., Ohmura, A., and Morris, E. M.). IAHS Publication No. 223. Wallingford: IAHS Press, pp. 227–236.
- Nakai, Y., Sakamoto, T., Terajima, T., Kitamura, K., and Shirai, T. (1999). Energy balance above a boreal coniferous forest: a difference in turbulent fluxes between snow-covered and snow-free canopies. *Hydrol. Process.*, **13**, 515–529.
- National Snow and Ice Data Center (NSIDC). (1996). *Arctic Ocean Snow and Meteorological Observations from Drifting Stations: 1937, 1950–1991*, CD-ROM Version 1.0. Boulder, CO: University of Colorado.
- Nazintsev, Yu. L. (1963). On the role of thermal processes in sea ice melting and in the transformation of the relief of multiyear ice floes in the central Arctic (in Russian). *Prob. Arkt. Antarkt.*, **12**, 69–75. (In Russian; English translation available from the CRREL Library).
- Nazintsev, Yu. L. (1964). Thermal balance of the surface of the perennial ice cover in the central Arctic. *Trudy, Arkt. Antarkt. Nauchno-Issl. Inst.*, **267**, 110–126. (In Russian; English translation available from the CRREL Library).
- Neumann, N. and Marsh, P. (1998). Local advection of sensible heat in the snowmelt landscape of Arctic tundra. *Hydrol. Process.*, **12**, 1547–1560.
- Ni, W., Li, X., Woodstock, C. E., Roujean, J.-L., and Davis, R. E. (1997). Transmission of solar radiation in boreal conifer forests: measurements and models. *J. Geophys. Res.*, **102**(D24), 29 555–29 566.
- Ohmura, A. 2001. Physical basis for the temperature-based melt-index method. *J. Appl. Meteorol.*, **40**, 753–761.
- Oke, T. R. (1987). *Boundary Layer Climates*, 2nd edn. London: Routledge.
- Olyphant, G. and Isard, S. (1988). The role of advection in the energy balance of late-lying snowfields: Niwot Ridge, Front Range, Colorado. *Water Resources Res.*, **24**, 1962–1968.
- O'Neill, A. D. J. and Gray, D. M. (1973). Spatial and temporal variations of the albedo of a prairie snowpack. In *The Role of Snow and Ice in Hydrology: Proc., Banff Symposium*, vol. 1. Geneva-Budapest-Paris: UNESCO-WMO-IAHS, pp. 176–186.
- Owen, P. R. (1964). Saltation of uniform grains in air. *J. Fluid Mech.*, **20**, 225–242.
- Parviainen, J. and Pomeroy, J. W. (2000). Multiple-scale modelling of forest snow sublimation: initial findings. *Hydrol. Process.*, **14**(15), 2669–2681.

- Perovich, D. K., Grenfell, T. C., Light, B., and Hobbs, P. V. (2002). Seasonal evolution of the albedo of multiyear Arctic sea ice. *J. Geophys. Res.*, **107**(C10), 8044, doi:10.1029/2000JC000438.
- Persson, P. O. G., Fairall, C. W., Andreas, E. L., Guest, P. S., and Perovich, D. K. (2002). Measurements near the Atmospheric Surface Flux Group tower at SHEBA: near-surface conditions and surface energy budget. *J. Geophys. Res.*, **107**(C10), 8043, doi:10.1029/2000JC000705.
- Plüss, C. (1997). *The Energy Balance over an Alpine Snowcover – Point Measurements and Areal Distribution*. Zürcher Geographische Schriften (ZGS), Heft vol. 65. Zürich: Swiss Federal Institute of Technology ETHZ.
- Plüss, C. and Ohmura, A. (1997). Longwave radiation on snow-covered mountainous surfaces. *J. Appl. Meteorol.*, **36**, 818–824.
- Poggi, A. (1976). Heat balance in the ablation area of the Ampere Glacier (Kerguelen Islands). *J. Appl. Meteorol.*, **16**, 48–55.
- Pomeroy, J. W. (1989). A process-based model of snow drifting. *Ann. Glaciol.*, **13**, 237–240.
- Pomeroy, J. W. (1991). Transport and sublimation of snow in wind-scoured alpine terrain. In *Snow, Hydrology and Forests in High Alpine Areas* (ed. Bergmann, H., Lang, H., Frey, W., Issler, D., and Salm, B.). IAHS Publication No. 205. Wallingford: IAHS Press, pp. 131–140.
- Pomeroy, J. W., Davies, T. D., Jones, H. G., *et al.* (1999a). Transformations of snow chemistry in the boreal forest: accumulation and volatilization. *Hydrol. Process.*, **13**, 2257–2273.
- Pomeroy, J. W. and Dion, K. (1996). Winter radiation extinction and reflection in a boreal pine canopy: measurements and modelling. *Hydrol. Process.*, **10**, 1591–1608.
- Pomeroy, J. W. and Essery, R. (1999). Turbulent fluxes during blowing snow: field tests of model sublimation predictions. *Hydrol. Process.*, **13**, 2963–2975.
- Pomeroy, J. W., Essery, R. L. H., Gray, D. M., *et al.* (1999b). Modelling snow–atmosphere interactions in cold continental environments. In *Interactions Between the Cryosphere, Climate and Greenhouse Gases* (ed. Tranter, M., Armstrong, R., Brun, E., *et al.*). IAHS Publication No. 256. Wallingford: IAHS Press, pp. 91–101.
- Pomeroy, J. W. and Granger, R. J. (1997). Sustainability of the western Canadian boreal forest under changing hydrological conditions – I – Snow accumulation and ablation. In *Sustainability of Water Resources under Increasing Uncertainty* (ed. Rosjberg, D., Boutayeb, N., Gustard, A., Kundzewicz, Z., and Rasmussen, P.). IAHS Publication No. 240. Wallingford: IAHS Press, pp. 237–242.
- Pomeroy, J. W. and Gray, D. M. (1990). Saltation of snow. *Water Resources Res.*, **26**(7), 1583–1594.
- Pomeroy, J. W. and Gray, D. M. (1995). *Snowcover Accumulation, Relocation and Management*. NHRI Science Report No. 7. Saskatoon: National Hydrology Research Institute.
- Pomeroy, J. W., Gray, D. M., and Landine, P. G. (1993). The prairie blowing snow model: characteristics, validation, operation. *J. Hydrol.*, **144**, 165–192.
- Pomeroy, J. W., Gray, D. M., Shook, K. R., *et al.* (1998b). An evaluation of snow accumulation and ablation processes for land surface modelling. *Hydrol. Process.*, **12**(15), 2339–2367.
- Pomeroy, J. W., Hedstrom, N., and Parviainen, J. (1999c). The snow mass balance of Wolf Creek. In *Wolf Creek Research Basin: Hydrology, Ecology, Environment* (ed. Pomeroy, J. and Granger, R.). Saskatoon: National Water Research Institute, Minister of Environment, pp. 15–30.

- Pomeroy, J. W. and Li, L. (2000). Prairie and Arctic areal snow cover mass balance using a blowing snow model. *J. Geophys. Res.*, **105**(D21), 26 619–26 634.
- Pomeroy, J. W. and Male, D. H. (1992). Steady-state suspension of snow. *J. Hydrol.*, **136**, 275–301.
- Pomeroy, J. W., Marsh, P., and Gray, D. M. (1997). Application of a distributed blowing snow model to the Arctic. *Hydrol. Process.*, **11**, 1451–1464.
- Pomeroy, J. W., Parviainen, J., Hedstrom, N., and Gray, D. M. (1998a). Coupled modelling of forest snow interception and sublimation. *Hydrol. Process.*, **12**, 2317–2337.
- Pomeroy, J. W. and Schmidt, R. A. (1993). The use of fractal geometry in modelling intercepted snow accumulation and sublimation. *Proc. Eastern Snow Conf.*, **50**, 1–10.
- Raderschall, N. (1999). *Statistische Uebertragung von Modelldaten eines Numerischen Wettervorhersagemodells auf Alpine Standorte*. Diplomarbeit des Meteorologischen Instituts der Rheinischen Friedrich-Wilhelms-Universitaet Bonn, unpublished.
- Radionov, V. F., Bryazgin, N. N., and Aleksandrov, E. I. (1996). *The Snow Cover of the Arctic Basin*. St. Petersburg: Gidrometeoizdat. (In Russian; English translation available as: Radionov, V. F., Bryazgin, N. N., and Aleksandrov, E. I. (1997). *The Snow Cover of the Arctic Basin*. Technical Report APL-UW TR 9701, Applied Physics Laboratory, University of Washington, Seattle.)
- Schmidt, R. A. (1972). *Sublimation of Wind-transported Snow – A Model*. USDA Forest Service Research Paper RM-90. Fort Collins, CO: Rocky Mountain Forest and Range Experiment Station.
- Schmidt, R. A. (1991). Sublimation of snow intercepted by an artificial conifer. *Agric. Forest Meteorol.*, **54**, 1–27.
- Schmidt, R. A. and Gluns, D. R. (1991). Snowfall interception on branches of three conifer species. *Can. J. Forest Res.*, **21**, 1262–1269.
- Shine, K. P. (1984). Parametrization of the shortwave flux over high albedo surfaces as a function of cloud thickness and surface albedo. *Q. J. Roy. Meteorol. Soc.*, **110**, 747–764.
- Shook, K. (1993). Fractal geometry of snowpacks during ablation. M.Sc. Thesis, University of Saskatchewan, Saskatoon.
- Shook, K. (1995). Simulation of the ablation of prairie snowcovers. Ph.D. Thesis, University of Saskatchewan, Saskatoon.
- Shook, K. and Gray, D. M. (1994). Determining the snow water equivalent of shallow prairie snowcovers. *Proc. Eastern Snow Conf.*, **51**, 89–95.
- Shook, K. and Gray, D. M. (1996). Small scale spatial structure of shallow snowcovers. *Hydrol. Process.*, **10**, 1283–1292.
- Shook, K. and Gray, D. M. (1997). Snowmelt resulting from advection. *Hydrol. Process.*, **11**, 1725–1736.
- Smeets, C. J. P. P., Duynkerke, P. G., and Vugts, H. F. (1998). Observed wind profiles and turbulence fluxes over an ice surface with changing surface roughness. *Bound.-Lay. Meteorol.*, **92**, 101–123.
- Steppuhn, H. (1981). Snow and agriculture. In *Handbook of Snow: Principles, Processes, Management and Use* (ed. Gray, D. M. and Male, D. H.). Toronto: Pergamon Press, pp. 60–125.
- Steppuhn, H. and Dyck, G. E. (1974). Estimating true basin snowcover. In *Advanced Concepts in the Technical Study of Snow and Ice Resources. Interdisciplinary Symposium*. Washington, DC: US National Academy of Sciences, pp. 314–328.
- Stull, R. B. (1988). *An Introduction to Boundary Layer Meteorology*. Dordrecht: Kluwer Academic Publishers.

- Sturm, M. (1992). Snow distribution and heat flow in the taiga. *Arctic Alpine Res.*, **24**(2), 145–152.
- Sturm, M., Holmgren, J., König, M., and Morris, K. (1997). The thermal conductivity of seasonal snow. *J. Glaciol.*, **43**, 26–41.
- Sturm, M., Holmgren, J., and Liston, G. E. (1995). A seasonal snow cover classification system for local to global applications. *J. Climate*, **8**, 1261–1283.
- Sturm, M., Perovich, D. K., and Holmgren, J. (2002). Thermal conductivity and heat transfer through the snow on the ice of the Beaufort Sea. *J. Geophys. Res.*, **107**(C10), 8045, doi:10.1029/2000JC000466.
- Sverdrup, H. H. (1936). The eddy conductivity of the air over a smooth snowfield. *Geophys. Publ.*, **11**(7), 5–49.
- Tabler, R. D. (1980). Self similarity of wind profiles in blowing snow allows outdoor modelling. *J. Glaciol.*, **26**(94), 421–434.
- Tabler, R. D. and Schmidt, R. A. (1986). Snow erosion, transport and deposition. In *Proc. Symposium on Snow Management for Agriculture* (ed. Steppuhn, H. and Nicholaichuk, W.). Great Plains Agricultural Council Publication No. 120. Lincoln: University of Nebraska, pp. 12–58.
- Thomas, G. and Rowntree, P. R. (1992). The boreal forest and climate. *Q. J. Roy. Meteorol. Soc.*, **118**, 469–497.
- Thorpe, A. D. and Mason, B. J. (1966). The evaporation of ice spheres and ice crystals. *Br. J. Appl. Phys.*, **17**, 541–548.
- Uttal, T., Curry, J. A., McPhee, M. G., *et al.* (2002). Surface heat budget of the Arctic Ocean. *Bull. Amer. Meteor. Soc.*, **83**(2), 255–275.
- Van den Broeke, M. R. (1997). Structure and diurnal variation of the atmospheric boundary layer over a mid-latitude glacier in summer. *Bound.-Lay. Meteorol.*, **83**, 183–205.
- Varley, M. J., Beven, K. J., and Oliver, H. R. 1996. Modelling solar radiation in steeply sloping terrain. *J. Climate*, **16**, 93–104.
- Webb, E. K. (1970). Profile relationships: the log-linear range and extension to strong stability. *Q. J. Roy. Meteorol. Soc.*, **96**, 67–90.
- Weisman, R. W. (1977). Snowmelt: a two-dimensional turbulent diffusion model. *Water Resources Res.*, **13**(2), 337–342.
- Woo, M-K. and Steer, P. (1986). Monte Carlo simulation of snow depth in a forest. *Water Resources Res.*, **22**(6), 864–868.
- Yamazaki, T., Fukabori, K., and Kondo, J. (1996). Albedo of forest with crown snow. *Seppyo, J. Jpn. Soc. Snow Ice*, **58**, 11–18 (in Japanese with English summary).
- Yang, D., Goodison, B. E., Metcalfe, J. R., *et al.* (1995). Accuracy of Tretyakov precipitation gauge: result of WMO intercomparison. *Proc. Eastern Snow Conf.*, **52**, 95–106.
- Zhao, L., Gray, D. M., and Male, D. H. (1997). Numerical analysis of simultaneous heat and mass transfer during infiltration into frozen ground. *J. Hydrol.*, **200**, 345–363.

# Index

- ablation 95
- accretion 18
- Advanced Earth Observing Satellite (ADEOS) 202
- albedo 4, 5, 12, 53, 54, 55, 57, 61, 74, 137, 138, 146, 151, 152, 155, 193
- alpine snow cover 94, 98
- Alter shield 191
- AMIP 159
- AMIP-2 160
- AMSR-E (Advanced Microwave Scanning Radiometer) 202
- Antarctica 14
- Aqua 202
- Arctic 192, 207
- Arctic Ocean 165
- avalanches 13
- AVHRR 193, 194
  
- backscatter coefficient 201
- barometric pressure 46
- Beer's Law 156
- bi-directional reflectance 54
- black body 58
- blowing snow 86
- bonds 26
- boreal forest 109
- BOREAS 111, 156
- Bowen ratio 79
- Brooks and Corey formula 49
- buoyancy 44
  
- Canadian Climate Center (CCC) GCM 165
- Canadian Meteorological Centre 204, 206
- Canadian snow course observations 205
- capillary forces 61
- capillary pressure 25, 47, 48
- Central Sierra Snow Laboratory 127
- chemical exchange 41
- chromatic elution 32
- Clausius-Clapeyron equation 24, 79, 89
- CliC (Climate and Cryosphere)
- climate change 156, 181
  
- climate models 181
- CO<sub>2</sub> 164, 168, 169, 170
- Col de Porte 98, 137, 143, 144
- cold calorimetry 32
- compaction 32, 33, 46
- conductivity 40
- convection 42
- CROCUS model 98, 137, 138, 144, 148, 190, 206
- cryosphere 1
- crystal habit 16
- curvature 24, 26, 31
  
- Darcy's law 41
- Deardoff's parameterization 141
- deformation 33
- deformation rate 33
- deformation strain 33
- degree day 126
- density (see snow density)
- deposition 16
- depth hoar 33, 42
- diamond dust 14
- dielectric measurements 32
- diffuser 53
- diffusion coefficient 31, 38
  
- ECMWF 90, 115
- elastic 32
- emissivity 58, 61
- energy balance 71, 92, 153
- energy budget 39
- equilibrium form 28
- equilibrium vapor pressure 27
- evaporation 73
  
- faceted crystals 28, 33, 56
- feedback mechanisms 12
- Fick's law 88
- flow fingers 51, 53, 61
- fluid flow 40
- FMCW radar 52
- forced convection 45

- Fourier equation 36, 126  
 friction velocity 78, 87  
 frozen soil 32
- GCM 130, 136, 137, 140, 146, 147, 151, 154, 170, 206, 207  
 Gibbs-Duhem equation 25, 29  
 Global Climate Observing System (GCOS) 203  
 global warming 40, 162, 170  
 Global Telecommunications System (GTS) 204  
 GOES 194  
 grain shape 30  
 grain size 29  
 ground heat flux 72, 154  
 growth rate 31
- Hadley Centre GCM 168  
 hazard 7  
 heat flux 154  
 heat transfer 33  
 hot calorimetry 32
- ice nuclei 15  
 impurities 53, 54, 55, 56  
 infiltration 48  
 insolation 42  
 Interactive Multisensor Snow and Ice Mapping System (IMS) 193, 204  
 interception 19  
 IPCC 7, 163, 207
- Kernen Farm 105  
 kinematic viscosity 81  
 kinetic growth form 28
- Landsat Thematic Mapper 195  
 Laplace equation 24, 29, 47  
 latent heat 72, 76, 87  
 latent heat of fusion 5, 38, 72  
 latent heat of sublimation 38  
 liquid water content 30, 32  
 long-wave radiation 58, 61, 72, 75, 146, 147  
 lysimeter 48, 50
- MAGS 111  
 mass balance 72, 92, 153  
 melt-freeze crust 58  
 melt-freeze cycles 29  
 melting point depression 25  
 melting point temperature 29  
 meniscus 29  
 metamorphism 3, 27, 30, 31, 33  
 METEOSAT 193  
 microstructure 21, 27, 35  
 microwave 158, 201  
 mixing ratio 31  
 MODIS (Moderate Resolution Imaging Spectroradiometer) 202, 204  
 molality 27
- NASA Earth Observing System (EOS) 202  
 National Operational Hydrological Remote Sensing Center (NOHRSC) 196, 204  
 natural convection 45  
 Natural Resources Conservation Service (NRCS) 205  
 net radiation 76  
 Newtonian fluid 33  
 NOAA Climate Prediction Center 206  
 NOAA-NESDIS 193  
 NSIDC 194, 202, 203, 205  
 nucleation 15  
 numerical models 31  
 Nusselt number 89  
 NWPM (Numerical Weather Prediction Models) 130
- Obukhov length 77  
 optical grain size 56
- passive microwave 196  
 Peclet number 38  
 Penman-Monteith model 85  
 Perce-Neige model 128  
 permeability 41, 42, 43, 48, 49  
 permittivity 31  
 phase diagram 23  
 photon 53, 54  
 PILPS 2e 154  
 plastic 32  
 polar amplification 158  
 pore space 48  
 porosity 21, 40, 42, 44, 59, 148  
 porous media 19, 20, 44  
 prairies 104, 200  
 precipitation 14, 190, 191  
 precipitation particles 30
- QuickSCAT 202
- radar 201  
 radiative properties 31  
 radius of curvature 47  
 Rayleigh number 45  
 RCM (Regional Climate Model) 130  
 reflectance 31  
 refractive index 31  
 Reynolds number 81, 82, 89  
 rheological properties 32, 33  
 Richardson number 78, 141  
 riming 18  
 Rocky Mountains 155  
 roughness length 79, 82
- saltation 87, 92  
 sastruggi 57  
 Satellite Analysis Branch (SAB) 206  
 satellite remote sensing 192  
 satellites 182  
 saturated or one-phase flow 41  
 saturation pressure 13  
 sea ice 101  
 sensible heat 72, 76

- SHEBA 101, 103  
 Sherwood number 89  
 short-wave radiation 61, 72, 74, 138  
 short-wave spectrum 58  
 sintering 18, 30, 42  
 Sleepers River Research Watershed 127  
 SMMR 196, 197, 200  
 SNOTEL 189, 205  
 snow classification 21  
 snow course 188, 189  
 snow density 4, 19, 20, 21, 31, 33, 36, 59, 72, 148, 191  
 snow depth climatologies 206  
 snow drift 33  
 snow line 8  
 snow pillows 189  
 snow pit 190  
 snow water equivalent (SWE) 4  
 snow-climate feedback 161, 162, 170  
 snowfall rates 59  
 snowflakes 18  
 SNOWMIP 128, 145  
 SNOWPACK 95, 148, 190  
 SNTHERM 50, 115, 148, 190, 206  
 solar radiation 74  
 specific heat 36, 72  
 specific humidity 77  
 specular reflection 54  
 SPOT 195  
 SSARR 126  
 SSM/I 194, 196, 200, 205  
 Stanford Watershed Model 126  
 Stefan-Boltzmann equation 75  
 sublimation 17, 28, 33, 73, 85, 86, 87, 88, 89, 90  
 supersaturation 16, 23  
 surface hoar 56  
 surface roughness 46, 77  
 surface tension 26  
 Synthetic Aperture Radar (SAR) 201  
 temperature gradient 28, 30, 31, 45, 60  
 tensiometer 48  
 Terra 202  
 TESSEL surface scheme 155  
 texture 21  
 thermal conductivity 5, 13, 35, 36, 60  
 thermal properties 5, 35  
 thermal spectrum 61  
 triple point 23  
 turbulence 46  
 turbulent fluxes 72, 76  
 U.S. Air Force snow depth climatology 158  
 ultrasonic snow depth sensors 186  
 unsaturated flow 46  
 van Genuchten function 48  
 vapor diffusion 28, 31  
 vapor pressure 16, 23, 27, 28  
 vegetation 83, 155  
 ventilation 39, 40, 46  
 viscosity 34  
 viscous 32  
 von Kármán's constant 77  
 water retention 47  
 WCRP Climate and Cryosphere (CliC) 203  
 Weissfluhjoch 94  
 wet snow metamorphism 29, 31, 33  
 wetting front 49, 51, 53  
 windpumping 40, 60  
 World Meteorological Organization 128, 129